(NASA-TP-1919) WIND-TUNNEL RESULTS FOR A MODIFIED 17-PERCENT-THICK LOW-SPEED AIRFOIL SECTION (NASA) 87 p HC A05/MF A01 CSCL 01A

N82-11033

Unclas

H1/02 01860

Wind-Tunnel Results for a Modified 17-Percent-Thick Low-Speed Airfoil Section

Robert J. McGhee and William D. Beasley

NOVEMBER 1981

NASA

NASA Technical Paper 1919

Wind-Tunnel Results for a Modified 17-Percent-Thick Low-Speed Airfoil Section

Robert J. McGhee and William D. Beasley
Langley Research Center
Hampton, Virginia

NASA
National Aeronautics
and Space Administration

Scientific and Technical
Information Branch

1981

SUMMARY

An investigation was conducted in the Langley Low-Turbulence Pressure Tunnel to evaluate the effects on performance of modifying a 17-percent-thick low-speed airfoil. The airfoil contour was altered to reduce the pitching-moment coefficient by increasing the forward loading and to increase the climb lift-drag ratio by decreasing the aft upper surface pressure gradient. The tests were conducted over a Mach number range from 0.07 to 0.32, a chord Reynolds number range from 1.0×10^6 to 12.0×10^6, and an angle-of-attack range from about −10° to 20°.

The results of the investigation indicate that the modification to the airfoil contour produced the design objectives of reduced pitching-moment coefficient at cruise and increased lift-drag ratio at climb. The magnitude of the pitching-moment coefficient was reduced about 20 percent at the design lift coefficient of 0.40, and the lift-drag ratio was increased about 10 percent at the climb lift coefficient of 1.0. The maximum lift coefficient was also increased about 10 percent at Reynolds numbers of 2.0×10^6 and 4.0×10^6. However, the stall characteristics of the modified airfoil were less desirable at Reynolds numbers greater than 2.0×10^6 because of a rapid forward movement of the trailing-edge separation point.

INTRODUCTION

Research on advanced-technology airfoils for low-speed general-aviation applications has received considerable attention at the Langley Research Center since the development of the LS(1)-0417 airfoil (formerly GA(W)-1) of reference 1. This 17-percent-thick airfoil provided higher lift-drag ratios during climb and higher maximum lift coefficients (with or without flaps) when compared with the older NACA (National Advisory Committee for Aeronautics) airfoils. However, because of the large amount of aft camber incorporated in the airfoil, the quarter-chord pitching-moment coefficient at design lift was about −0.10. This airfoil has been analytically reshaped with two objectives in mind: to reduce the pitching-moment coefficient by increasing the forward loading and to increase further the climb lift-drag ratio by decreasing the aft upper surface pressure gradient. This report presents the basic low-speed section characteristics of this modified airfoil and evaluates the effects on performance resulting from the change in airfoil shape.

The investigation was performed in the Langley Low-Turbulence Pressure Tunnel at free-stream Mach numbers from 0.07 to 0.32. The chord Reynolds number varied from about 1.0×10^6 to 12.0×10^6, and the geometric angle of attack varied from about −10° to 20°.

SYMBOLS

Values are given in both SI and U.S. Customary Units. The measurements and calculations were made in U.S. Customary Units.

C_p pressure coefficient, $\dfrac{p_l - p_\infty}{q_\infty}$

c	airfoil chord, cm (in.)
c_c	section chord-force coefficient, $\oint c_p \, d\left(\frac{z}{c}\right)$
c_d	section profile-drag coefficient, $\int_{\text{Wake}} c_d' \, d\left(\frac{h}{c}\right)$
c_d'	point-drag coefficient,

$$2\left(\frac{p}{p_\infty}\right)^{6/7}\left[\frac{\left(\frac{p_t}{p}\right)^{2/7}-1}{\left(\frac{p_{t,\infty}}{p_\infty}\right)^{2/7}-1}\right]^{1/2}\left\{\left(\frac{p_t}{p_{t,\infty}}\right)^{1/7}-\left[\frac{\left(\frac{p_t}{p_\infty}\right)^{2/7}-1}{\left(\frac{p_{t,\infty}}{p_\infty}\right)^{2/7}-1}\right]^{1/2}\right\}$$

c_l	section lift coefficient, $c_n \cos \alpha - c_c \sin \alpha$
c_m	section pitching-moment coefficient about quarter-chord point,

$$-\oint c_p\left(\frac{x}{c} - 0.25\right) d\left(\frac{x}{c}\right) + \oint c_p \frac{z}{c} \, d\left(\frac{z}{c}\right)$$

c_n	section normal-force coefficient, $-\oint c_p \, d\left(\frac{x}{c}\right)$
h	vertical distance in wake profile, cm (in.)
l/d	section lift-drag ratio
M	free-stream Mach number
p	static pressure, Pa (lb/ft^2)
p_t	total pressure, Pa (lb/ft^2)
q	dynamic pressure, Pa (lb/ft^2)
R	Reynolds number based on free-stream conditions and airfoil chord
V/V_∞	ratio of local velocity to free-stream velocity
x	airfoil abscissa, cm (in.)
z	airfoil ordinate, cm (in.)
z_c	mean camber-line ordinate, cm (in.)
z_t	mean thickness, cm (in.)
α	geometric angle of attack, deg

Subscripts:

ℓ local point on airfoil

max maximum

s separation

∞ free-stream conditions

Airfoil designations:

LS(1)-0417 low speed (first series); 0.4 design lift coefficient, 17 percent thick

Mod modified

AIRFOIL MODIFICATION

The airfoil contour was changed with two objectives in mind: to reduce the pitching-moment coefficient by increasing the forward loading and to increase the climb lift-drag ratio (c_l = 1.0) by decreasing the aft upper surface pressure gradient. The maximum thickness ratio, trailing-edge thickness, and design lift coefficient (c_l = 0.40) of the original airfoil were retained.

The upper surface modification to the original airfoil was accomplished by using the computer code of reference 2. This inverse method calculates inviscid coordinates of an airfoil from a prescribed velocity distribution. A boundary-layer correction is made to allow for viscous effects by computing the displacement thickness of the turbulent boundary layer, which is subtracted from the inviscid coordinates. The inviscid velocity distributions for both airfoils are shown in figure 1, and figure 2 illustrates the change in airfoil shape. The design conditions for the airfoil were a lift coefficient of 0.40, a Reynolds number of 4.0×10^6, and a Mach number of 0.15. Figure 3 compares the mean thickness distributions and camber lines for the two airfoils. Coordinates for the modified airfoil are presented in table I.

Theoretical chordwise pressure distributions (ref. 2) for both airfoils are shown in figure 4 for a Reynolds number of 4.0×10^6. Boundary-layer transition was specified at x/c = 0.03 for the calculations to ensure a turbulent boundary-layer development on the airfoils. A reduction in the pitching-moment coefficient at design lift of about 28 percent is indicated by the theoretical calculations. Note that a flat pressure distribution or reduced pressure-gradient region extends for about 0.20c prior to the start of the aft upper surface pressure recovery for the modified airfoil. This reduced pressure-gradient region with the "corner" located at x/c = 0.60 is considered to be an important feature of the airfoil design. Research reported in reference 3 for a modified 13-percent-thick airfoil clearly indicated that this reduced pressure-gradient region retards the rapid forward movement of upper surface separation at the onset of stall and promotes docile stall behavior for airfoils which stall from the trailing edge. The chordwise location of the corner is determined by the aft pressure gradient which must be gradual enough to avoid separation at climb lift coefficients (c_l = 1.0). Thus, the chordwise location of the corner is dependent on airfoil thickness ratio and design lift coefficient. The chordwise extent of the reduced pressure-gradient region must be determined from experimental tests, since present computer codes are inadequate when large regions of separation are present. The theoretical separation points and pressure distributions for both airfoils are shown in figure 4(b) at a climb lift coefficient of 1.0. A reduction in the extent of separation of about 0.05c is indicated for the modified airfoil. Based on this theoretical prediction of reduced separation, some improvement in lift-drag ratio at $c_l = 1.0$ would be expected.

MODEL, APPARATUS, AND PROCEDURE

Model

The airfoil model was constructed with a metal core around which plastic fill and two thin layers of fiberglass were used to form the contour of the airfoil. The model had a chord of 61 cm (24 in.) and a span of 91 cm (36 in.) and was equipped with both upper and lower surface orifices located 5 cm (2 in.) off the midspan. The airfoil surface was sanded in the chordwise direction with No. 400 dry silicon carbide paper to provide a smooth aerodynamic finish. The model-contour accuracy was generally within ±0.10 mm (±0.004 in.).

Wind Tunnel

The Langley Low-Turbulence Pressure Tunnel (ref. 4) is a closed-throat, single-return tunnel which can be operated at stagnation pressures from 1.0 to 10.0 atm (1 atm = 101.3 kPa) with tunnel-empty test-section Mach numbers up to 0.42 and 0.22, respectively. The maximum Reynolds number is about 49.2×10^6 per m (15.0×10^6 per ft) at a free-stream Mach number of about 0.22. The tunnel test section is 91 cm (3 ft) wide and 229 cm (7.5 ft) high.

Hydraulically actuated circular plates provided positioning and attachment for the two-dimensional model. The plates are 102 cm (40 in.) in diameter, rotate with the airfoil, and are flush with the tunnel wall. The airfoil ends were attached to rectangular model-attachment plates (fig. 5), and the airfoil was mounted so that the center of rotation for the circular plates was at 0.25c on the model reference line. The air gaps in the tunnel walls between the rectangular plates and the circular plates were sealed with metal seals.

Wake Survey Rake

A fixed wake survey rake (fig. 6) at the model midspan was mounted from the tunnel sidewall and located 1 chord length behind the trailing edge of the airfoil. The wake rake used 0.15-cm-diameter (0.06-in.) total-pressure tubes and 0.32-cm-diameter (0.125-in.) static-pressure tubes. The total-pressure tubes were flattened to 0.10 cm (0.04 in.) for 0.61 cm (0.24 in.) from the tip of the tube. Each static-pressure tube had four flush orifices drilled 90° apart; these orifices were located eight tube diameters from the tip of the tube and in the plane of measurement for the total-pressure tubes.

Instrumentation

Measurements of the static pressures on the airfoil surfaces and of the wake-rake pressures were made by an automatic pressure-scanning system using variable-capacitance precision transducers. Basic tunnel pressures were measured with precision quartz manometers. Angle of attack was measured with a calibrated digital shaft encoder operated by a pinion gear and rack attached to the circular model-attachment plates. Data were obtained by a high-speed acquisition system and were recorded on magnetic tape.

TESTS AND METHODS

The airfoil was tested at free-stream Mach numbers from 0.07 to 0.32 over an angle-of-attack range from about -10° to 20°. Reynolds number based on the airfoil chord was varied from about 1.0×10^6 to 12.0×10^6. The airfoil was tested both in the smooth condition (natural transition) and with roughness located on both upper and lower surfaces at 0.075c. The roughness was sized for each Reynolds number according to the technique described in reference 5. The roughness was sparsely distributed and consisted of granular-type strips 0.13 cm (0.05 in.) wide which were attached to the surfaces with clear lacquer.

The static-pressure measurements at the airfoil surface were reduced to standard pressure coefficients and were machine integrated to obtain section normal-force and chord-force coefficients as well as section pitching-moment coefficients about the quarter-chord point. Section profile-drag coefficients were computed from the wake-rake total, and static pressures by the method reported in reference 6.

An estimate of the standard low-speed wind-tunnel boundary corrections (ref. 7) amounted to a maximum of about 2 percent of the measured coefficients; these corrections have not been applied to the data. An estimate of the displacement of the effective center of a total-pressure tube in a velocity gradient on the values of c_d showed these effects to be negligible. (See ref. 6.)

PRESENTATION OF RESULTS

The results of this investigation have been reduced to coefficient form and are presented in the following figures:

Figure

DISCUSSION OF RESULTS

Section Characteristics

Lift.- The lift-curve slope for the 17-percent-thick modified airfoil in a smooth condition (roughness off) was about 0.12 per degree for the Reynolds numbers investigated ($M = 0.15$) as indicated by figure 10(a). The angle of attack for zero lift coefficient was about -3.5°. Maximum lift coefficients increased from about 1.70 to 2.10 as the Reynolds number was increased from 1.0×10^6 to 12.0×10^6. (See fig. 19.) The largest effect of Reynolds number on maximum lift coefficient occurred for Reynolds numbers below 6.0×10^6. The stall characteristics of the airfoil are of the trailing-edge type as shown by the pressure data of figure 15. However, the nature of the stall was abrupt for Reynolds numbers greater than 2.0×10^6. (See fig. 7.) Abrupt stall characteristics were not expected for this airfoil, and a detailed discussion is included in a subsequent section entitled "Pressure Distributions."

The addition of a narrow roughness strip at 0.075c (fig. 9) resulted in the expected decambering effect for thick airfoils because of the increase in boundary-layer thickness. The lift coefficient at $\alpha = 0°$ decreased about 0.03 at the lower Reynolds numbers, but only small changes occurred at the higher Reynolds numbers. The roughness strip decreased the $c_{l,max}$ performance of the airfoil as much as 0.04 for the test Reynolds number range. (See fig. 19.)

The effects of Mach number on the airfoil lift characteristics at a Reynolds number of 6.0×10^6 with roughness located at 0.075c are shown in figure 12(a). Increasing the Mach number from 0.10 to 0.32 resulted in the expected increase in lift-curve slope, and the stall angle of attack was decreased about 2.2°. However, there were only small changes in $c_{l,max}$ due to Mach number effects. (See fig. 20.)

The lift data for the original and modified 17-percent-thick airfoils are compared in figure 13 for Reynolds numbers from 2.0×10^6 to 6.0×10^6 with fixed transition at 0.075c. The data indicate that the linearity of the lift curve is extended to higher angles of attack and that $c_{l,max}$ is increased for the modified airfoil. This result is attributed to reduced upper surface boundary-layer separation for the modified airfoil, as illustrated by the pressure-data comparison of figure 18(c). Note, however, that the nature of the stall is more abrupt for the modified airfoil for Reynolds numbers of 4.0×10^6 and 6.0×10^6. The variation of $c_{l,max}$ with Reynolds number and Mach number is compared for both airfoils in figures 19 and 20, respectively. In the low Reynolds number range ($R < 4.0 \times 10^6$), an increase in $c_{l,max}$ of about 10 percent is shown for the modified airfoil. However, for Reynolds numbers greater than 9.0×10^6, both airfoils develop about the same $c_{l,max}$. Increasing the Mach number results in a decrease in $c_{l,max}$ for the original airfoil (fig. 20); however, only small Mach number effects on $c_{l,max}$ are shown for the modified airfoil. Comparisons of the values of $c_{l,max}$ for the modified airfoil with the NACA 4- and 5-digit airfoils and 65-series airfoils are shown in figure 21 for Reynolds numbers from 3.0×10^6 to 9.0×10^6. Substantial improvements in $c_{l,max}$ throughout the Reynolds number range are indicated for the modified low-speed airfoil. For example, at a Reynolds number of 3.0×10^6 a 35-percent improvement in $c_{l,max}$ is shown for the modified airfoil compared with the NACA 23018 airfoil.

Pitching moment.- The pitching-moment-coefficient data of figures 9, 10(c), and 11(c) illustrate the expected positive increments in c_m due to decreasing the Reynolds number or adding roughness at a constant Reynolds number. This result is typical of the decambering effect associated with boundary-layer thickening for thick airfoils. At a Reynolds number of 6.0×10^6, increasing the Mach number from 0.10 to 0.32 (fig. 12(c)) shows small effects on the pitching-moment data to about $\alpha = 10°$. At the higher angles of attack, a positive increment in c_m is shown.

The pitching-moment data for the original and modified airfoils are compared in figure 13. The design objective of reducing c_m by increasing the forward loading of the airfoil was accomplished. A reduction in the magnitude of c_m of about 20 percent at $c_l = 0.40$ (cruise condition) is indicated for the modified airfoil. The theory indicated a reduction in c_m of about 28 percent. This result is important because of the expected reduced trim penalties for the modified airfoil at cruise conditions.

Drag and lift-drag ratio.- Natural transition usually occurs near the leading edge of wings in actual flight conditions of general aviation aircraft because of the roughness of construction or insect remains gathered in flight. Therefore, the discussion of the drag data is limited to data obtained with fixed transition at 0.075c.

The profile-drag coefficient at design lift ($c_l = 0.40$) decreased from about 0.0115 at $R = 2.0 \times 10^6$ to about 0.0085 at $R = 12.0 \times 10^6$. (See figs. 11(b) and 22.) This reduction in c_d is due to the decrease in the skin-friction coefficient of the turbulent boundary layer at the higher Reynolds numbers. There are only small effects of Mach number on c_d (fig. 12(b)) over a Mach number range from 0.10 to 0.32.

The drag data for the original and modified airfoils are compared in figure 13 for Reynolds numbers from 2.0×10^6 to 6.0×10^6 with fixed transition at 0.075c. The design objective of reduced c_d, at typical climb conditions ($c_l = 1.0$; $R = 4.0 \times 10^6$) by decreasing the aft upper surface pressure gradient was accomplished (c_d decreased about 0.0012). An increase in climb lift-drag ratio of about 10 percent was measured for the modified airfoil. (See fig. 23.)

Pressure Distributions

The chordwise pressure data of figure 15 illustrate the effects of angle of attack for several Reynolds numbers for the modified airfoil. As the angle of attack is increased, upper surface trailing-edge separation is first indicated by the approximate constant-pressure region on the airfoil. At a Reynolds number of 2.0×10^6, separation is indicated at about $\alpha = 12°$. (See fig. 15(a).) Additional increases in angle of attack result in this constant-pressure region moving forward along the airfoil, and the stall characteristics are docile. The lift curve is well rounded at stall as shown by figure 9(a). However, at $R = 4.0 \times 10^6$ (fig. 15(b)) the trailing-edge separation point moves rapidly forward for an increase in angle of attack from about 16° to 17°, and the stall characteristics are abrupt. The lift data of figure 9(b) illustrate the abrupt decrease in lift at stall. As discussed in a previous section entitled "Airfoil Modification," docile stall behavior was anticipated for this airfoil because of the flat pressure distribution (reduced pressure-gradient region) prior to the start of the aft upper surface pressure recovery at the design lift coefficient. However, as previously discussed, the rearward extent of this flat pressure distribution must be determined from experimental tests because the present airfoil theories are inadequate when large regions of separation are present. Thus, more desirable stall characteristics for this airfoil at the higher Reynolds number would be expected by reshaping the airfoil with a more rearward extent of this flat pressure distribution.

Comparisons of the pressure data for the original and modified airfoils are shown in figure 18 at a Mach number of 0.15 and a Reynolds number of 4.0×10^6. The pressure data at $\alpha = 0°$ (fig. 18(a)) illustrate the increase in forward loading and the decrease in the aft upper surface pressure gradient for the modified airfoil. This reduced pressure gradient has a favorable effect on the airfoil boundary-layer development (reduced thickness) and results in a decrease in c_d at typical climb lift coefficients. Comparisons of the airfoil pressure data at $\alpha = 12°$ (fig. 18(c)) indicate that the modified airfoil exhibits about 0.20c less separation than the original airfoil.

CONCLUDING REMARKS

Wind-tunnel tests have been conducted in the Langley Low-Turbulence Pressure Tunnel to evaluate the effects on performance of modifying a 17-percent-thick low-speed airfoil. The airfoil contour was altered to reduce the pitching-moment coefficient by increasing the forward loading and to increase the climb lift-drag ratio by decreasing the aft upper surface pressure gradient. The tests were conducted at free-stream Mach numbers from 0.07 to 0.32. The chord Reynolds number was varied from about 1.0×10^6 to 12.0×10^6.

The results show that the modification to the airfoil contour produced the design objectives of reduced pitching-moment coefficient at cruise and increased lift-drag ratio at climb. The magnitude of the pitching-moment coefficient was reduced about 20 percent at the design lift coefficient of 0.40, and the lift-drag ratio was increased about 10 percent at the climb lift coefficient of 1.0. The maximum lift coefficient was also increased about 10 percent at Reynolds numbers of 2.0×10^6 and 4.0×10^6. However, the stall characteristics of the modified airfoil were less desirable at Reynolds numbers greater than 2.0×10^6 because of a rapid forward movement of the trailing-edge separation point.

Langley Research Center
National Aeronautics and Space Administration
Hampton, VA 23665
August 18, 1981

REFERENCES

1. McGhee, Robert J.; and Beasley, William D.: Low-Speed Aerodynamic Characteristics of a 17-Percent-Thick Airfoil Section Designed for General Aviation Applications. NASA TN D-7428, 1973.

2. Bauer, Frances; Garabedian, Paul; and Korn, David: Supercritical Wing Sections III. Volume 150 of Lecture Notes in Economics and Mathematical Systems, Springer-Verlag, 1977.

3. McGhee, Robert J.; and Beasley, William D.: Low-Speed Wind-Tunnel Results for a Modified 13-Percent-Thick Airfoil. NASA TM X-74018, 1977.

4. Von Doenhoff, Albert E.; and Abbott, Frank T., Jr.: The Langley Two-Dimensional Low-Turbulence Pressure Tunnel. NACA TN 1283, 1947.

5. Braslow, Albert L.; and Knox, Eugene C.: Simplified Method for Determination of Critical Height of Distributed Roughness Particles for Boundary-Layer Transition at Mach Numbers From 0 to 5. NACA TN 4363, 1958.

6. Pankhurst, R. C.; and Holder, D. W.: Wind-Tunnel Technique. Sir Issac Pitman & Sons, Ltd. (London), 1965.

7. Pope, Alan; and Harper, John J.: Low-Speed Wind Tunnel Testing. John Wiley & Sons, Inc., c.1966.

TABLE I.- COORDINATES FOR LS(1)-0417 MOD AIRFOIL

Upper surface		Lower surface	
x/c	z/c	x/c	z/c
0	0	0	0
.00124	.01286	.00106	-.00728
.00239	.01665	.00248	-.01063
.00741	.02642	.00765	-.01683
.01300	.03408	.01338	-.02096
.02088	.04266	.01991	-.02441
.03133	.05170	.03183	-.02945
.04150	.05894	.04187	-.03294
.05080	.06464	.05110	-.03573
.07102	.07488	.07203	-.04101
.09992	.08593	.10088	-.04665
.12642	.09341	.12531	-.05040
.15195	.09875	.15156	-.05374
.17613	.10242	.17603	-.05633
.20136	.10503	.20151	-.05851
.22458	.10651	.22487	-.06016
.25191	.10731	.25229	-.06167
.27462	.10734	.27686	-.06259
.30195	.10678	.30180	-.06323
.32382	.10597	.32330	-.06355
.35017	.10471	.35239	-.06367
.37685	.10320	.37431	-.06353
.40344	.10157	.40000	-.06312
.42607	.10012	.42580	-.06243
.45228	.09836	.45148	-.06146
.47432	.09680	.47321	-.06042
.49983	.09488	.50145	-.05869
.52478	.09280	.52561	-.05681
.55306	.09013	.55215	-.05424
.57414	.08788	.57495	-.05155
.60250	.08445	.60089	-.04793
.62408	.08153	.62389	-.04432
.64961	.07770	.65070	-.03976
.67575	.07339	.67458	-.03552
.70240	.06864	.69911	-.03104
.72617	.06416	.72419	-.02632
.74966	.05956	.74967	-.02148
.77674	.05412	.77634	-.01652
.80302	.04870	.80123	-.01216
.82446	.04422	.82480	-.00841
.85023	.03874	.85026	-.00485
.87504	.03337	.87444	-.00195
.90244	.02737	.90007	.00032
.92463	.02238	.92418	.00147
.95022	.01657	.95022	.00160
.97593	.01034	.97586	.00013
1.00000	.00378	1.00000	-.00354

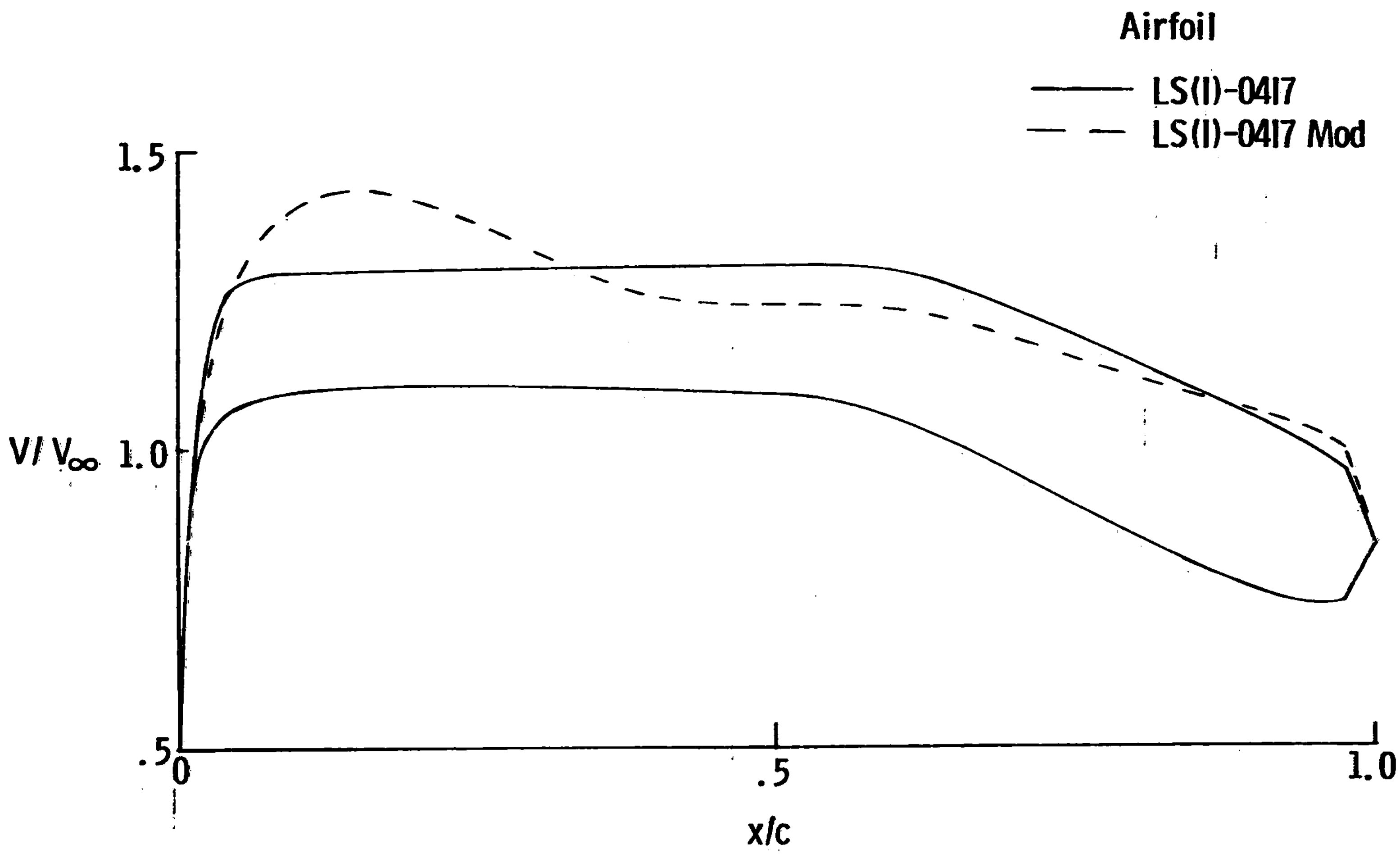

Figure 1.- Inviscid velocity distributions for LS(1)-0417 and LS(1)-0417 Mod airfoils. $c_l = 0.40$.

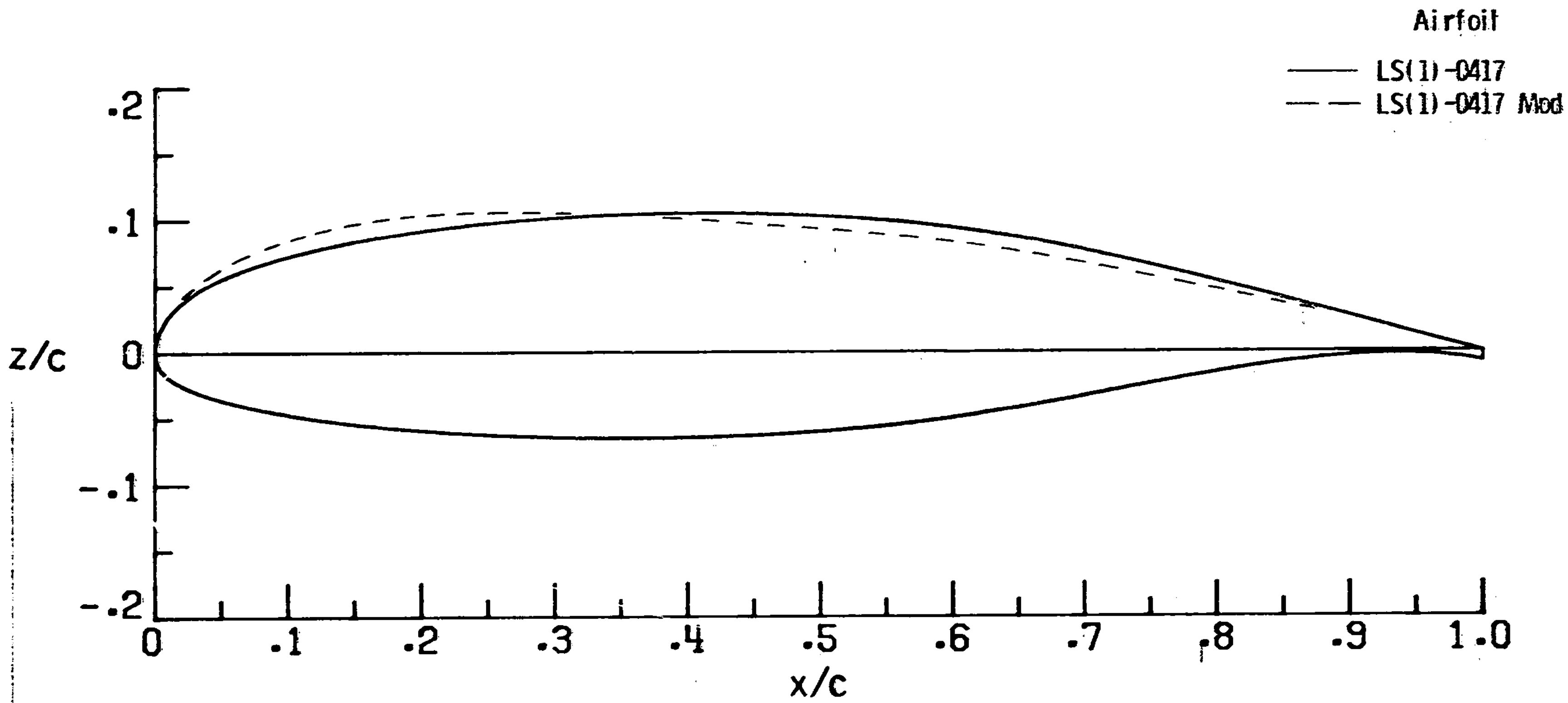

Figure 2.- Comparison of section shapes for LS(1)-0417 and LS(1)-0417 Mod airfoils.

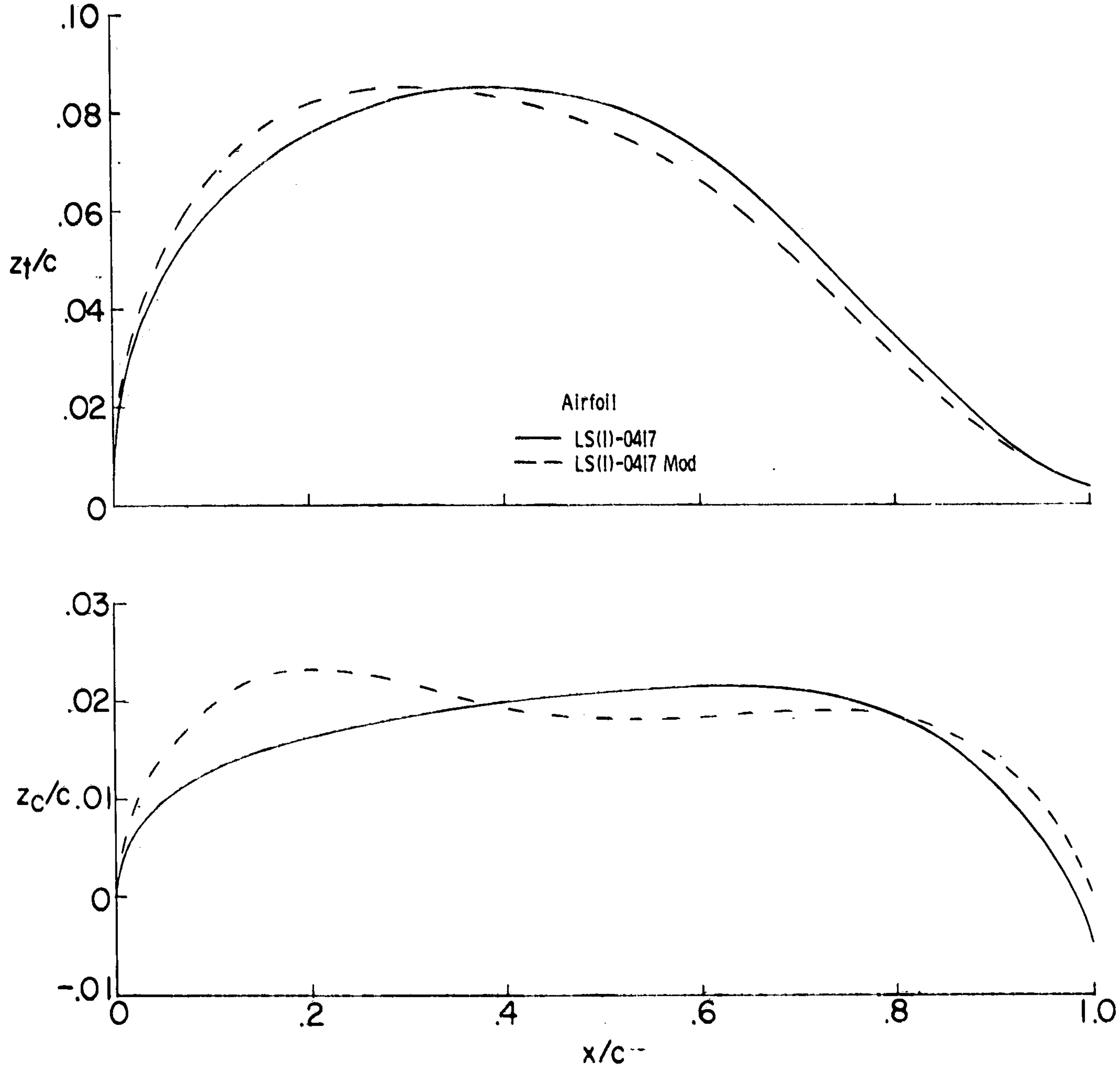

Figure 3.- Comparison of mean thickness distributions and camber lines for LS(1)-0417 and LS(1)-0417 Mod airfoils.

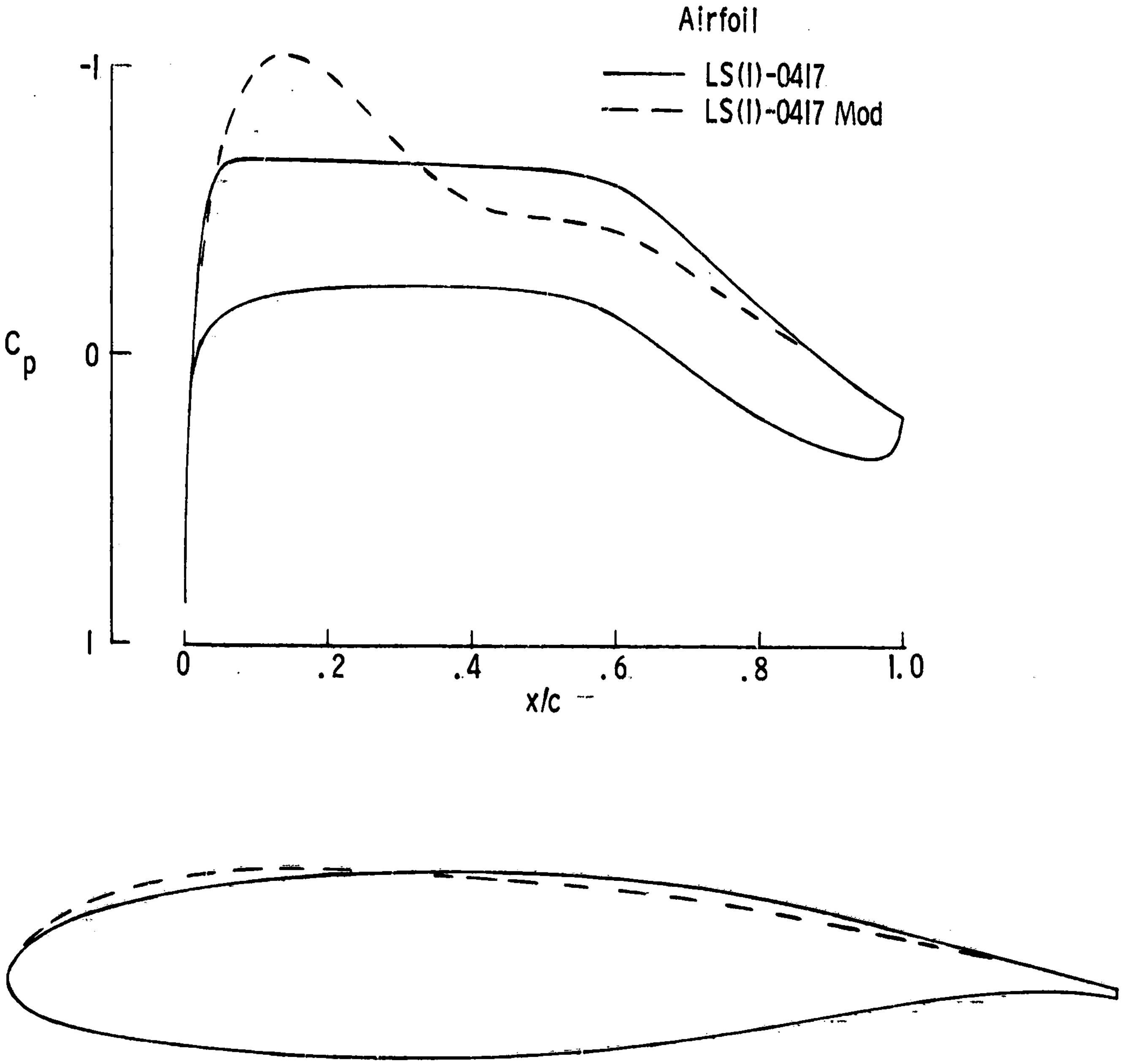

(a) $c_l = 0.40$.

Figure 4.- Theoretical chordwise pressure distributions for LS(1)-0417 and LS(1)-0417 Mod airfoils. $M = 0.15$; $R = 4.0 \times 10^6$.

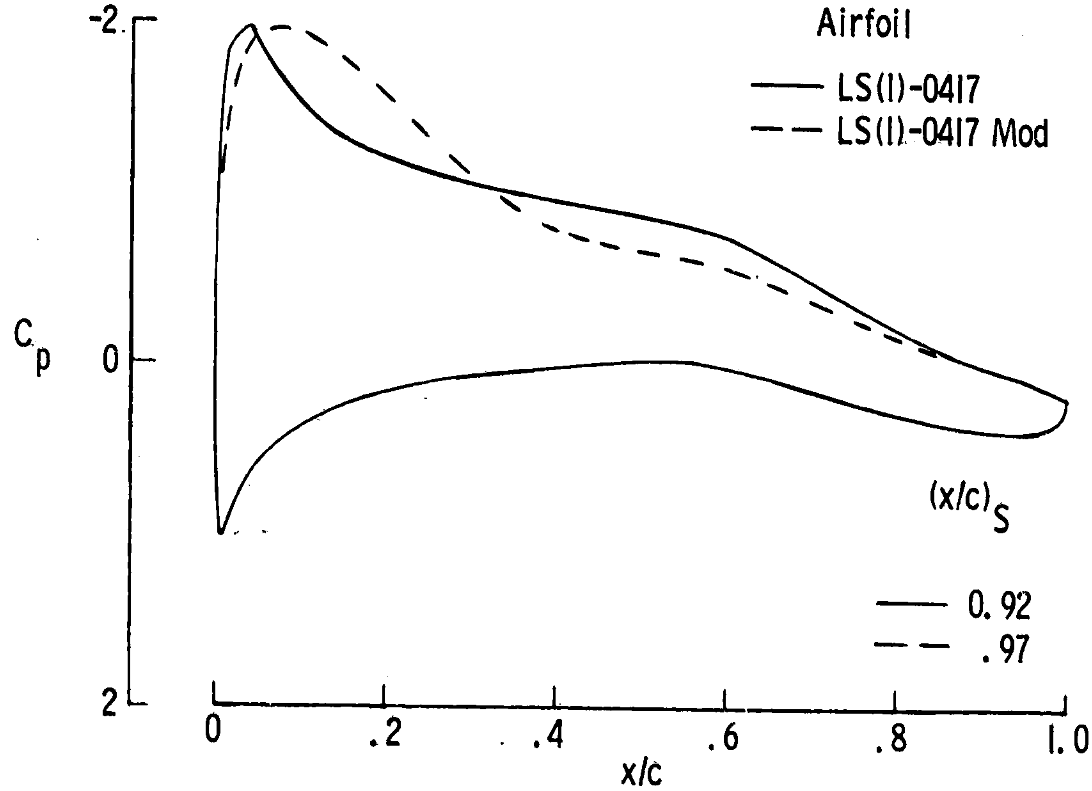

(b) $c_l = 1.0$.

Figure 4.- Concluded.

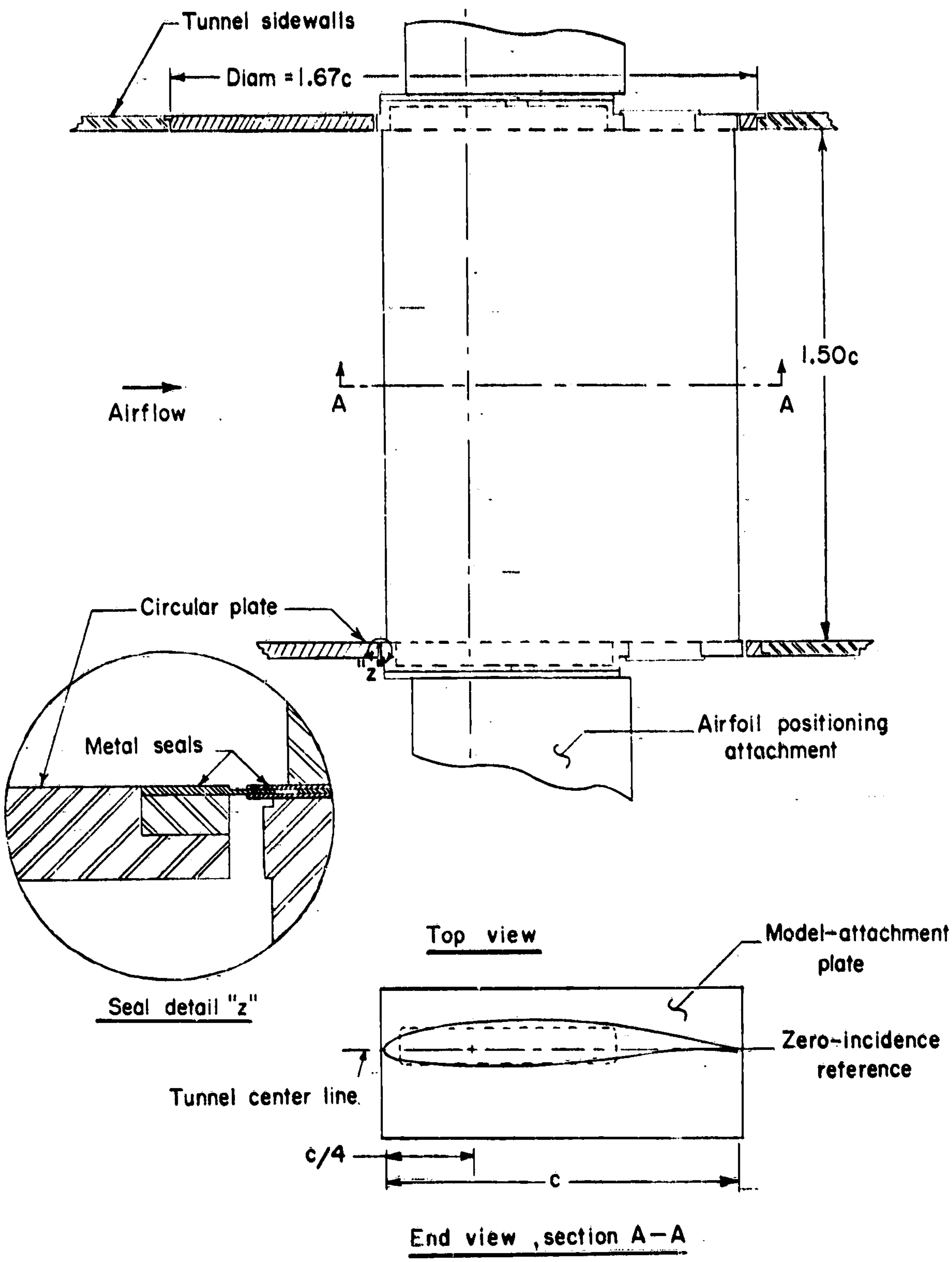

Figure 5.- Typical airfoil model mounted in wind tunnel.
c = 61 cm (24 in.).

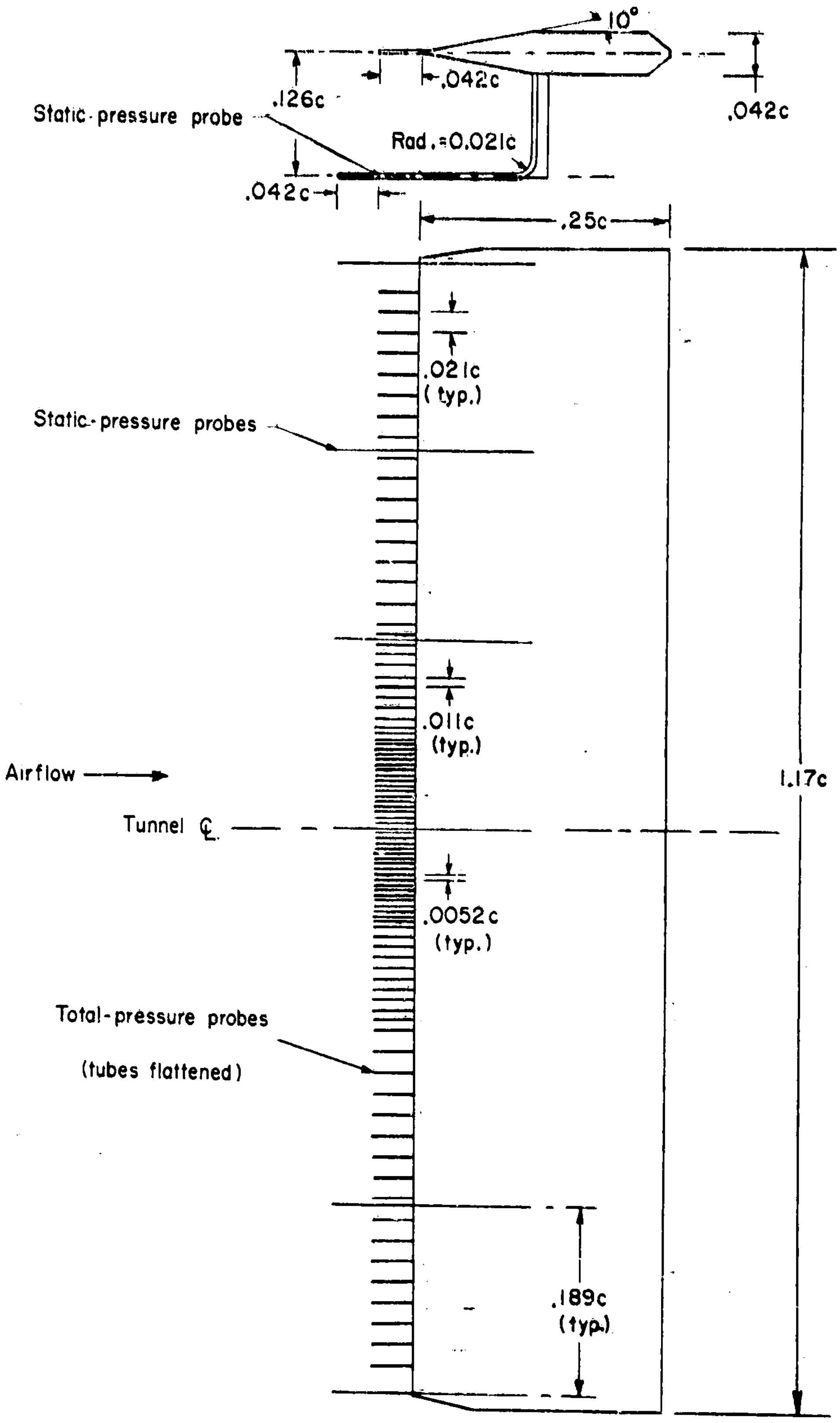

Figure 6.- Wake survey rake. c = 61 cm (24 in.).

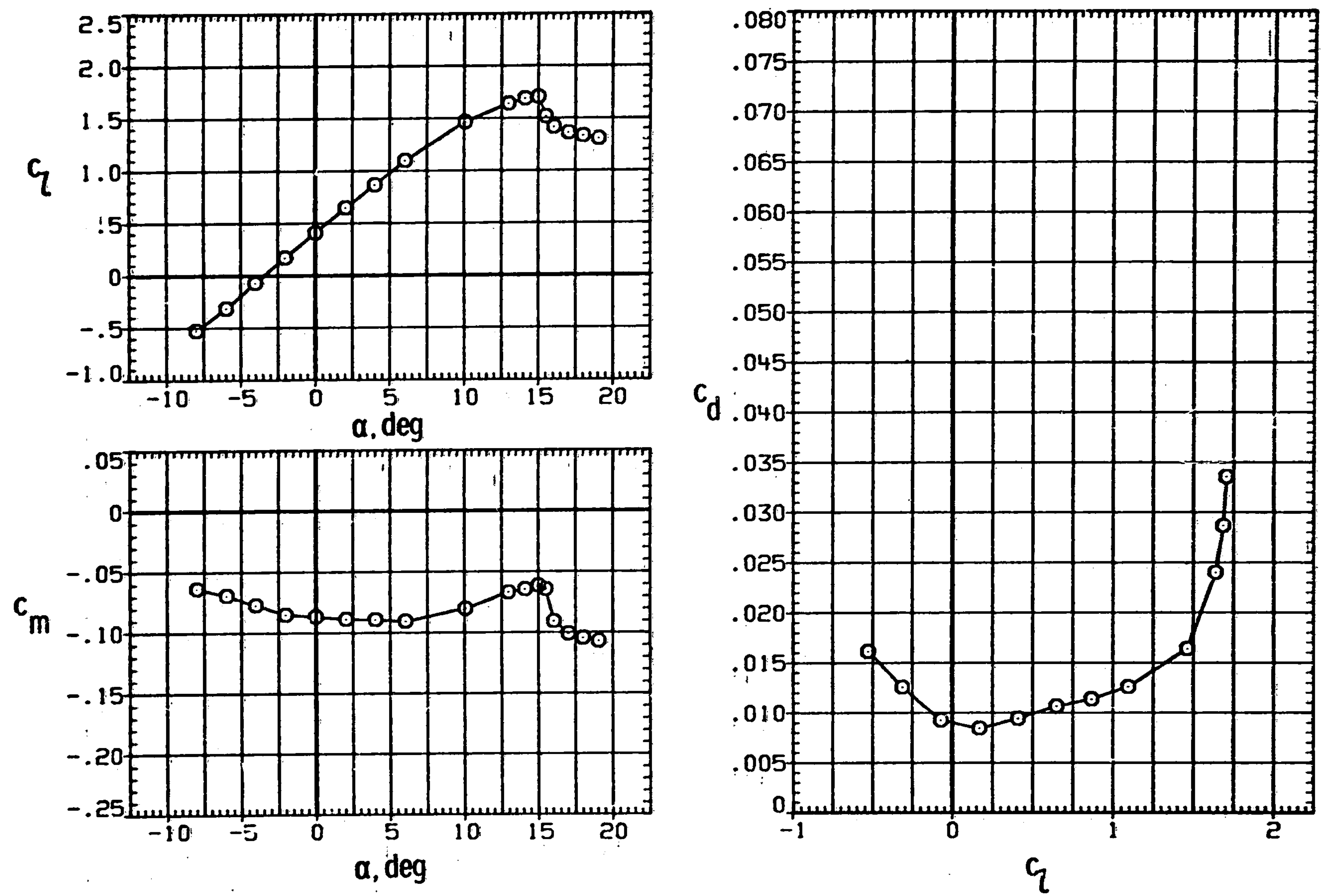

(a) $M = 0.07$; $R = 1.0 \times 10^6$.

Figure 7.- Section characteristics for LS(1)-0417 Mod airfoil. Model smooth.

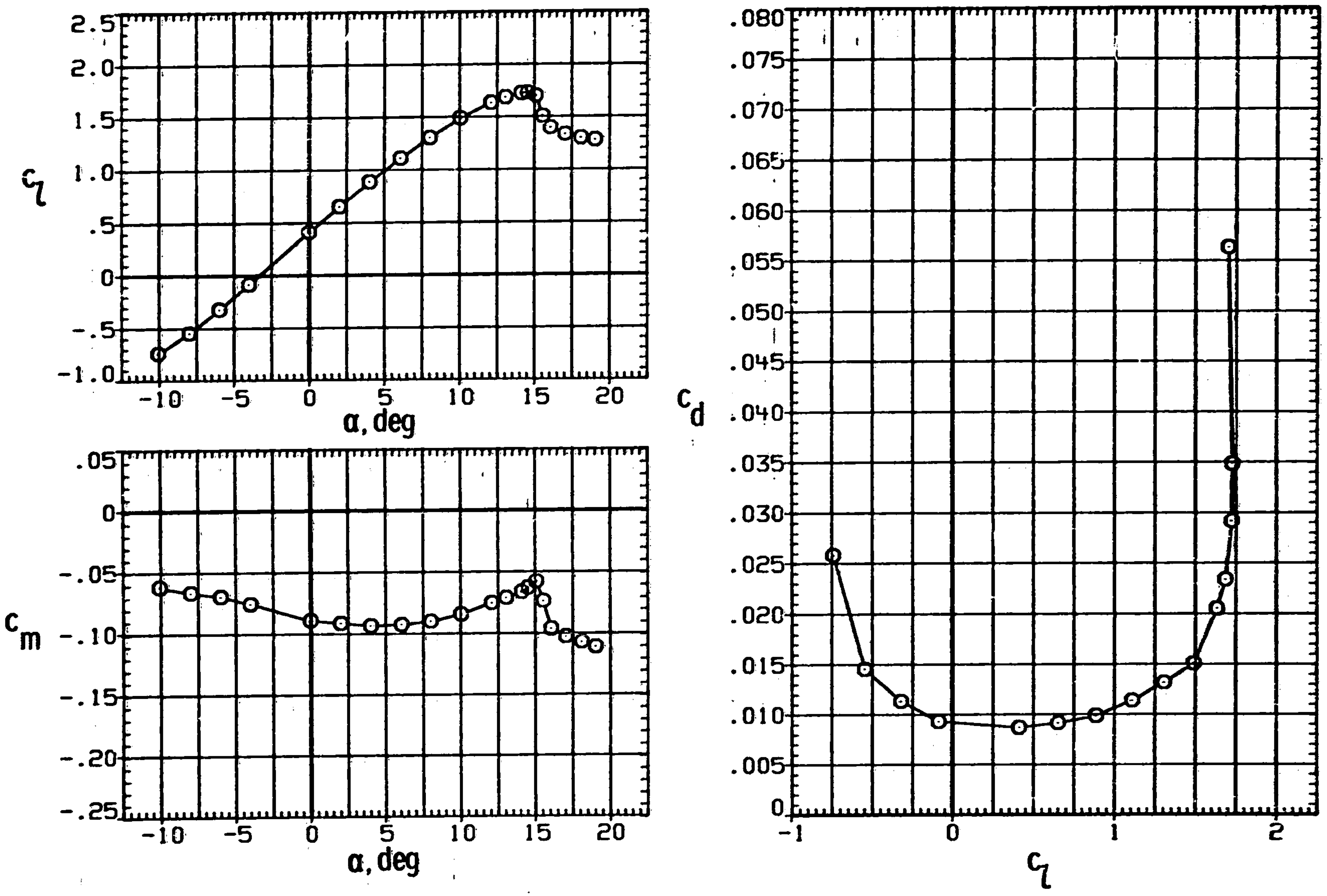

(b) $M = 0.10$; $R = 1.5 \times 10^6$.

Figure 7.- Continued.

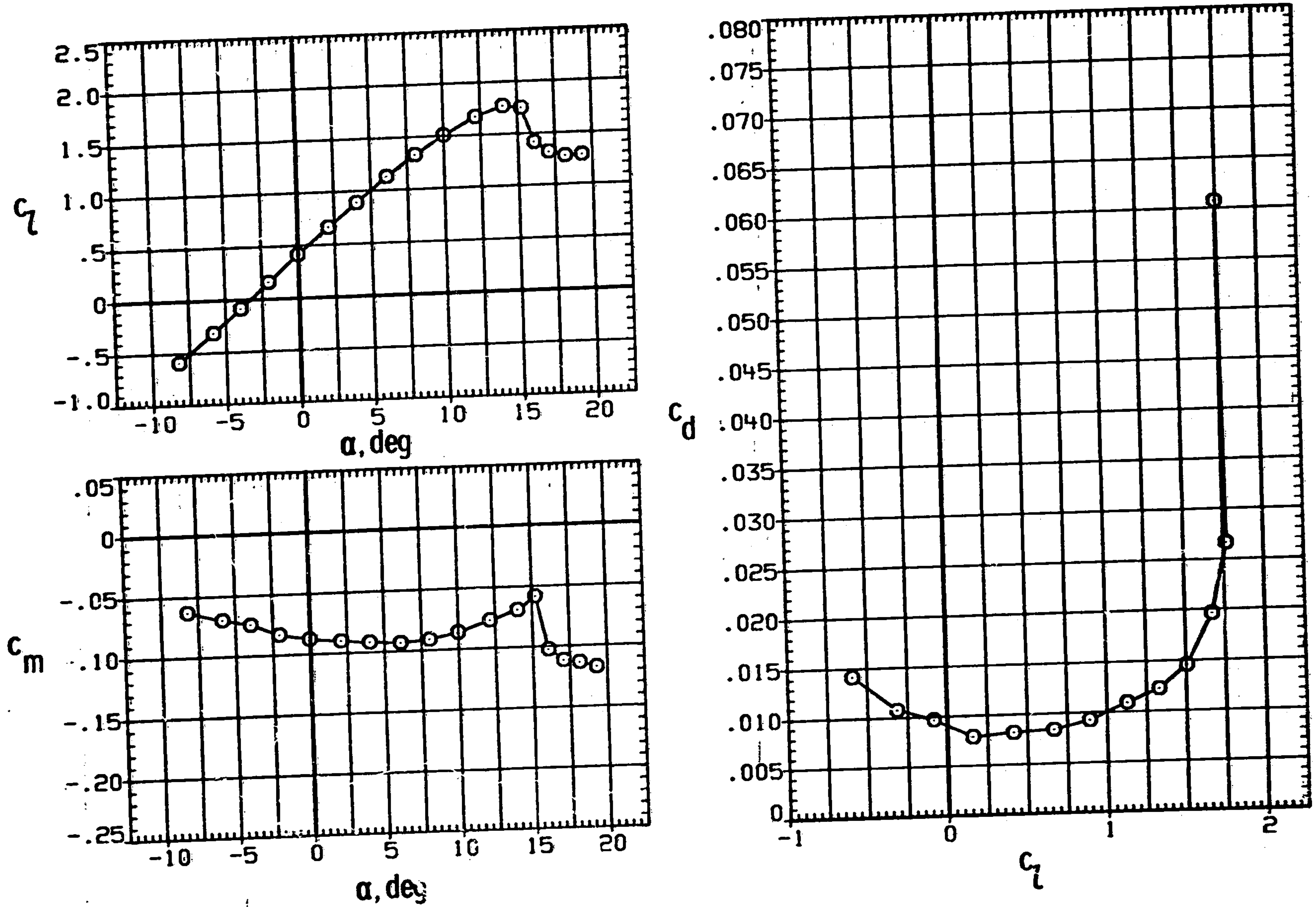

(c) M = 0.15; R = 2.0 × 10^6.

Figure 7.- Continued.

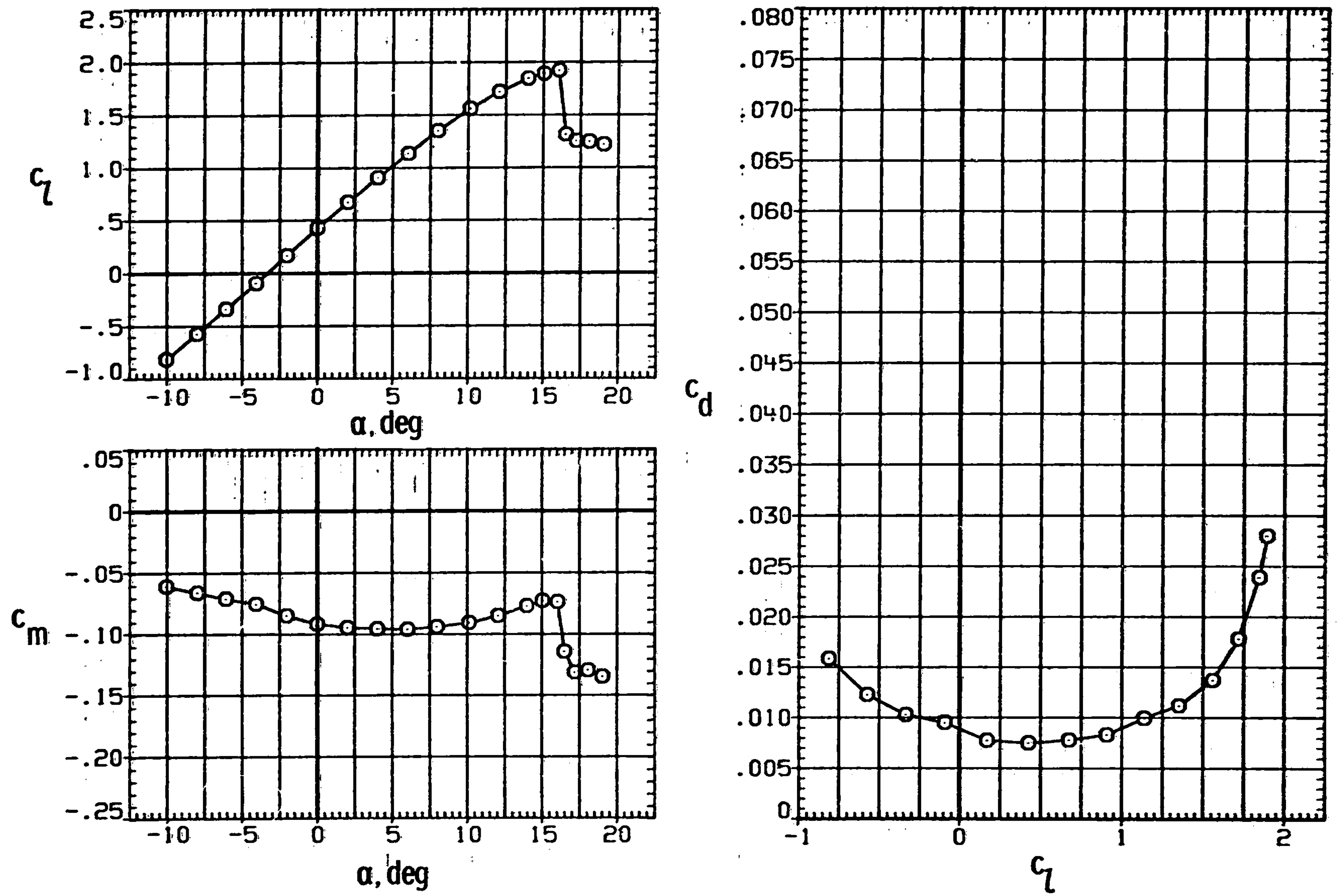

(d) M = 0.15; R = 3.0×10^6.

Figure 7.- Continued.

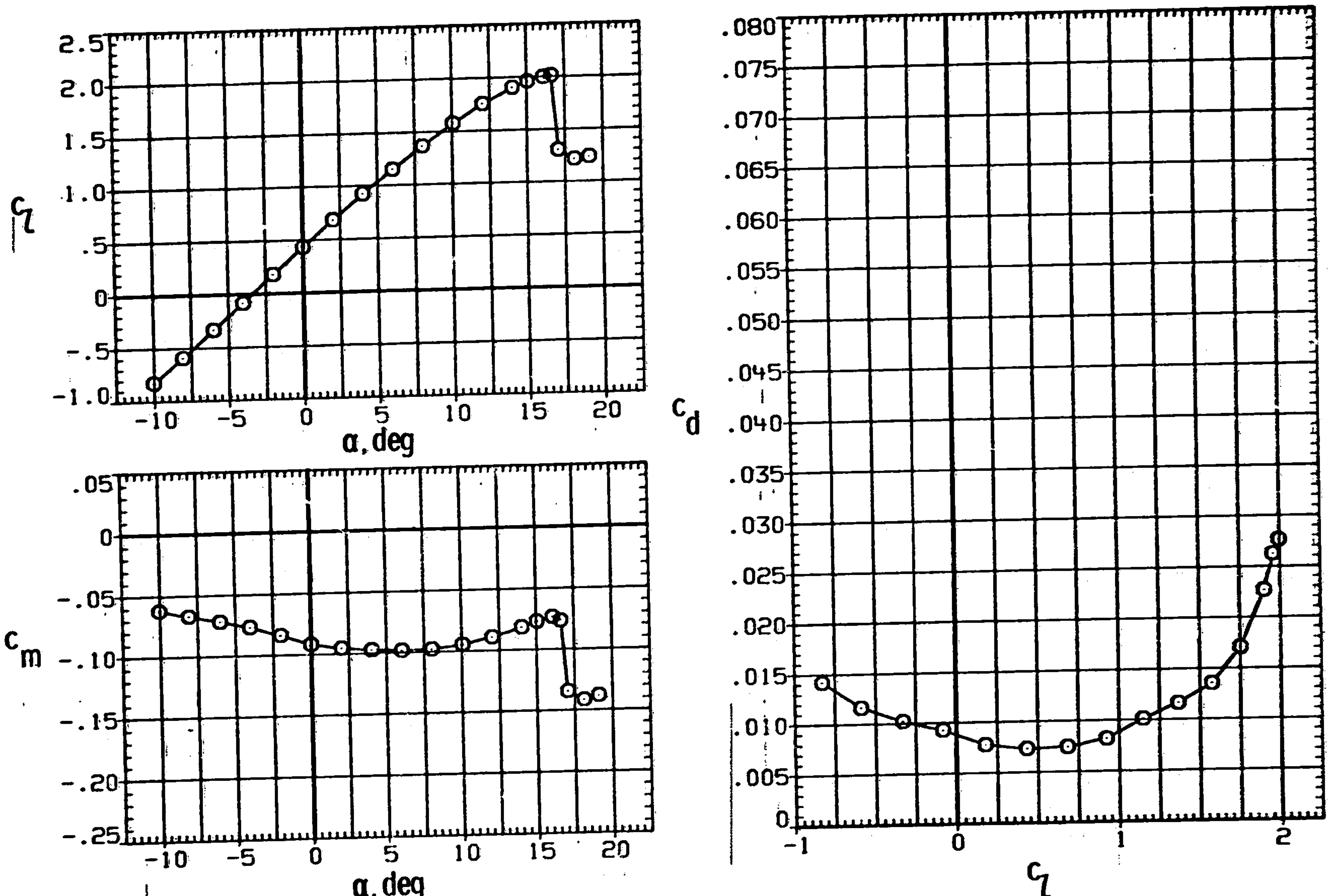

(e) $M = 0.15$; $R = 4.0 \times 10^6$.

Figure 7.- Continued.

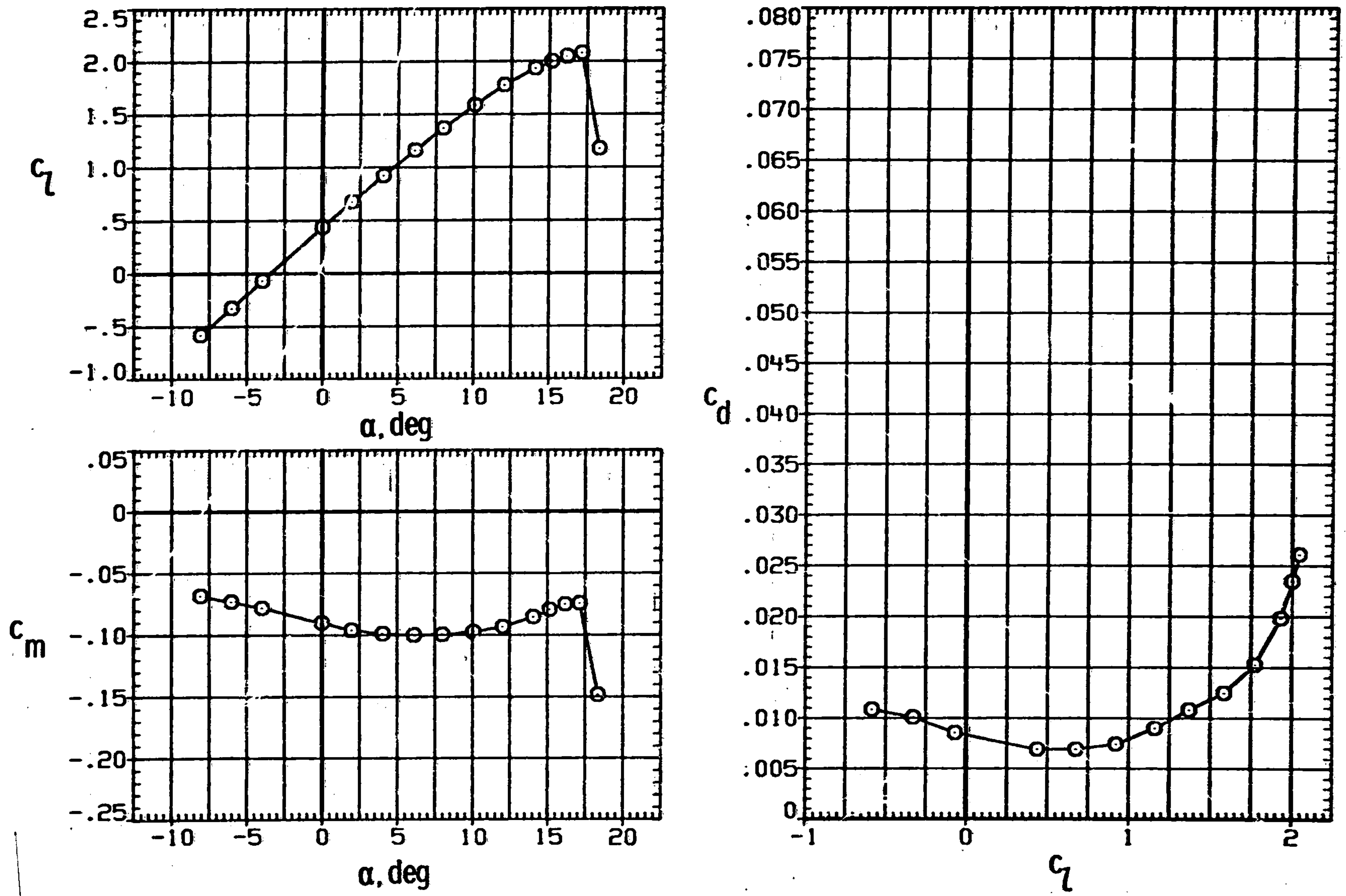

(f) $M = 0.15$; $R = 6.0 \times 10^6$.

Figure 7.- Continued.

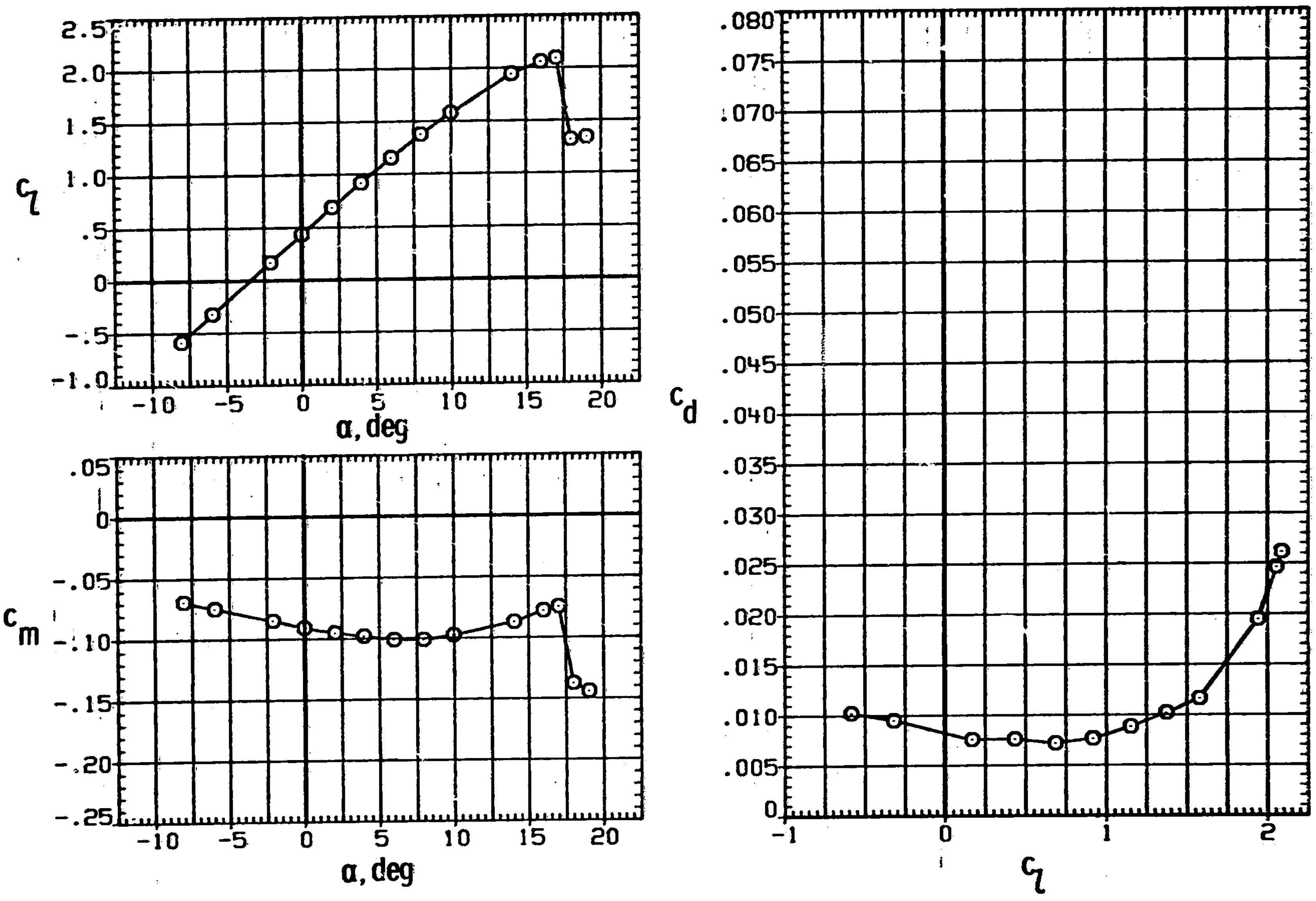

(g) $M = 0.15$; $R = 9.0 \times 10^6$.

Figure 7.- Continued.

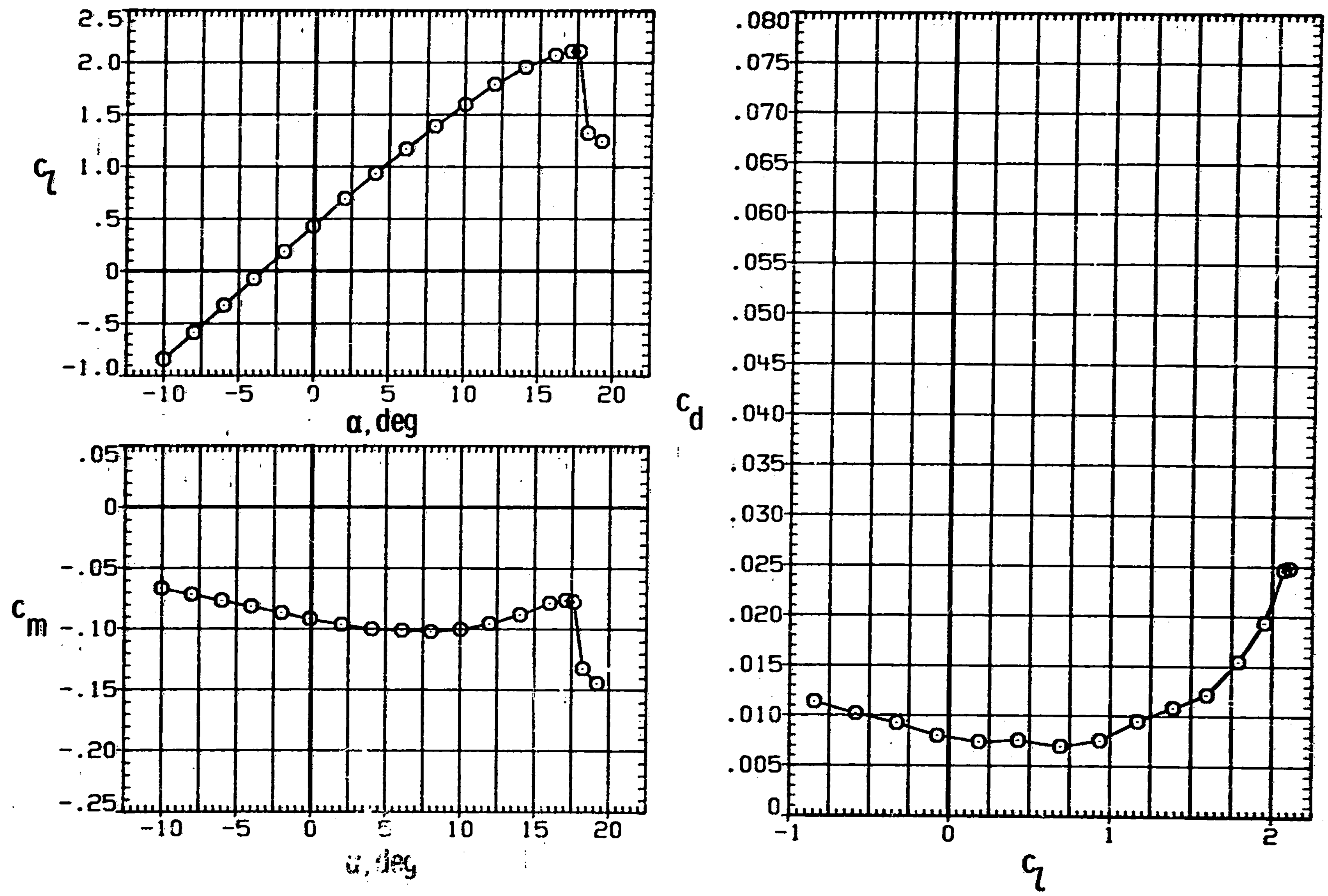

(h) M = 0.15; R = 12.0 × 10^6.

Figure 7.- Concluded.

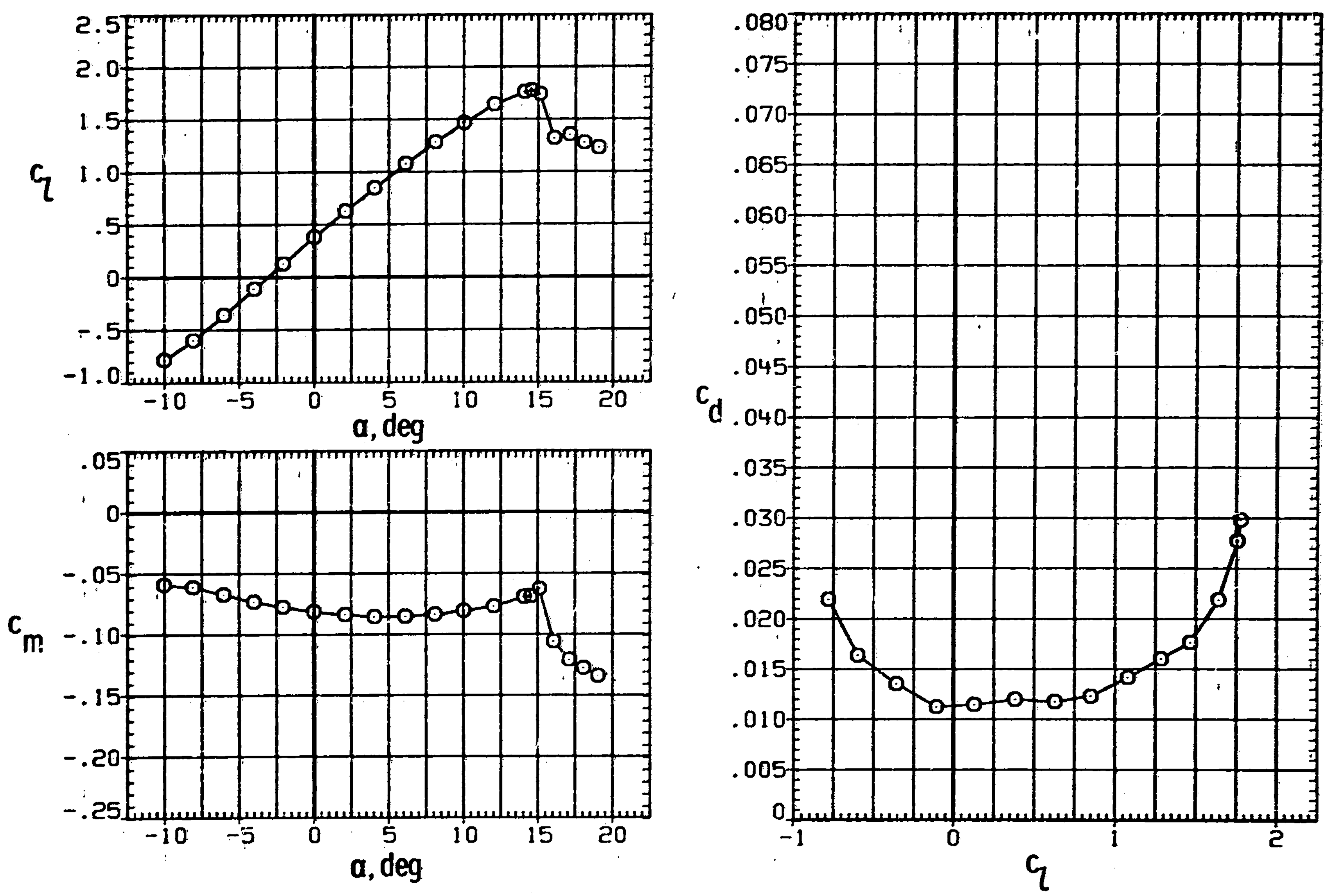

(a) $M = 0.15$; $R = 2.0 \times 10^6$.

Figure 8.- Section characteristics for LS(1)-0417 Mod airfoil. Roughness located at 0.075c.

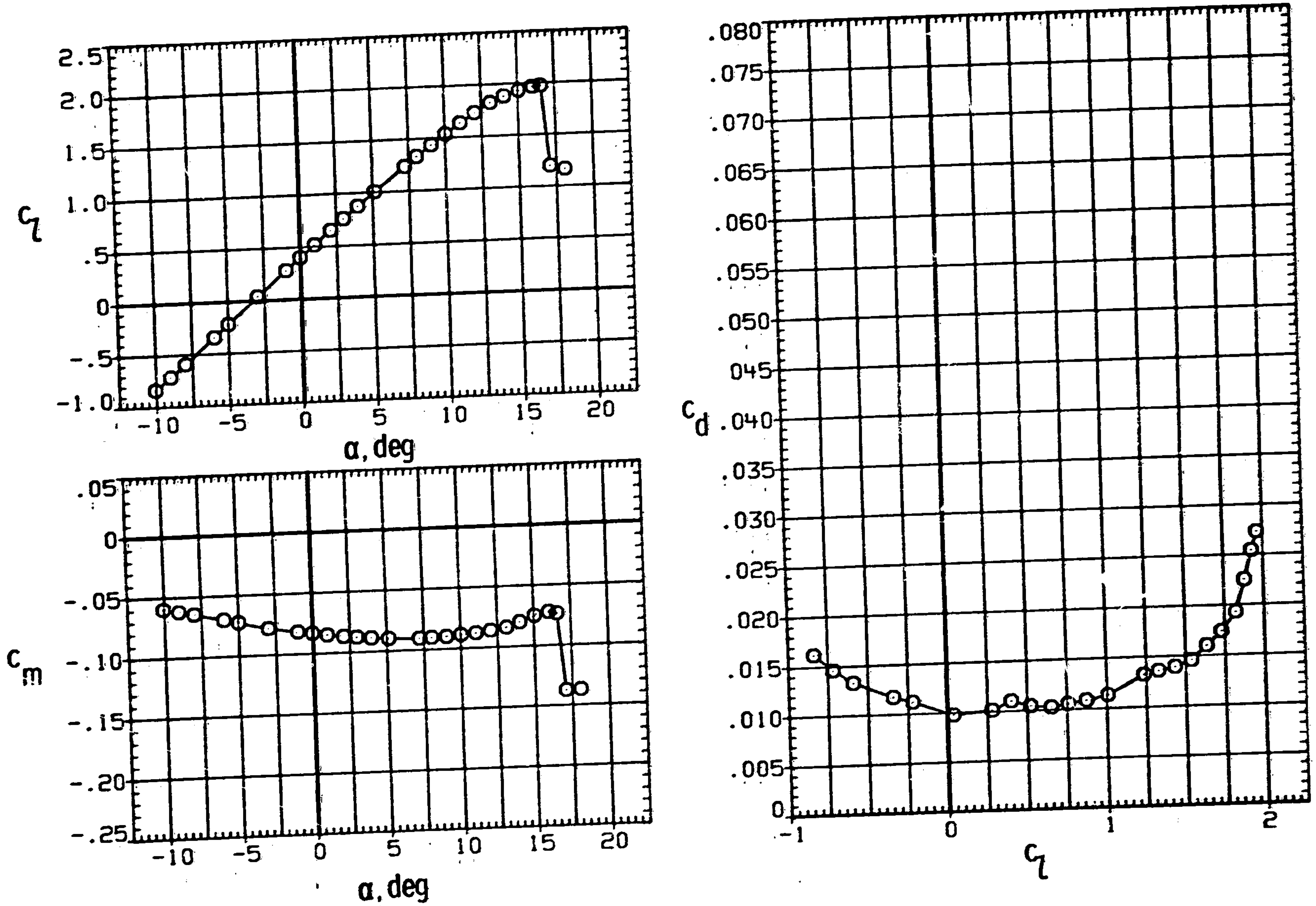

(b) $M = 0.15$; $R = 4.0 \times 10^6$.

Figure 8.- Continued.

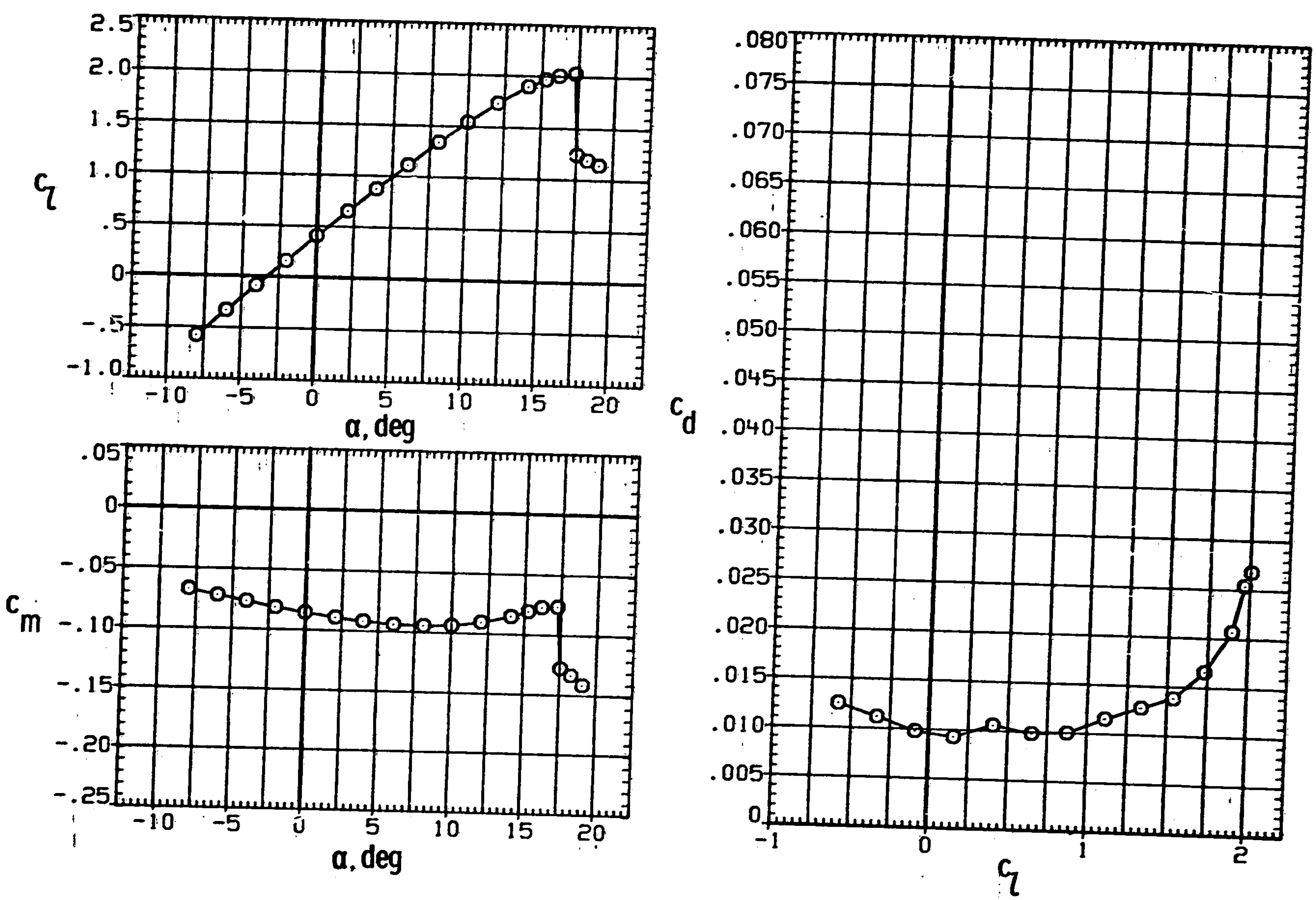

(c) $M = 0.10$; $R = 6.0 \times 10^6$.

Figure 8.- Continued.

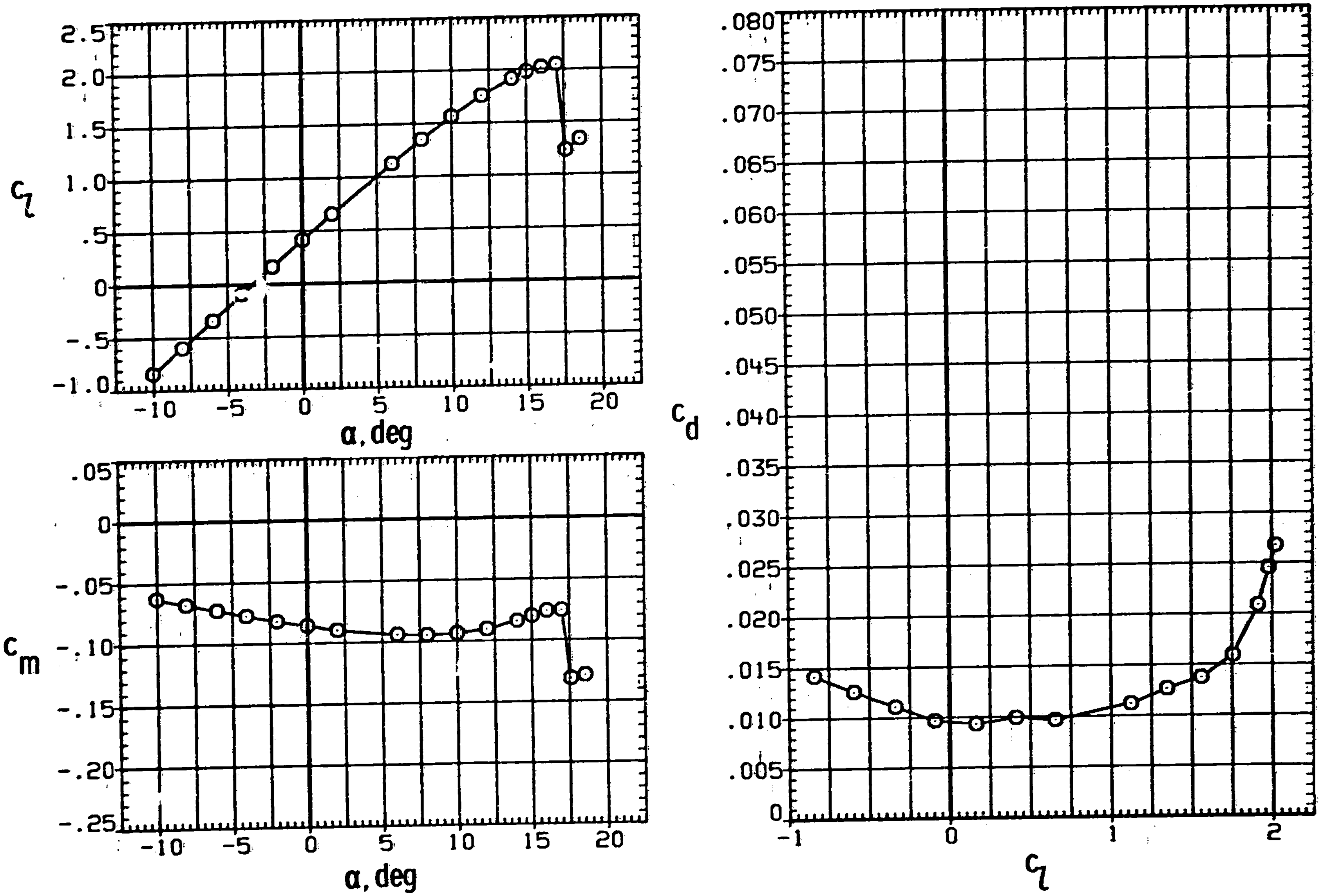

(d) $M = 0.15$; $R = 6.0 \times 10^6$.

Figure 8.- Continued.

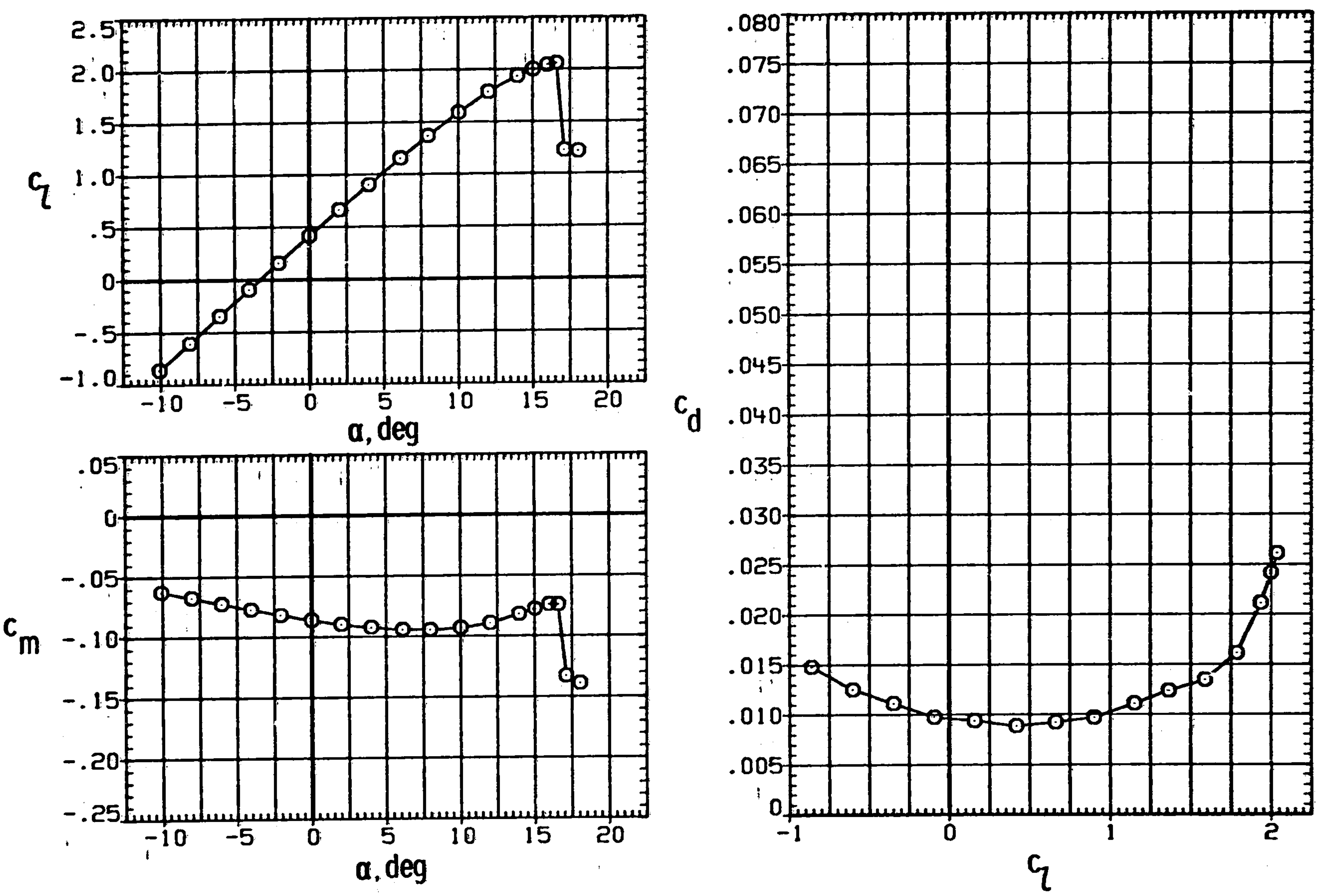

(e) $M = 0.20$; $R = 6.0 \times 10^6$.

Figure 8.- Continued.

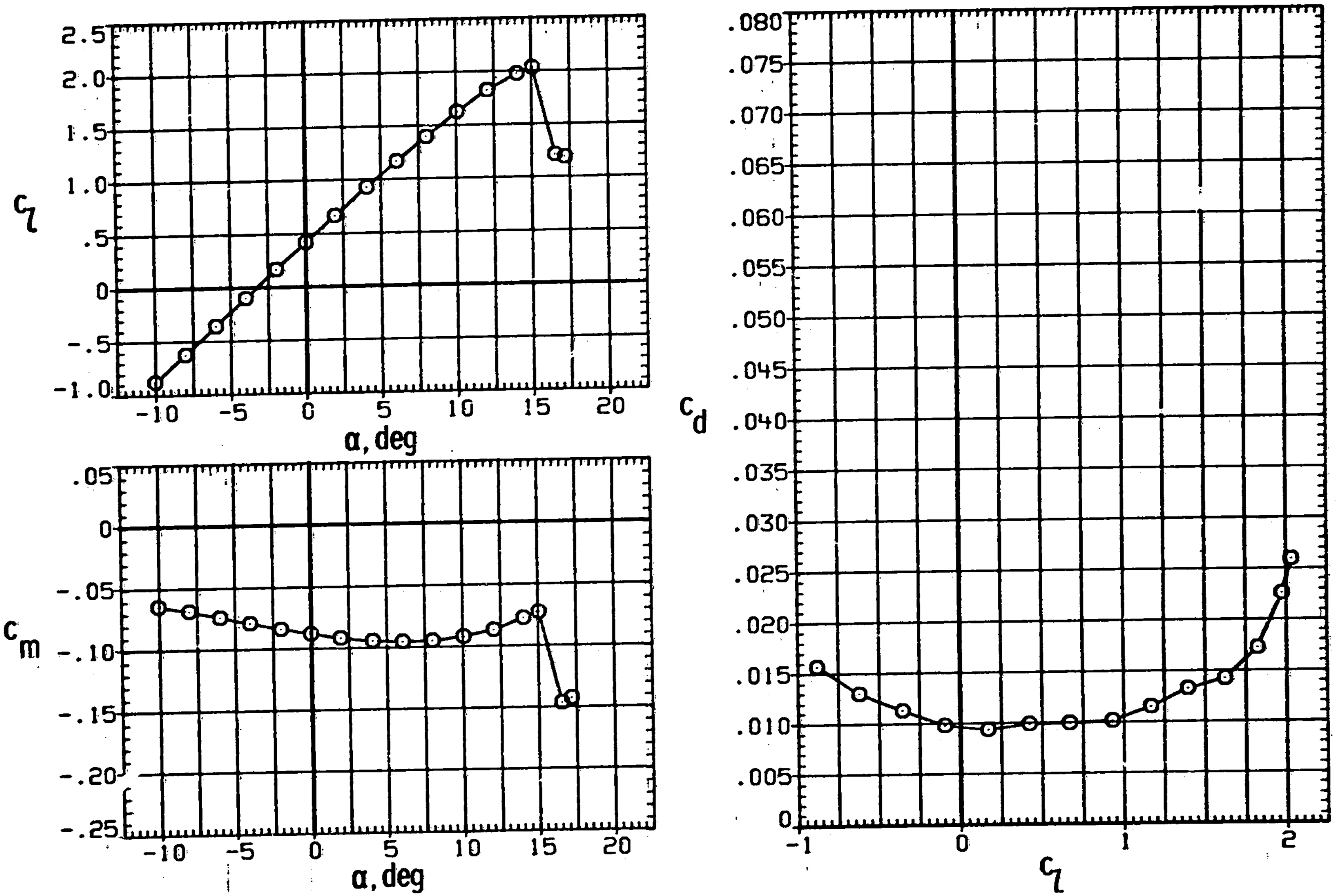

(f) $M = 0.28$; $R = 6.0 \times 10^6$.

Figure 8.- Continued.

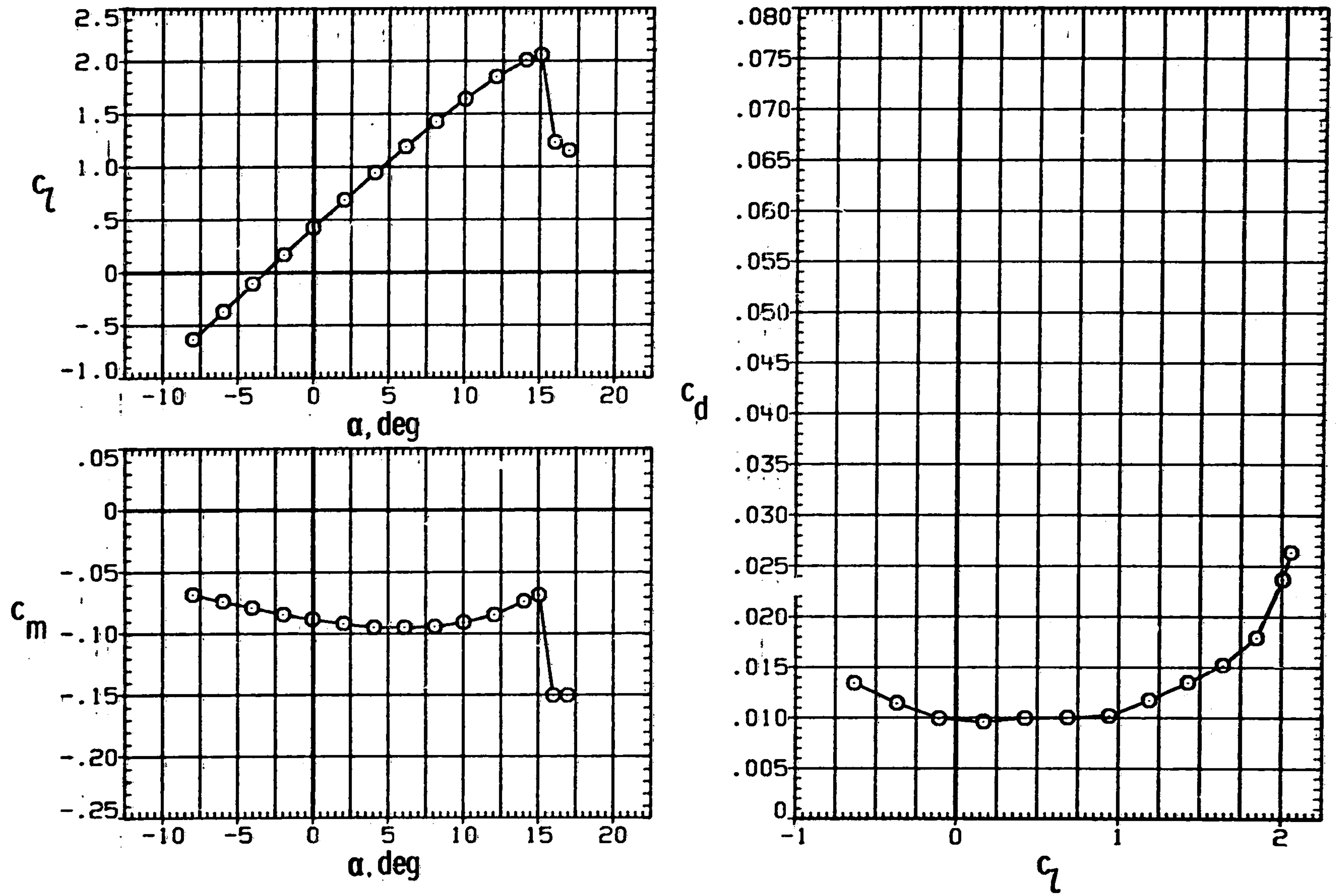

(g) $M = 0.32$; $R = 6.0 \times 10^6$.

Figure 8.- Continued.

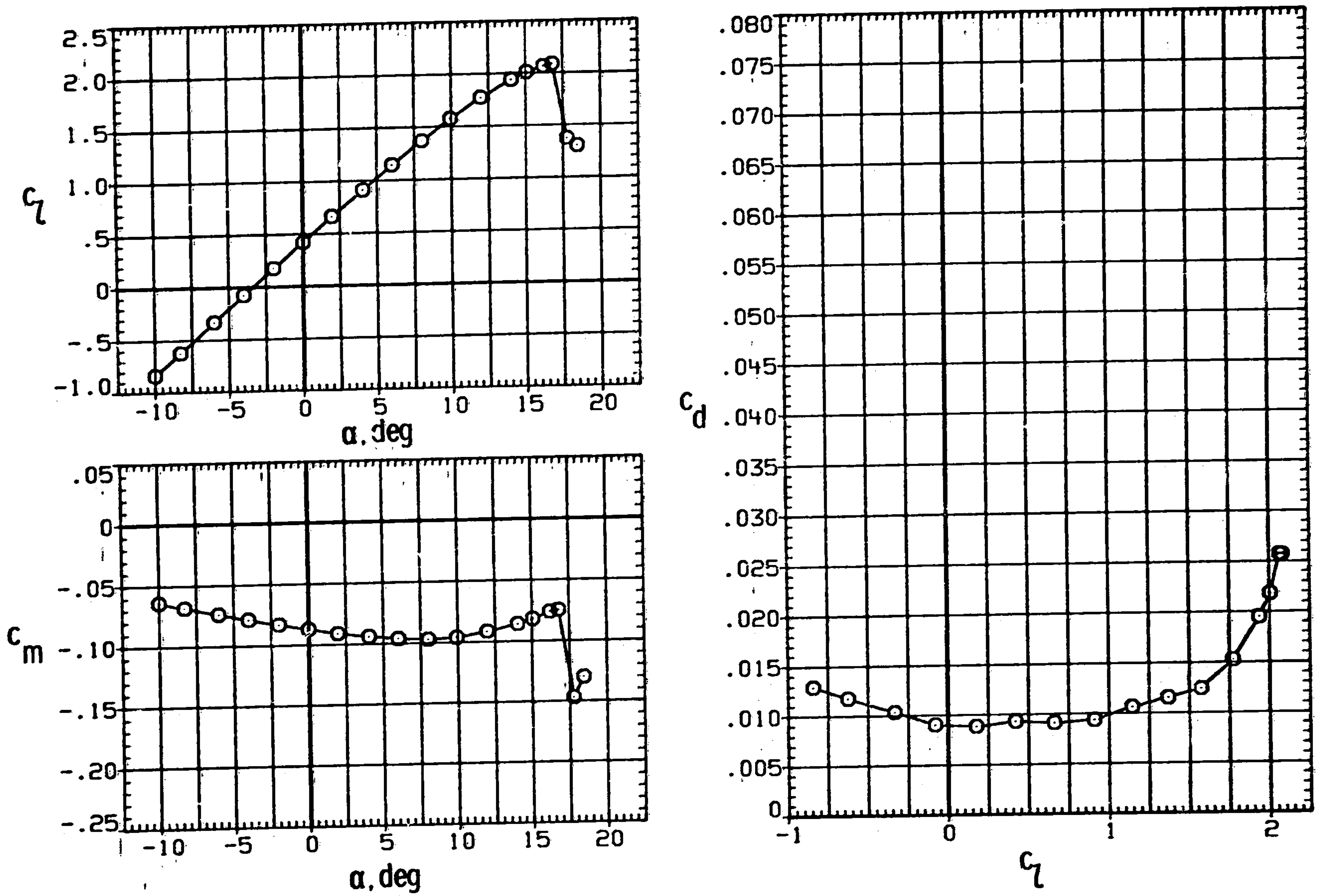

(h) $M = 0.15$; $R = 9.0 \times 10^6$.

Figure 8.- Continued.

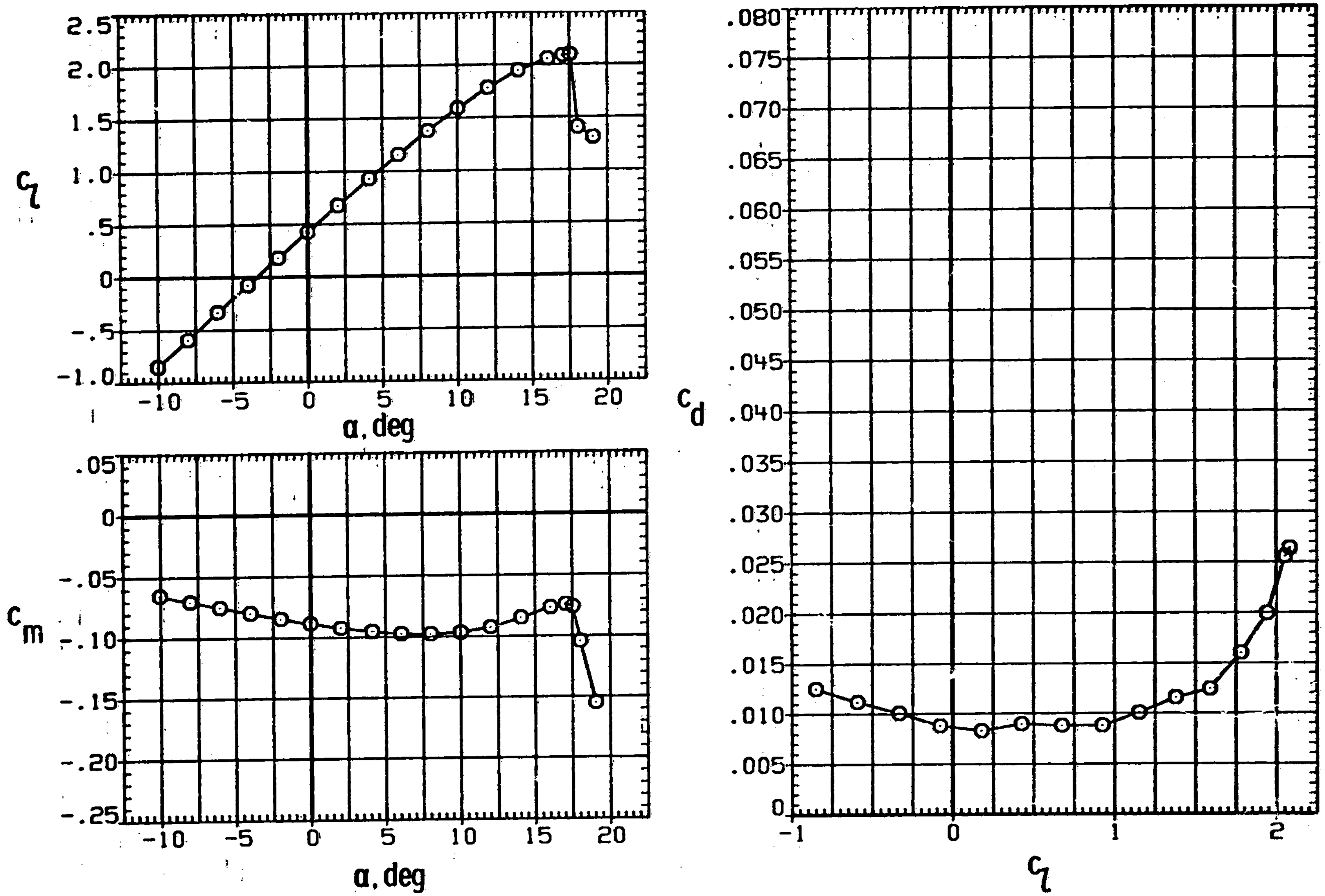

(i) $M = 0.15$; $R = 12.0 \times 10^6$.

Figure 8.- Concluded.

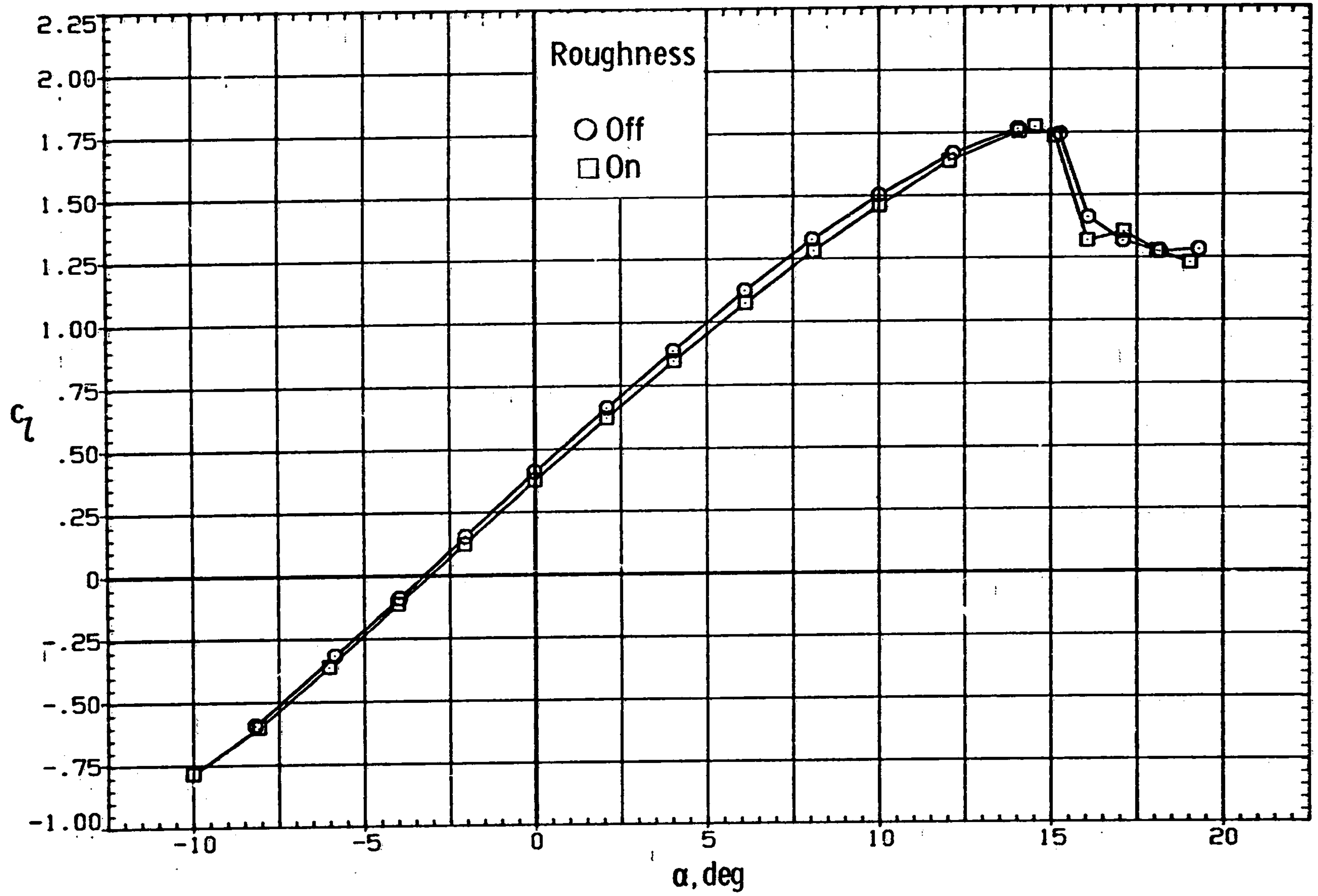

(a) $R = 2.0 \times 10^6$.

Figure 9.- Effect of roughness on section characteristics. M = 0.15.

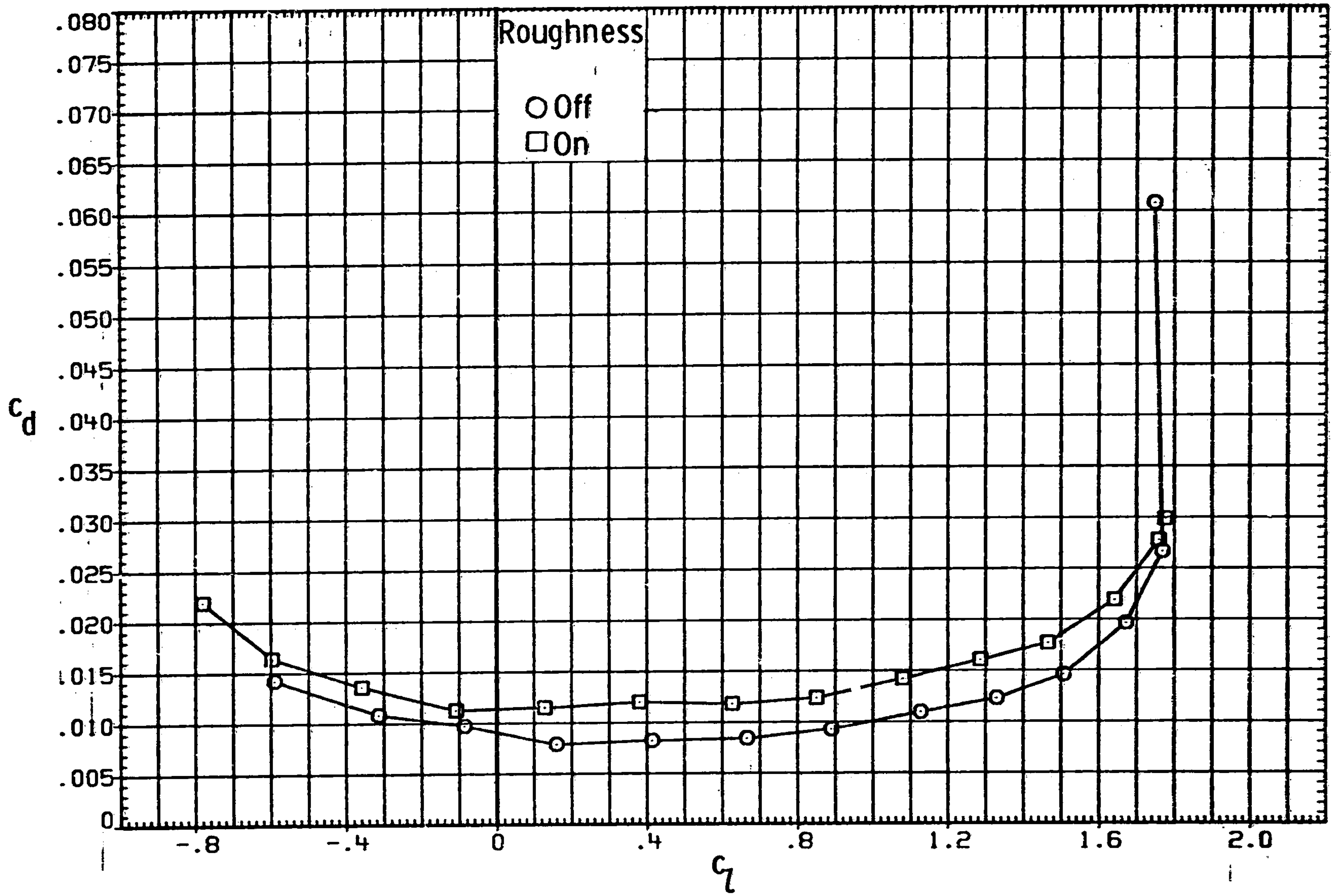

(a) $R = 2.0 \times 10^6$. Continued.

Figure 9.- Continued.

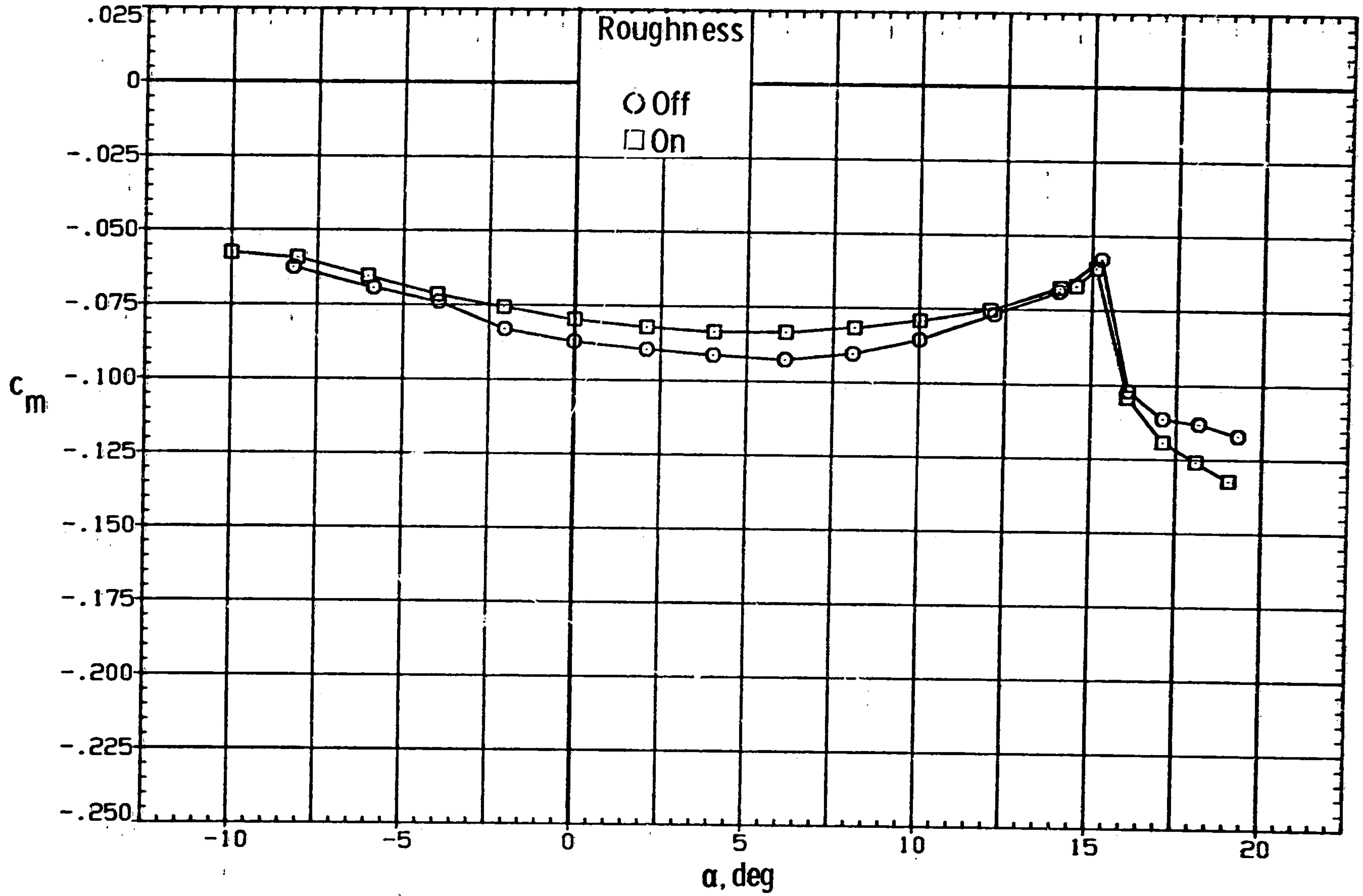

(a) $R = 2.0 \times 10^6$. Concluded.

Figure 9.- Continued.

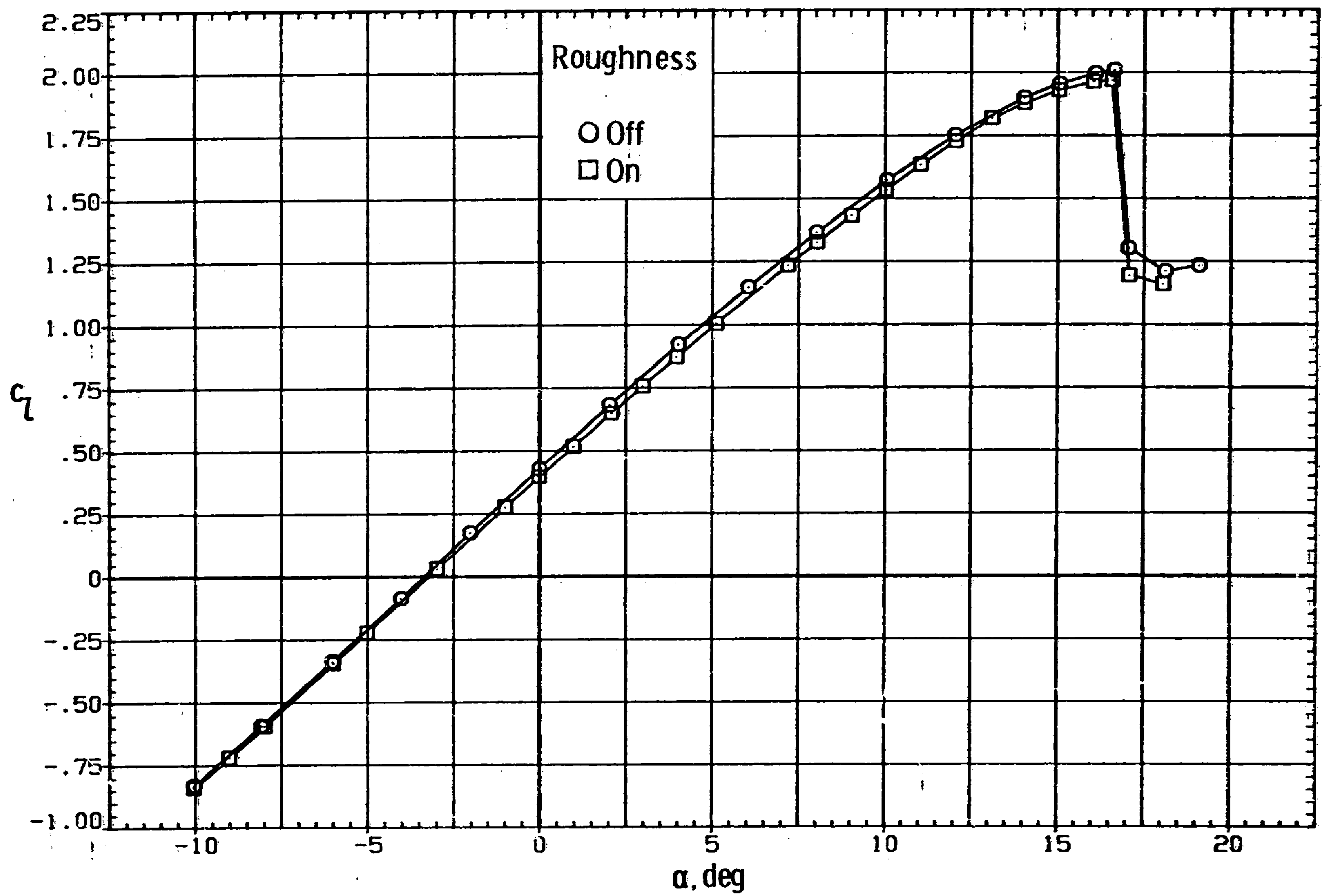

(b) $R = 4.0 \times 10^6$.

Figure 9.- Continued.

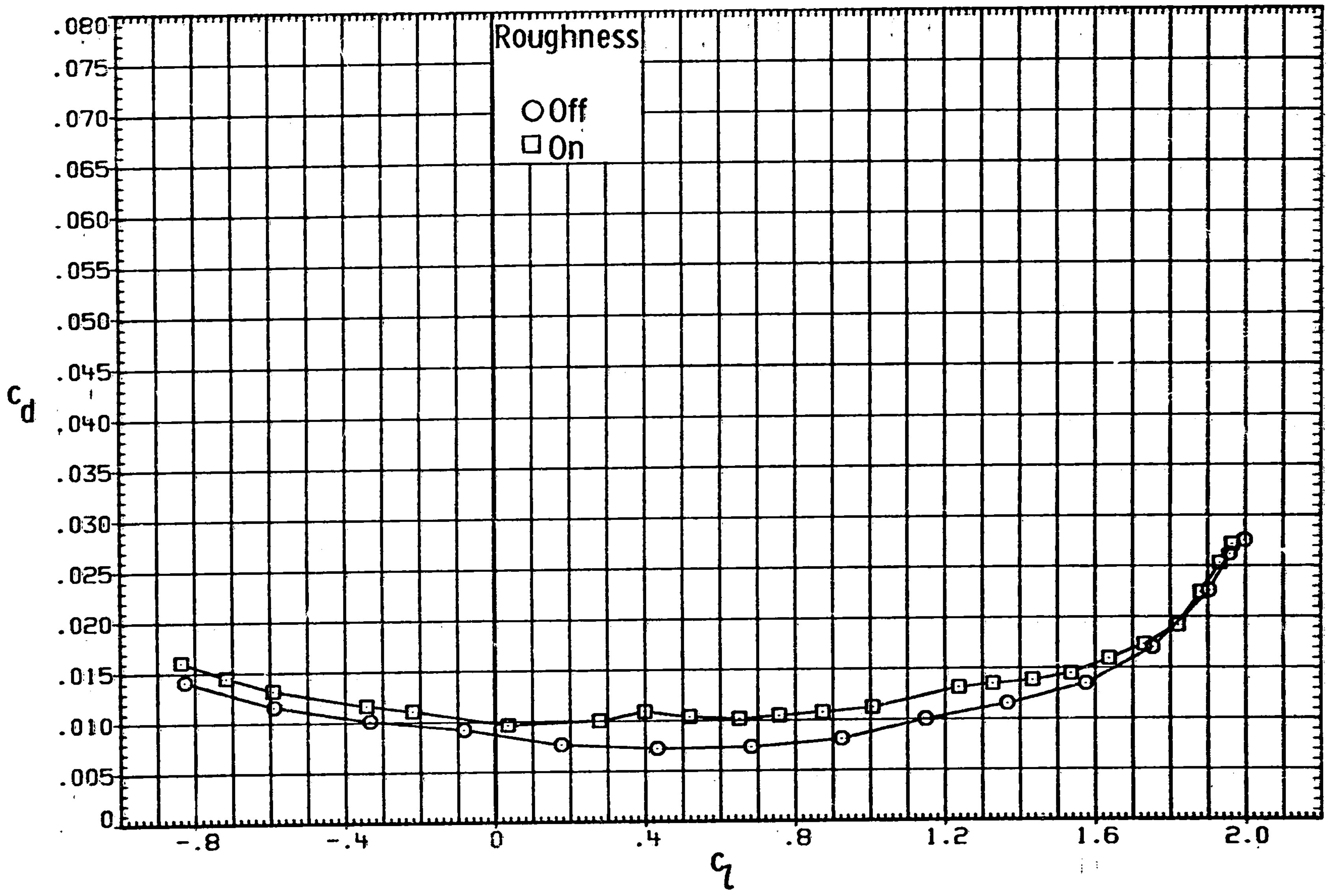

(b) $R = 4.0 \times 10^6$. Continued.

Figure 9.- Continued.

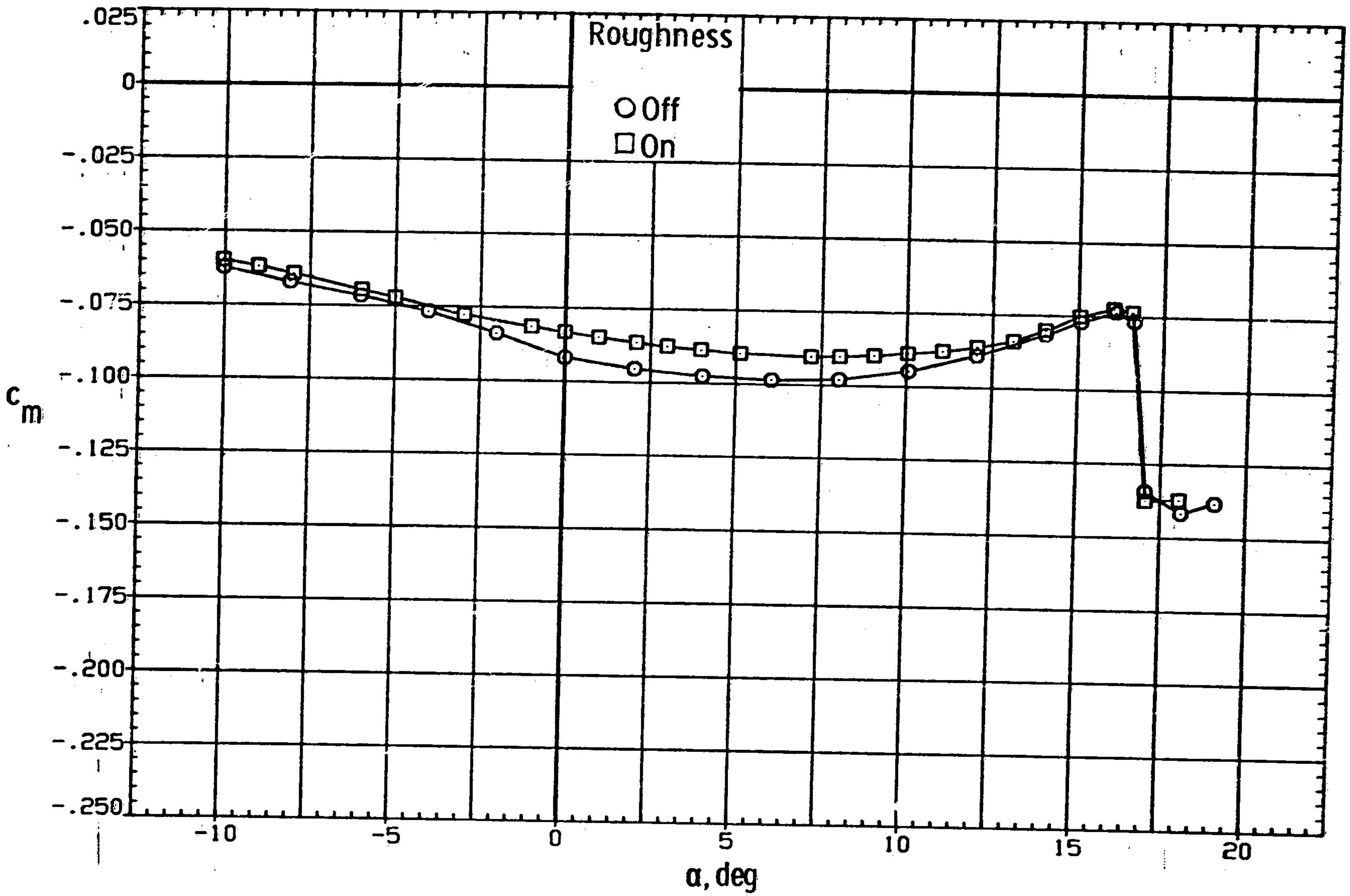

(b) $R = 4.0 \times 10^6$. Concluded.

Figure 9.- Continued.

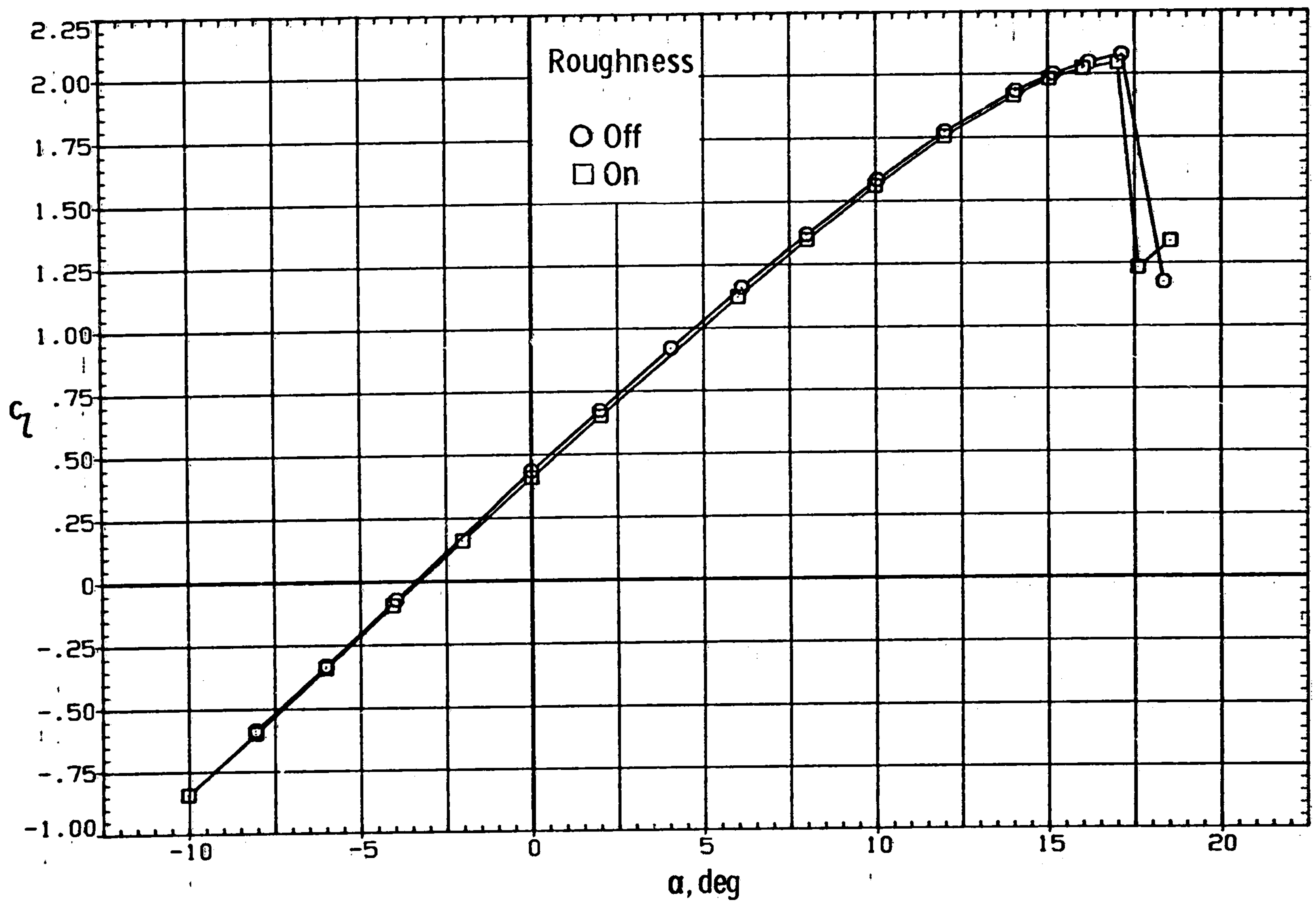

(c) $R = 6.0 \times 10^6$.

Figure 9.- Continued.

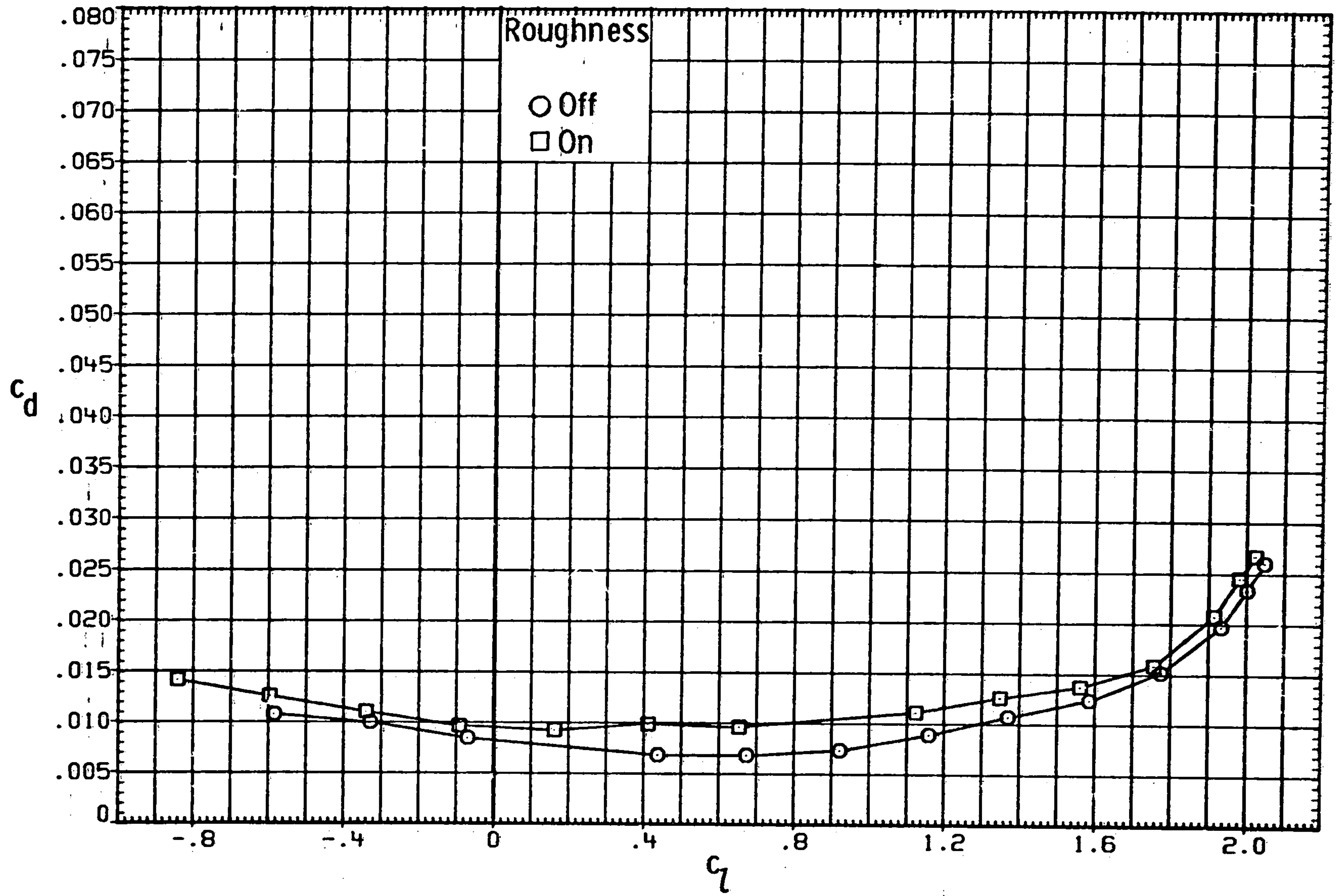

(c) $R = 6.0 \times 10^6$. Continued.

Figure 9.- Continued.

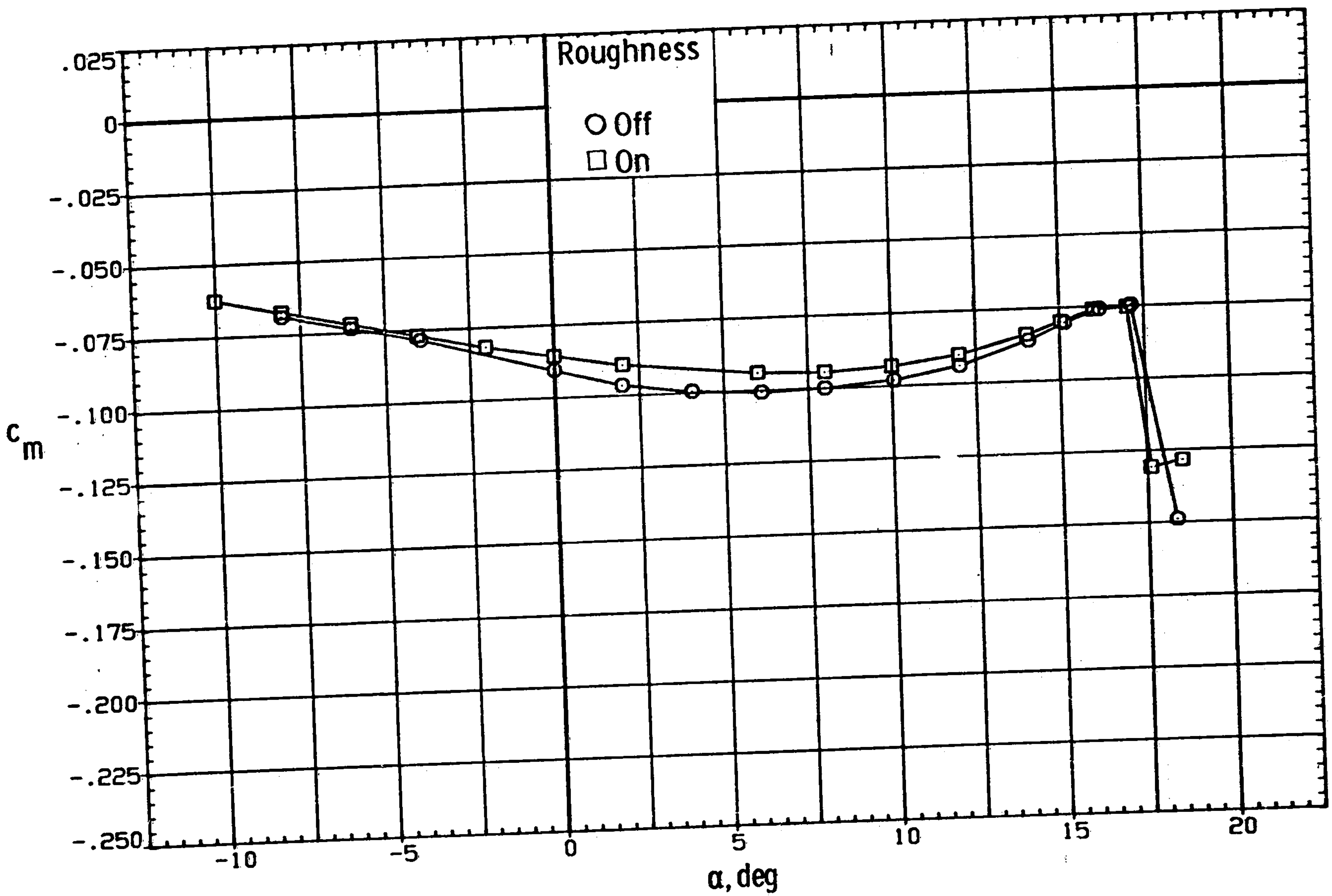

(c) $R = 6.0 \times 10^6$. Concluded.

Figure 9.- Continued.

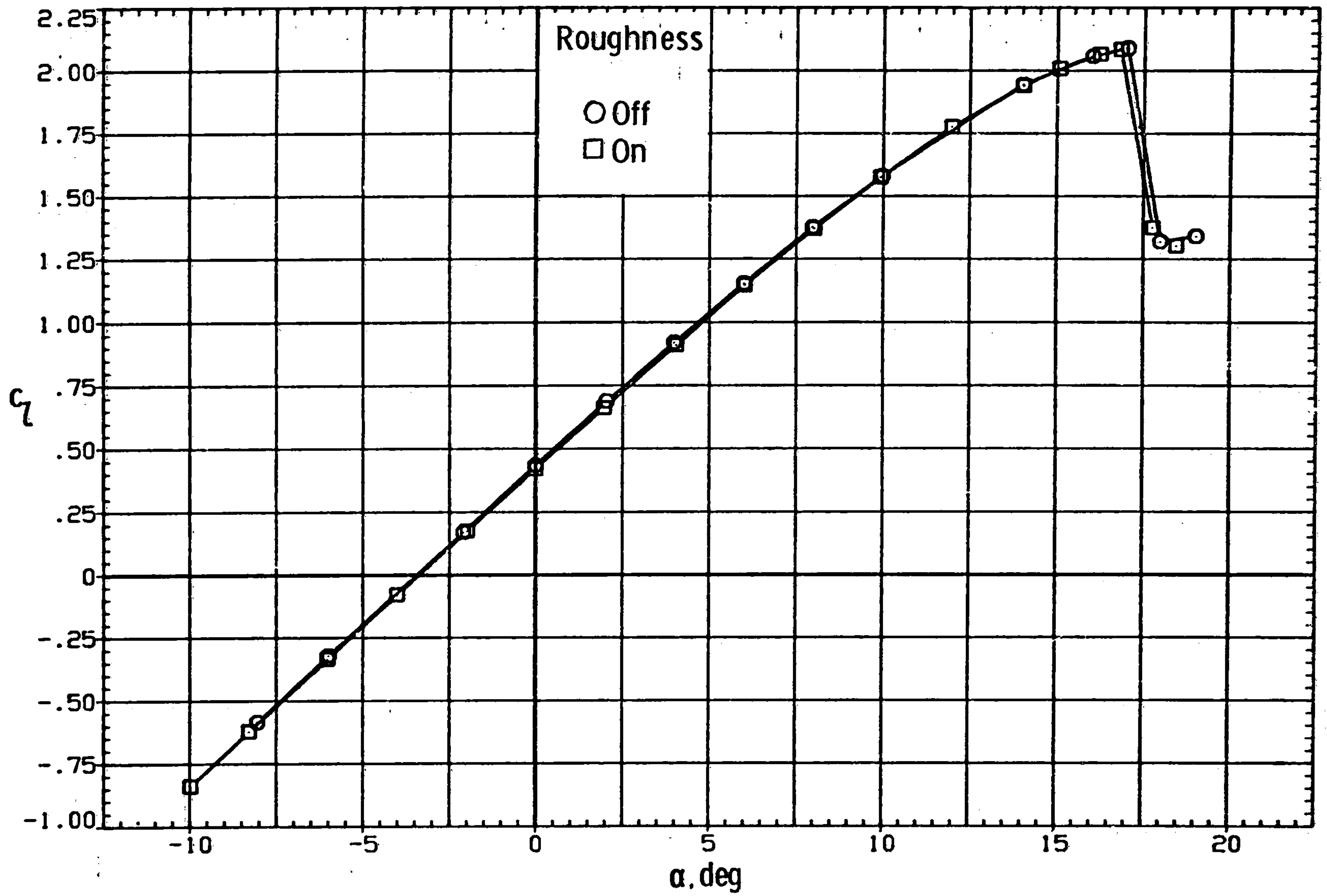

(d) $R = 9.0 \times 10^6$.

Figure 9.- Continued.

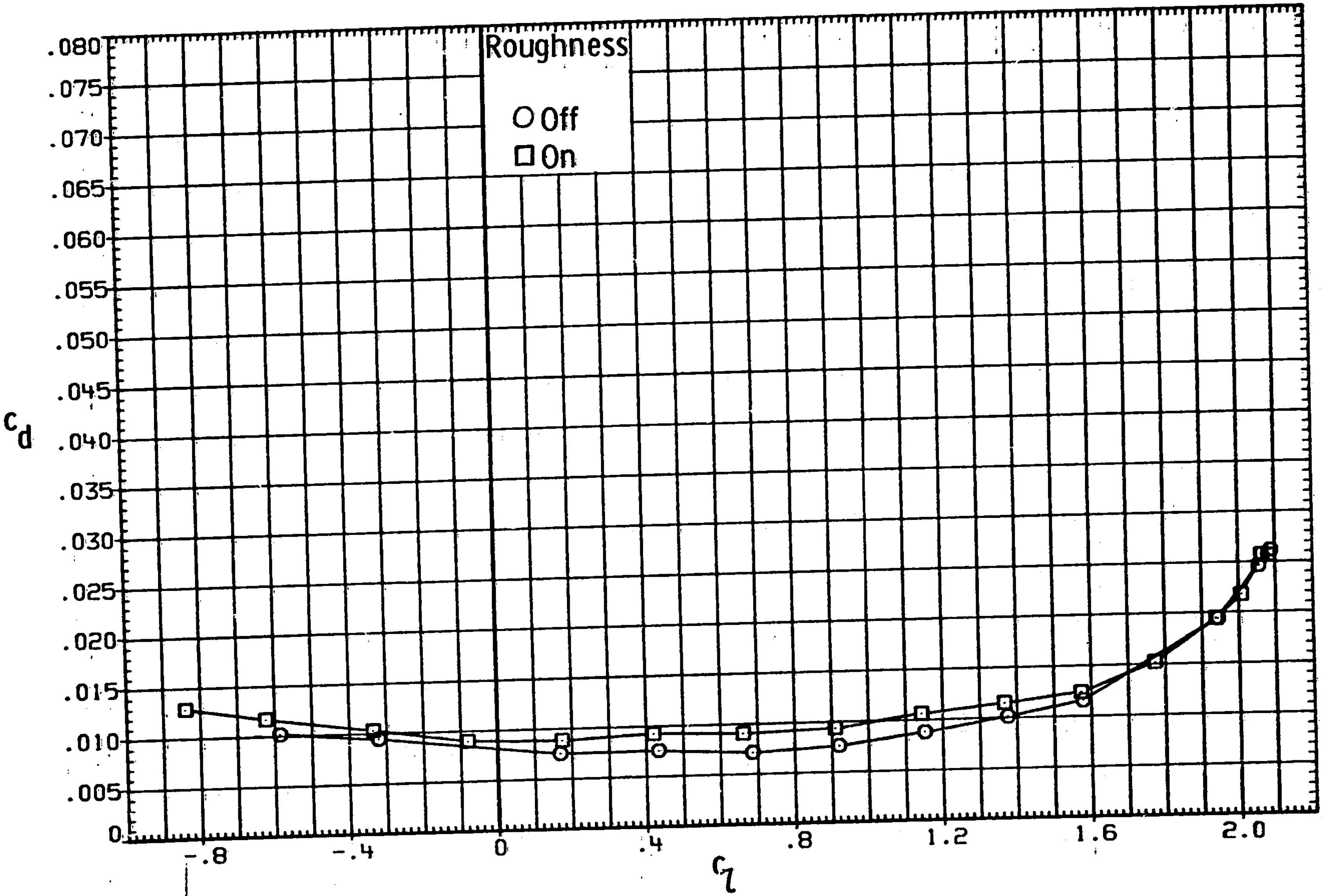

(d) $R = 9.0 \times 10^6$. Continued.

Figure 9.- Continued.

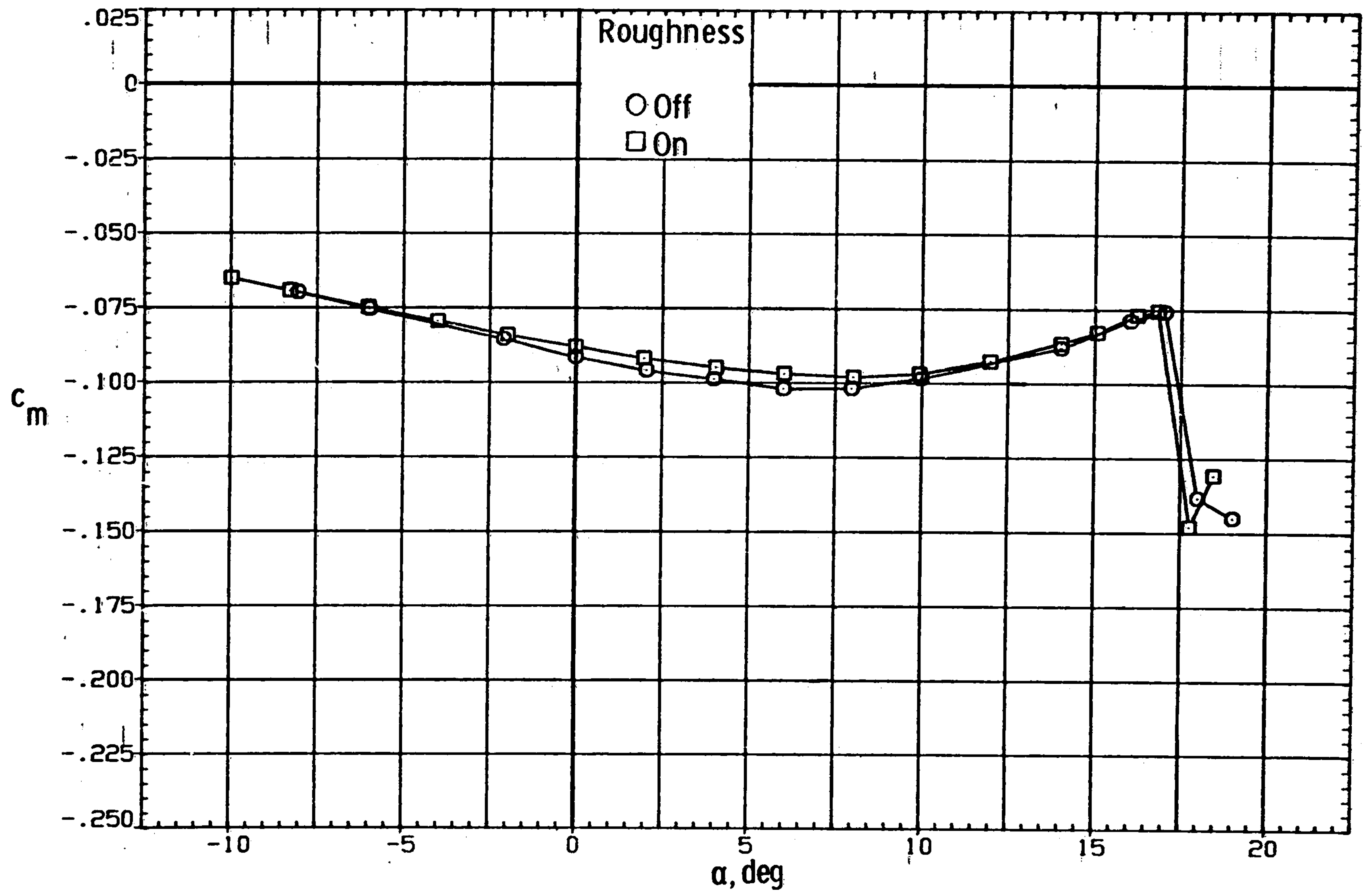

(d) R = 9.0 × 10^6. Concluded.

Figure 9.- Continued.

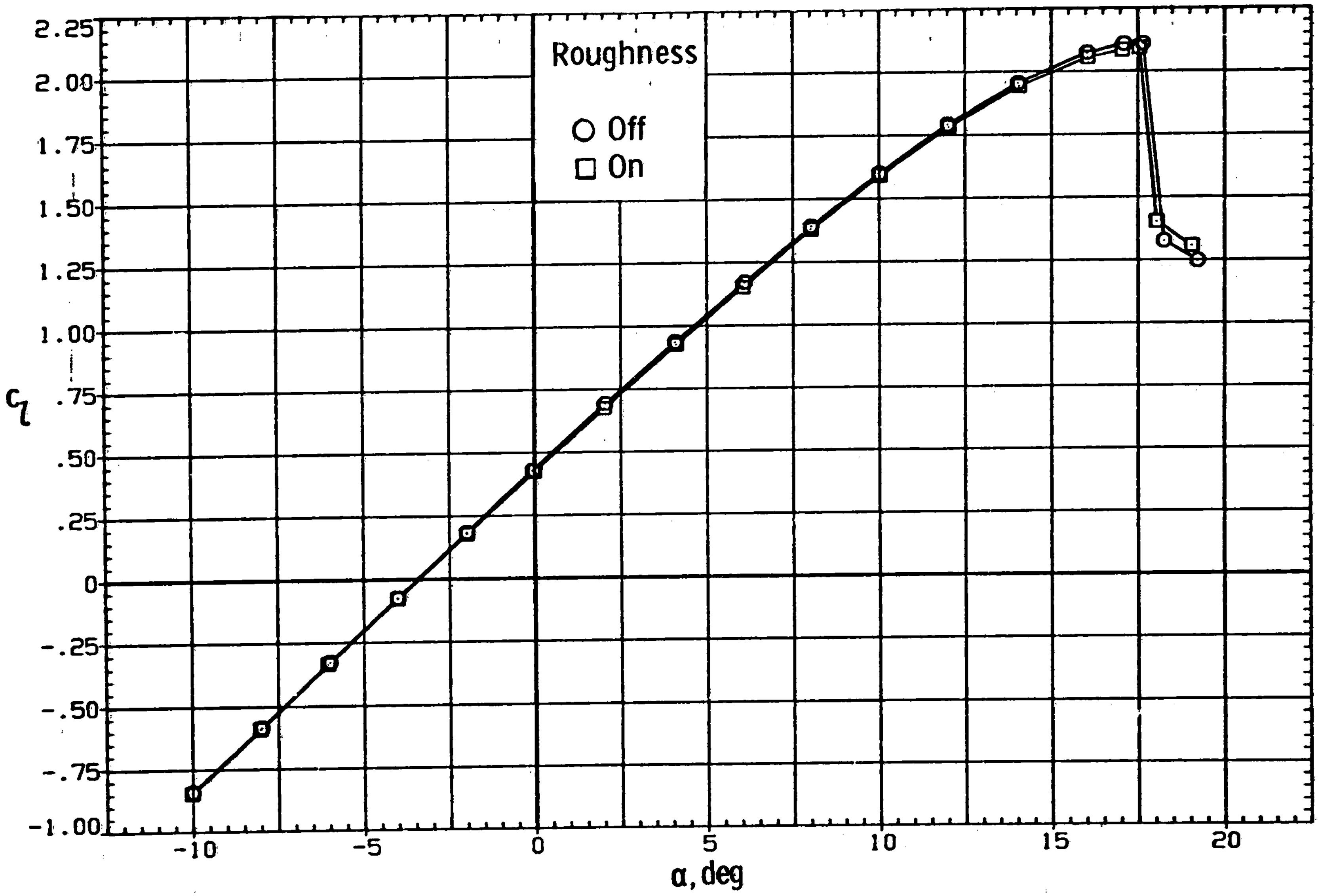

(e) $R = 12.0 \times 10^6$.

Figure 9.- Continued.

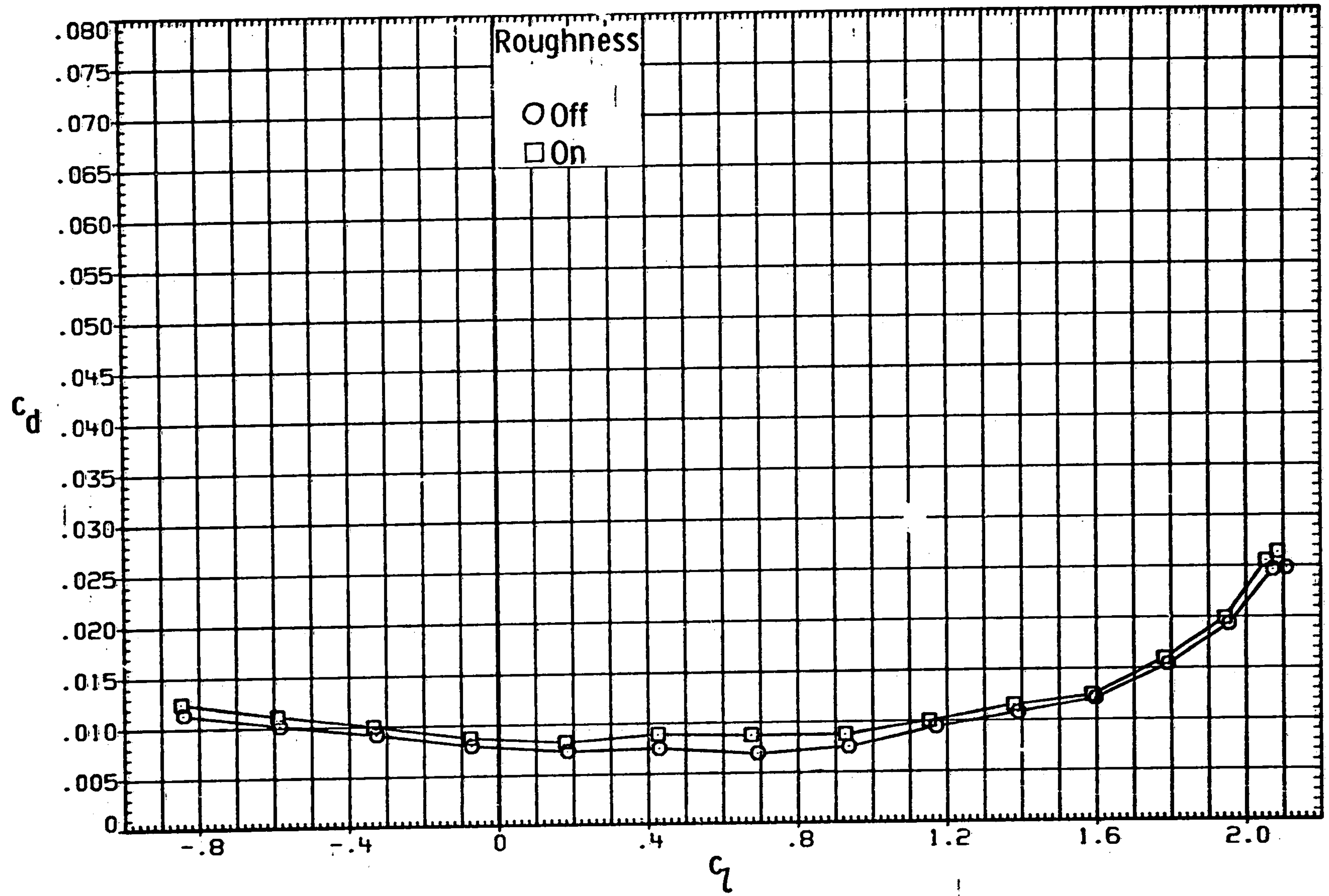

(e) $R = 12.0 \times 10^6$. Continued.

Figure 9.- Continued.

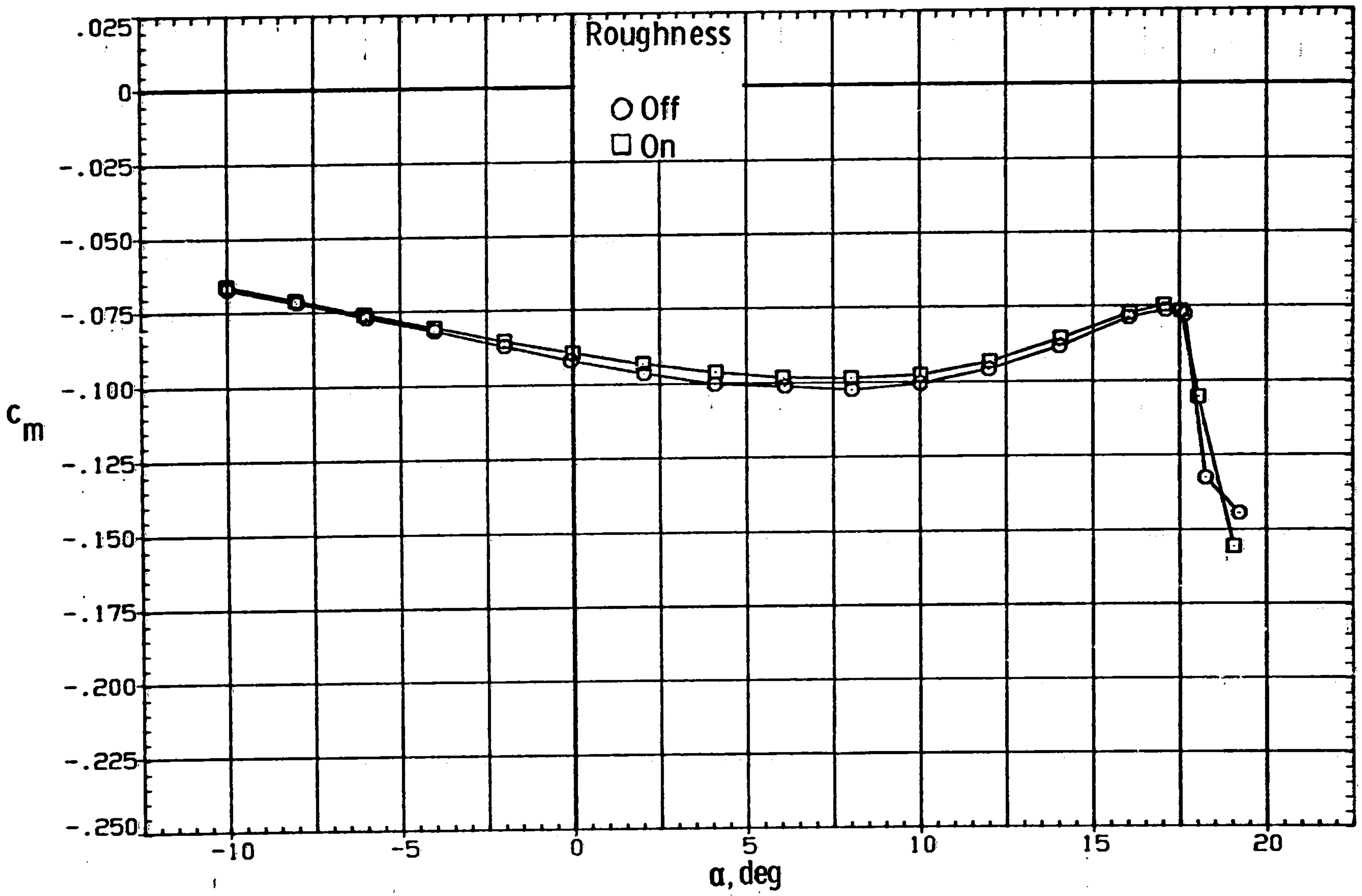

(e) $R = 12.0 \times 10^6$. Concluded.

Figure 9.- Concluded.

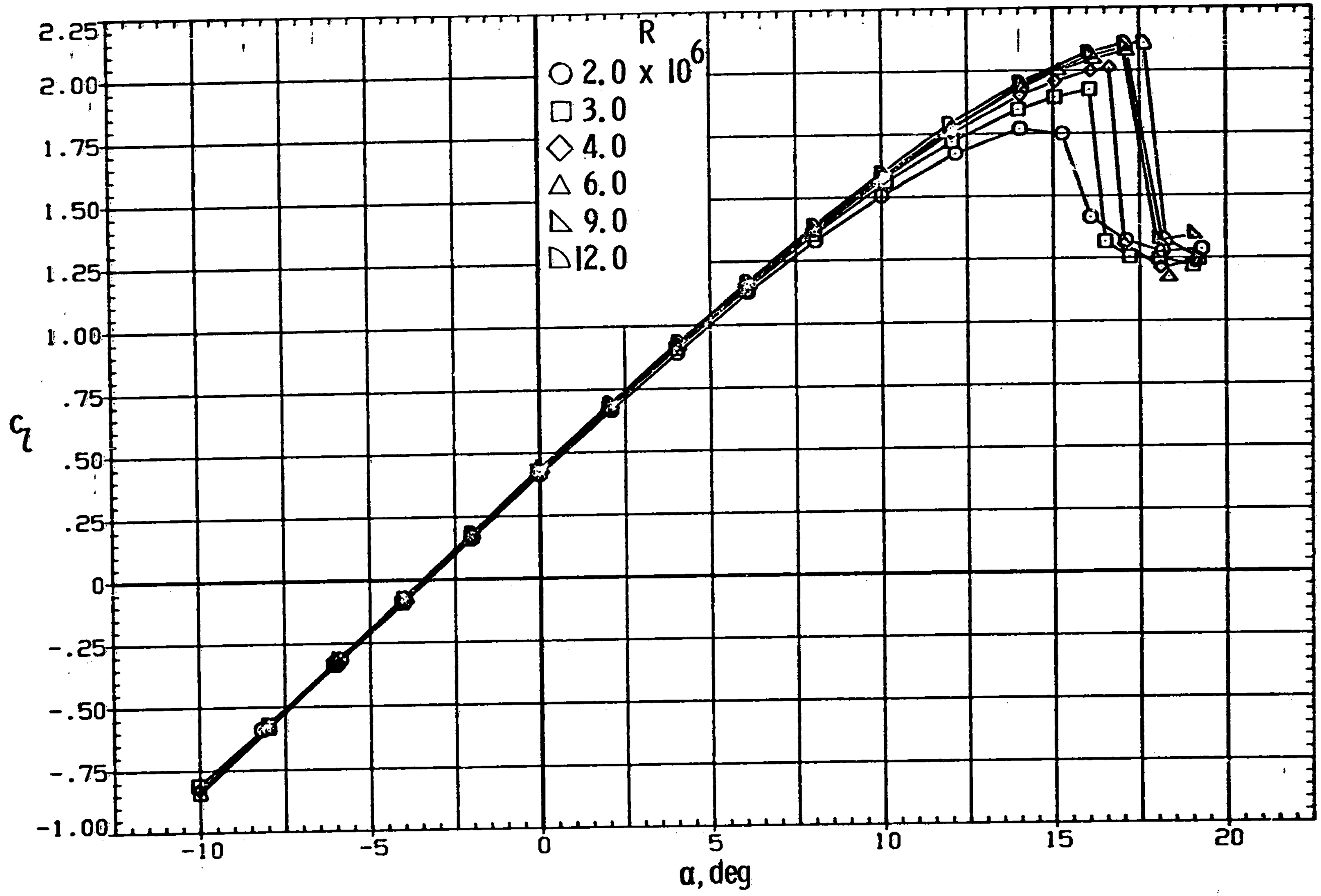

(a) Lift.

Figure 10.- Effect of Reynolds number on section characteristics. Model smooth; M = 0.15.

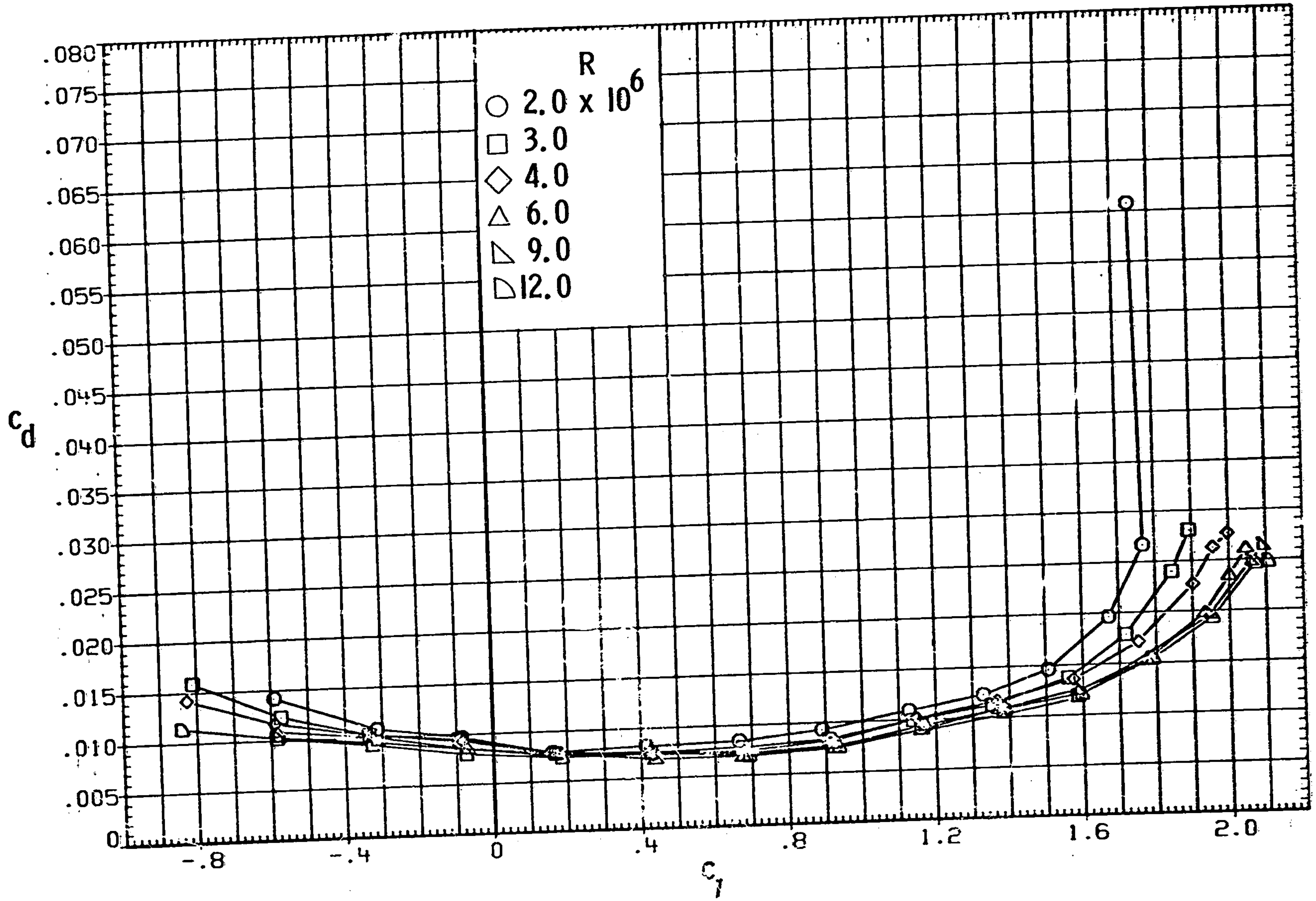

(b) Drag.

Figure 10.- Continued.

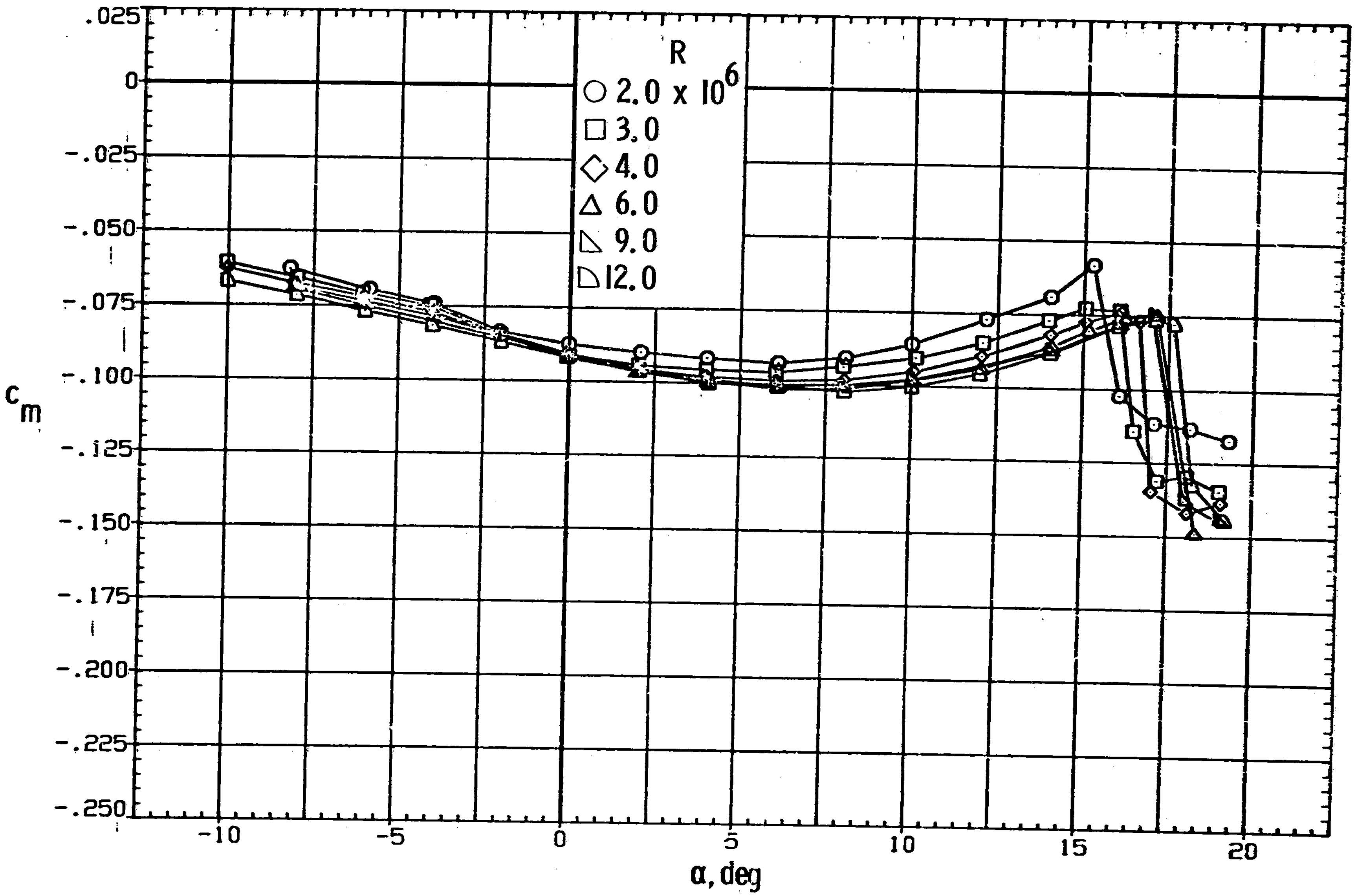

(c) Pitching moment.

Figure 10.- Concluded.

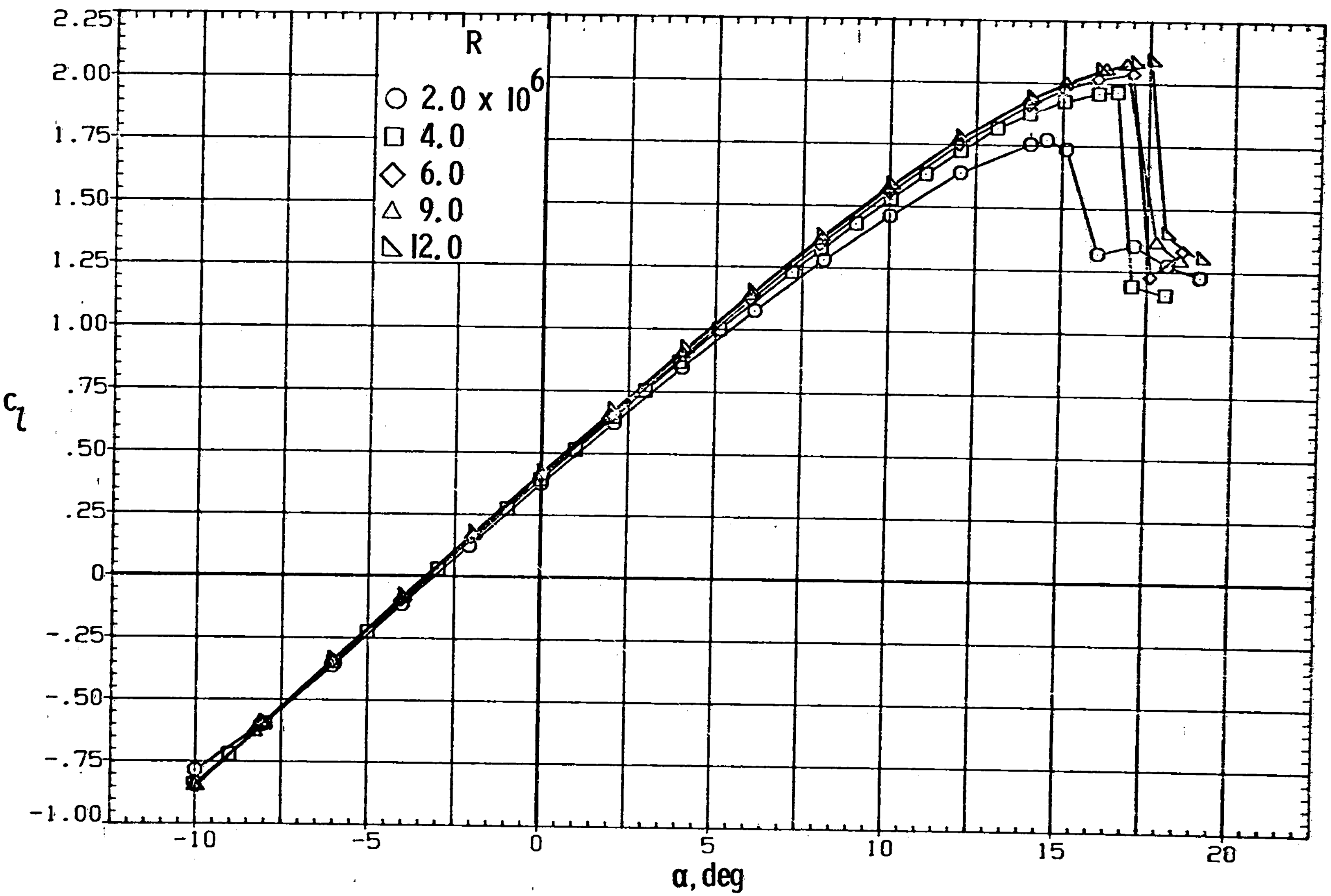

(a) Lift.

Figure 11.- Effect of Reynolds number on section characteristics. Roughness located at 0.075c; M = 0.15.

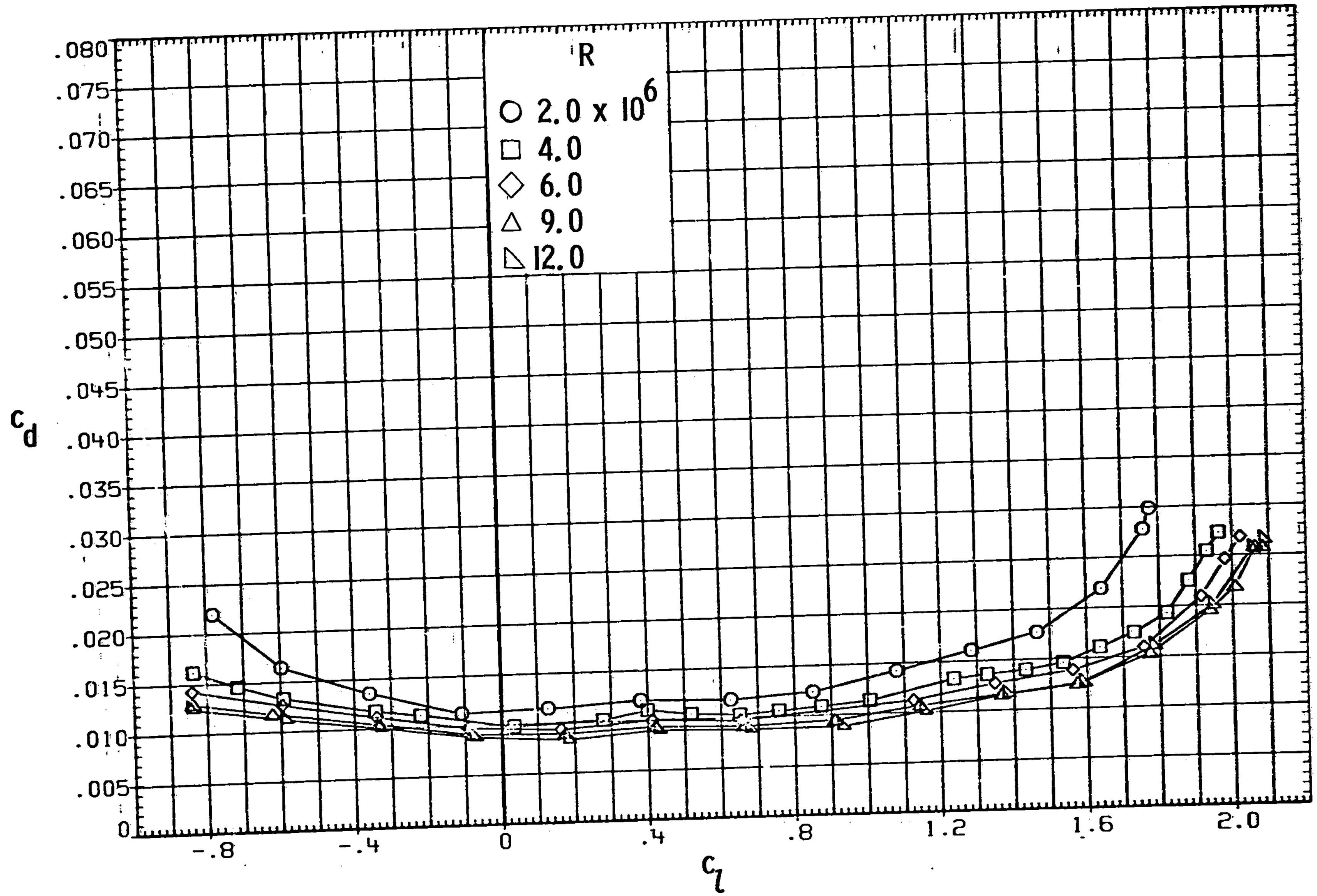

(b) Drag.

Figure 11.- Continued.

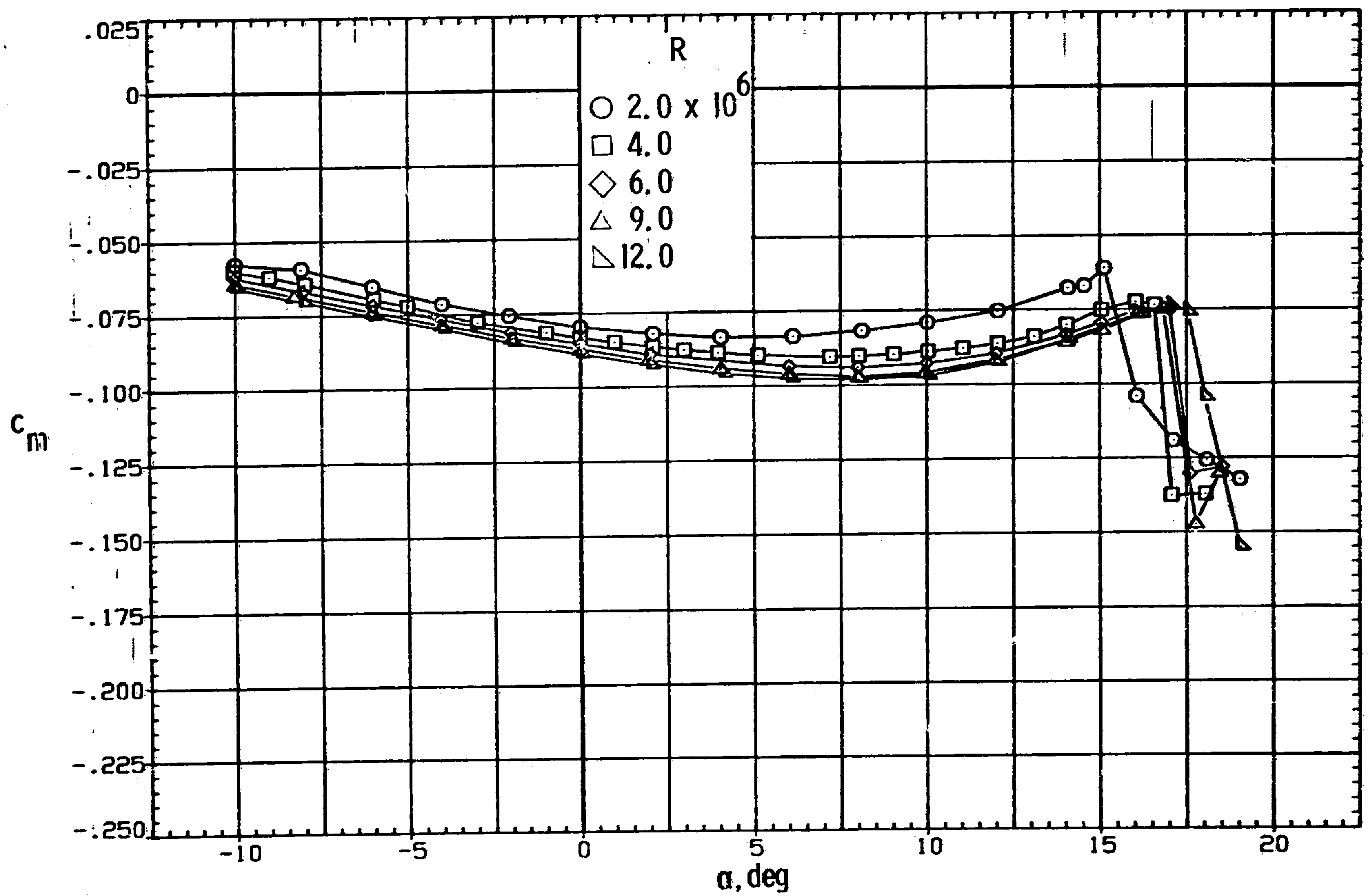

(c) Pitching moment.

Figure 11.- Concluded.

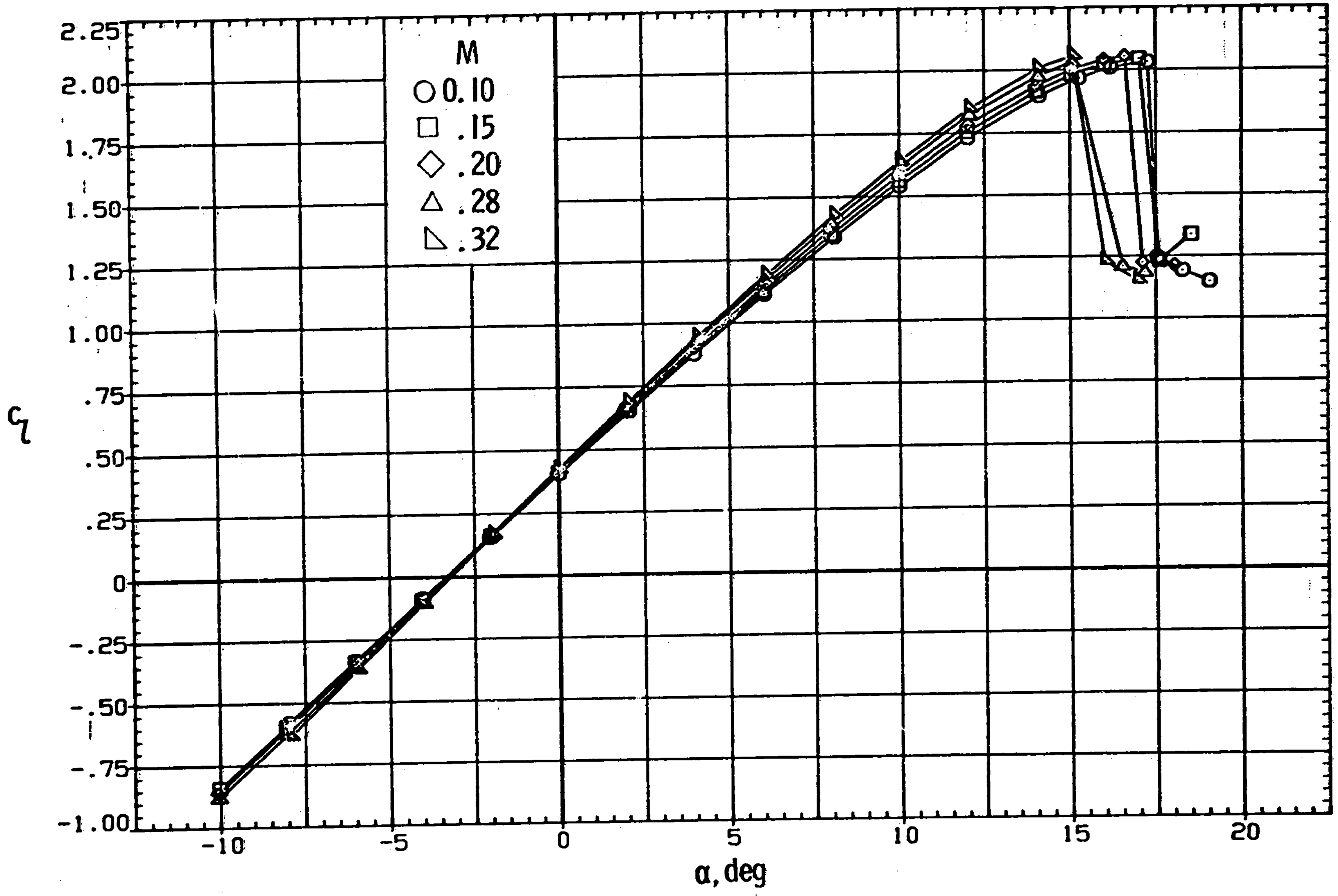

(a) Lift.

Figure 12.- Effect of Mach number on section characteristics. Roughness located at 0.075c; $R = 6.0 \times 10^6$.

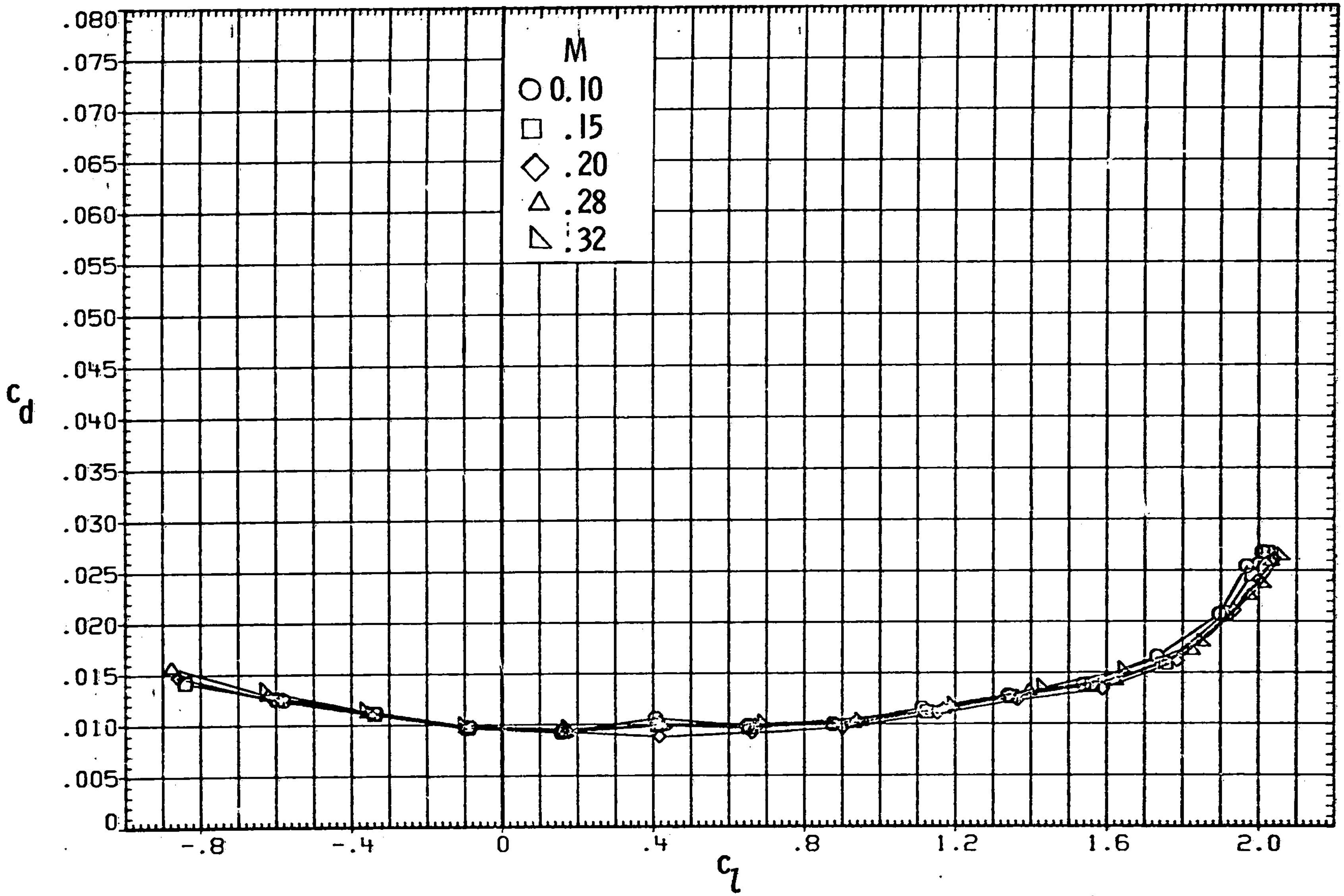

(b) Drag.

Figure 12.- Continued.

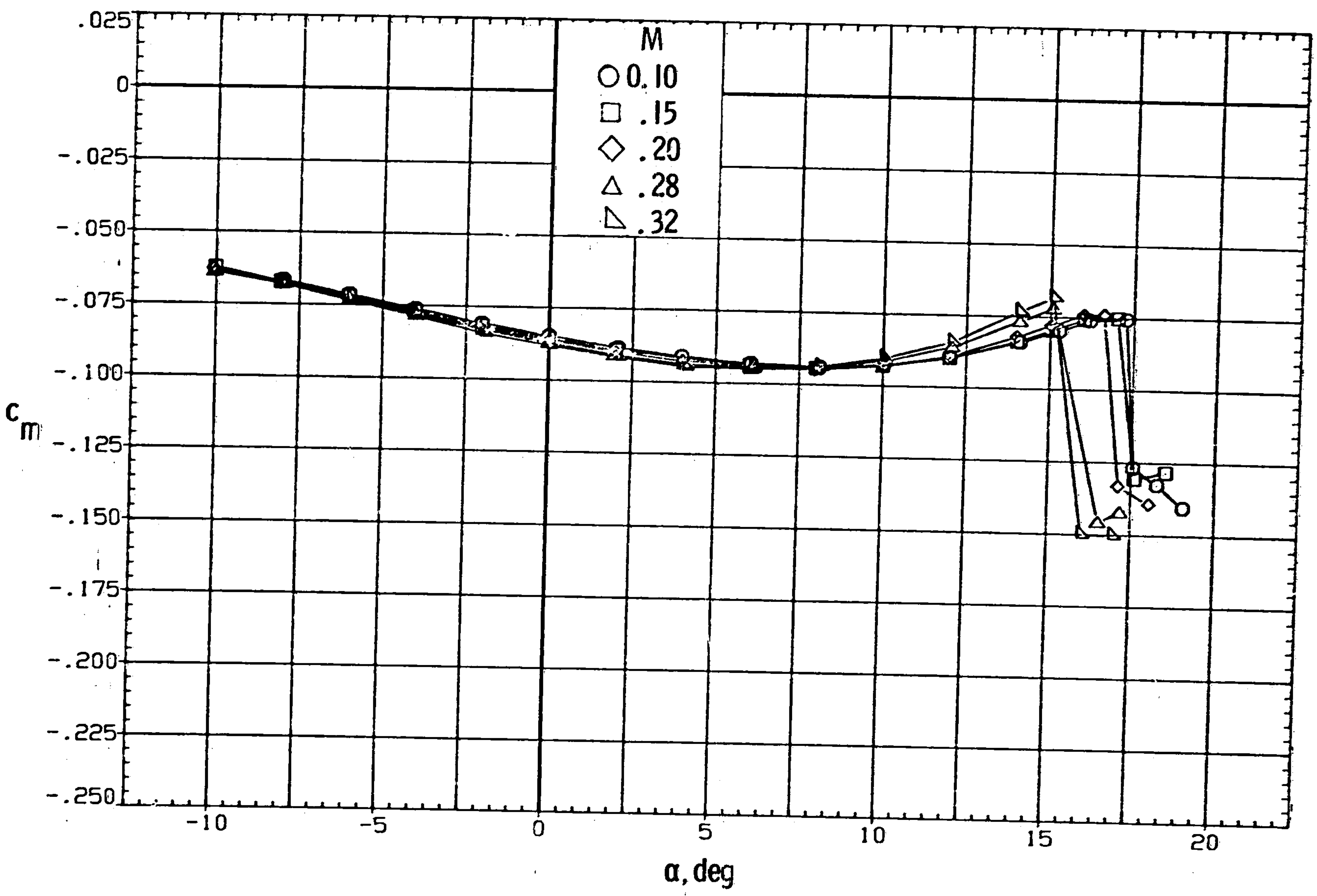

(c) Pitching moment.

Figure 12.- Concluded.

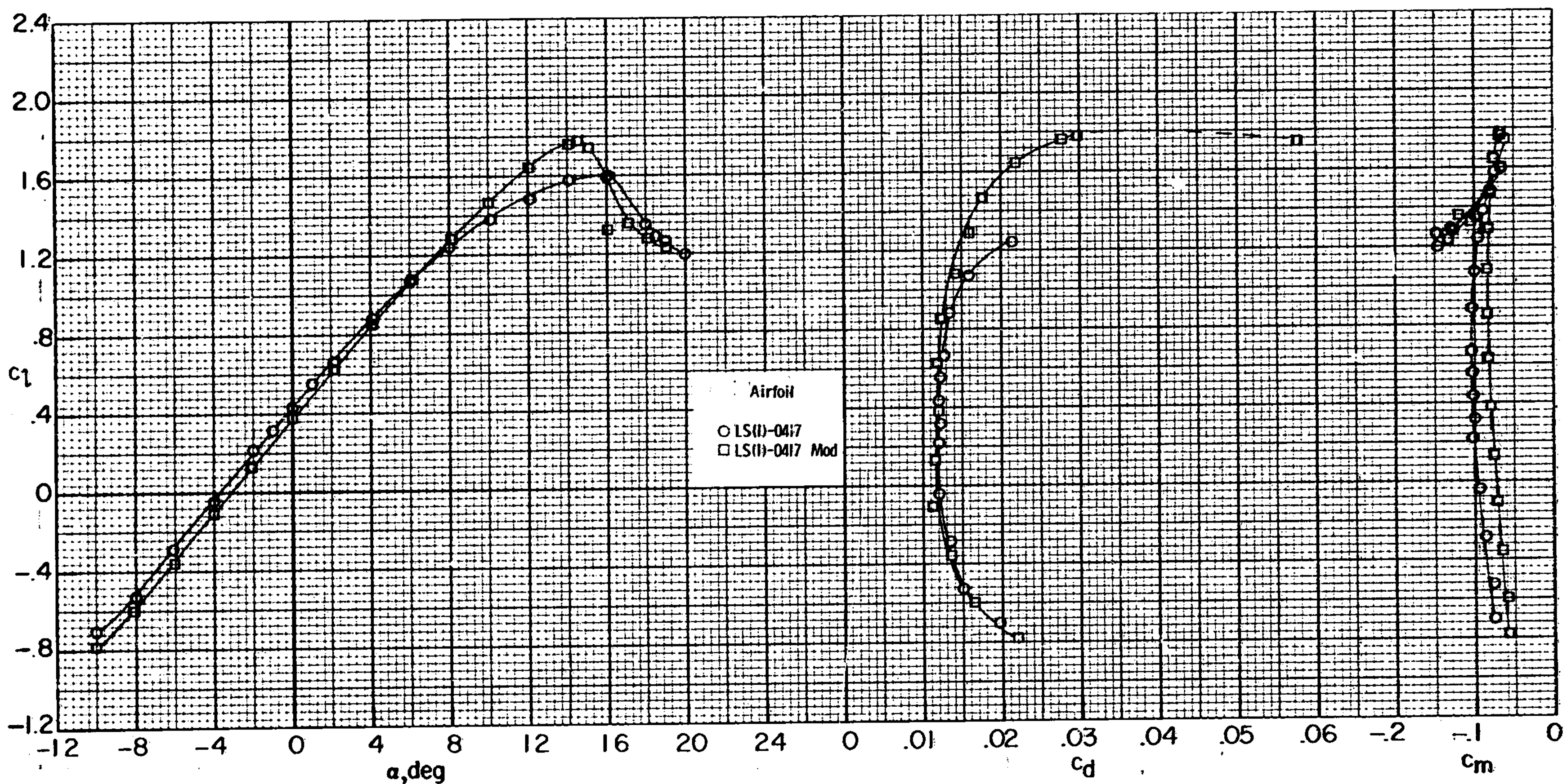

(a) $R = 2.0 \times 10^6$.

Figure 13.- Comparison of section characteristics for LS(1)-0417 and LS(1)-0417 Mod airfoils. Roughness on; $M = 0.15$.

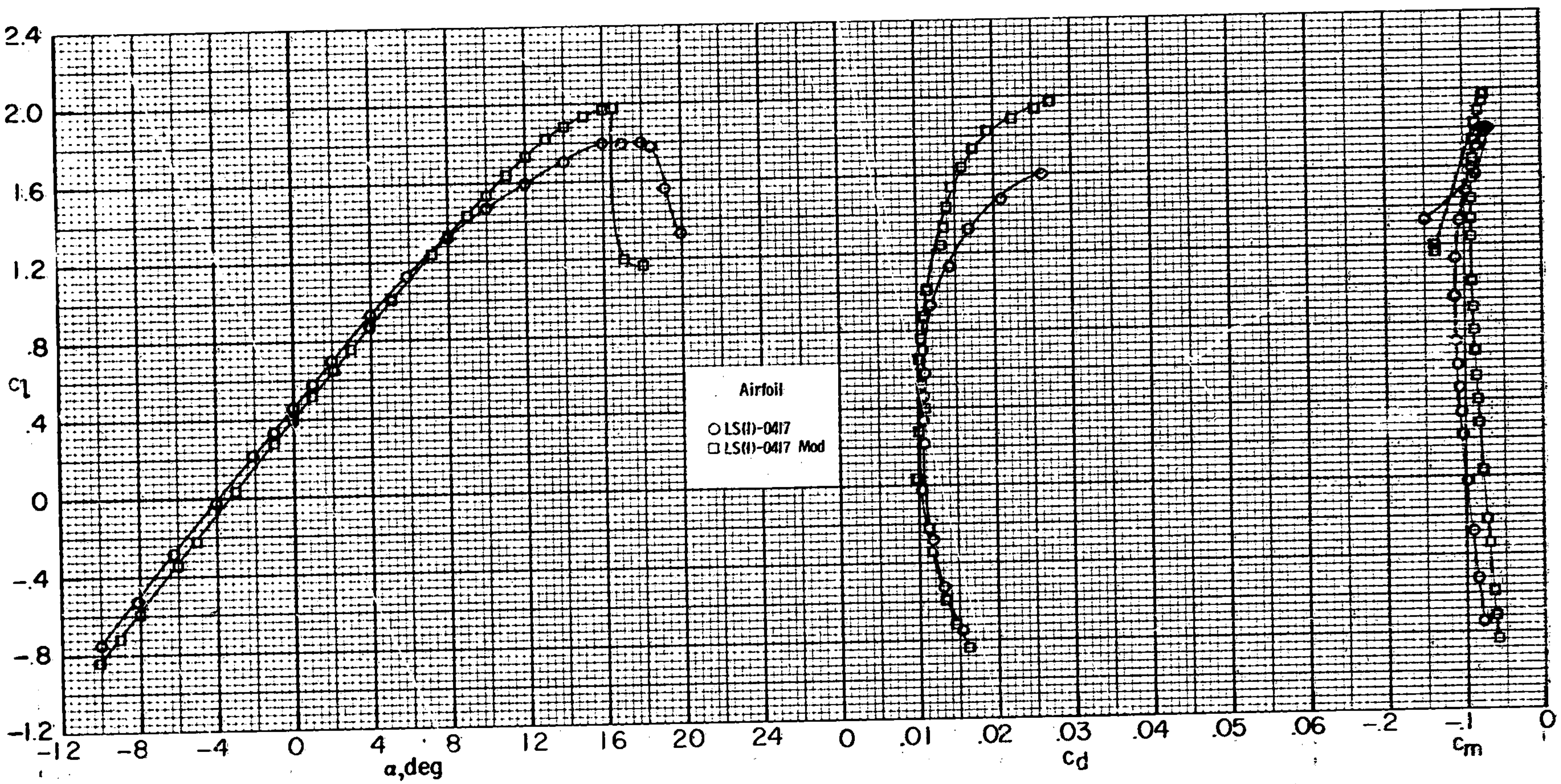

(b) $R = 4.0 \times 10^6$.

Figure 13.- Continued.

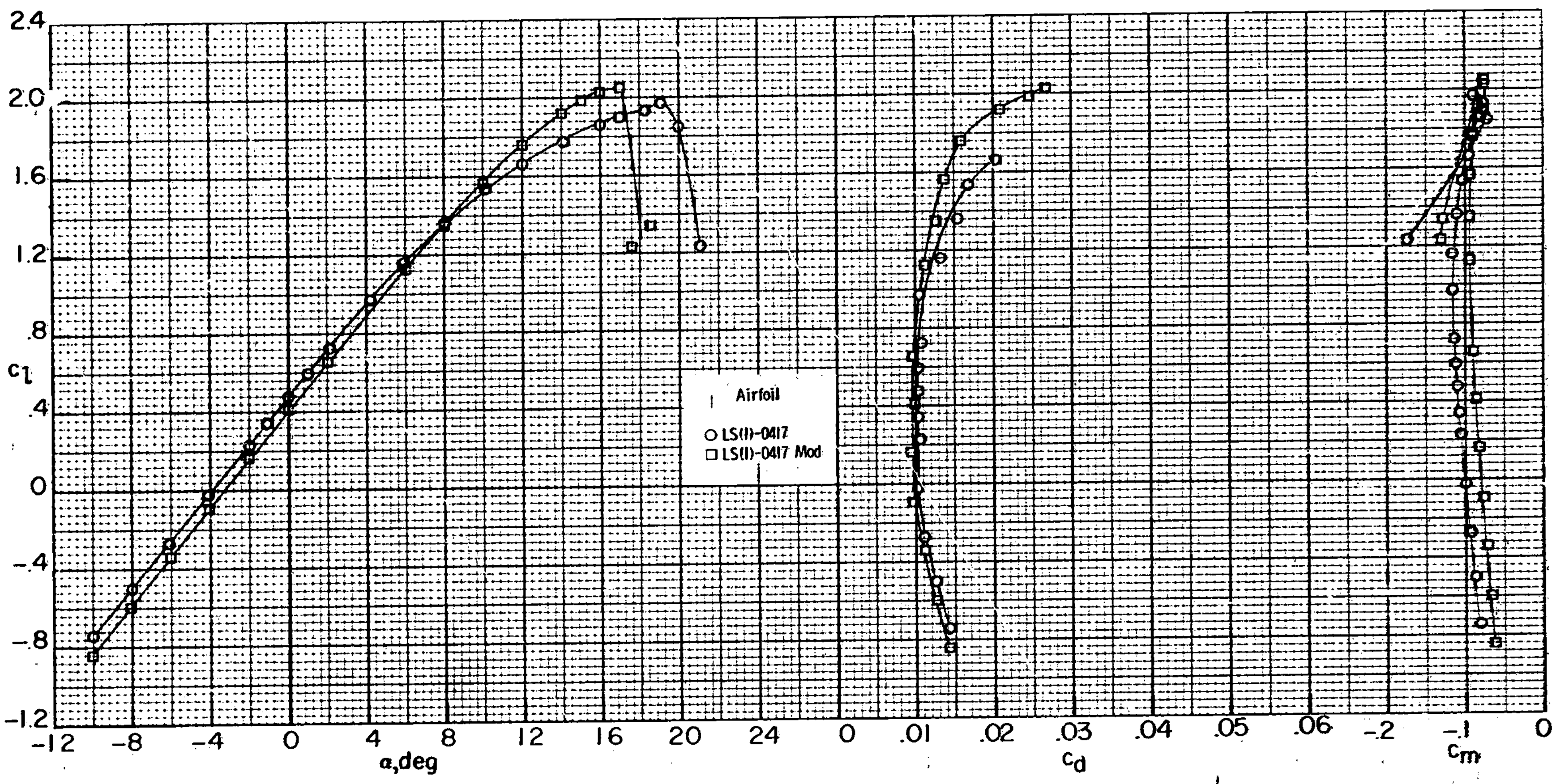

(c) $R = 6.0 \times 10^6$.

Figure 13.- Concluded.

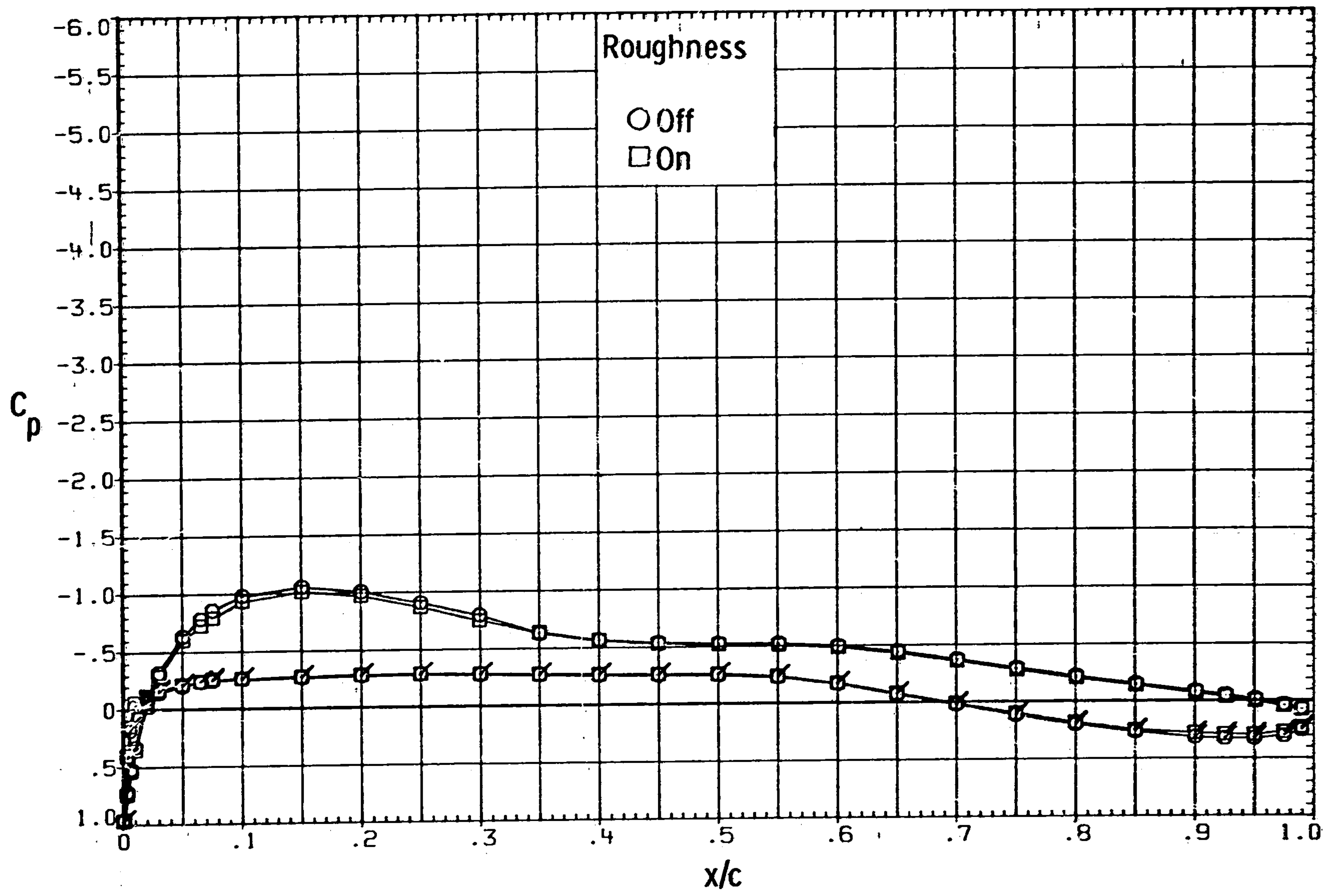

(a) $R = 2.0 \times 10^6$.

Figure 14.- Effect of roughness on chordwise pressure distributions for LS(1)-0417 Mod airfoil. $M = 0.15$; $\alpha = 0°$. Flagged symbols designate lower surface.

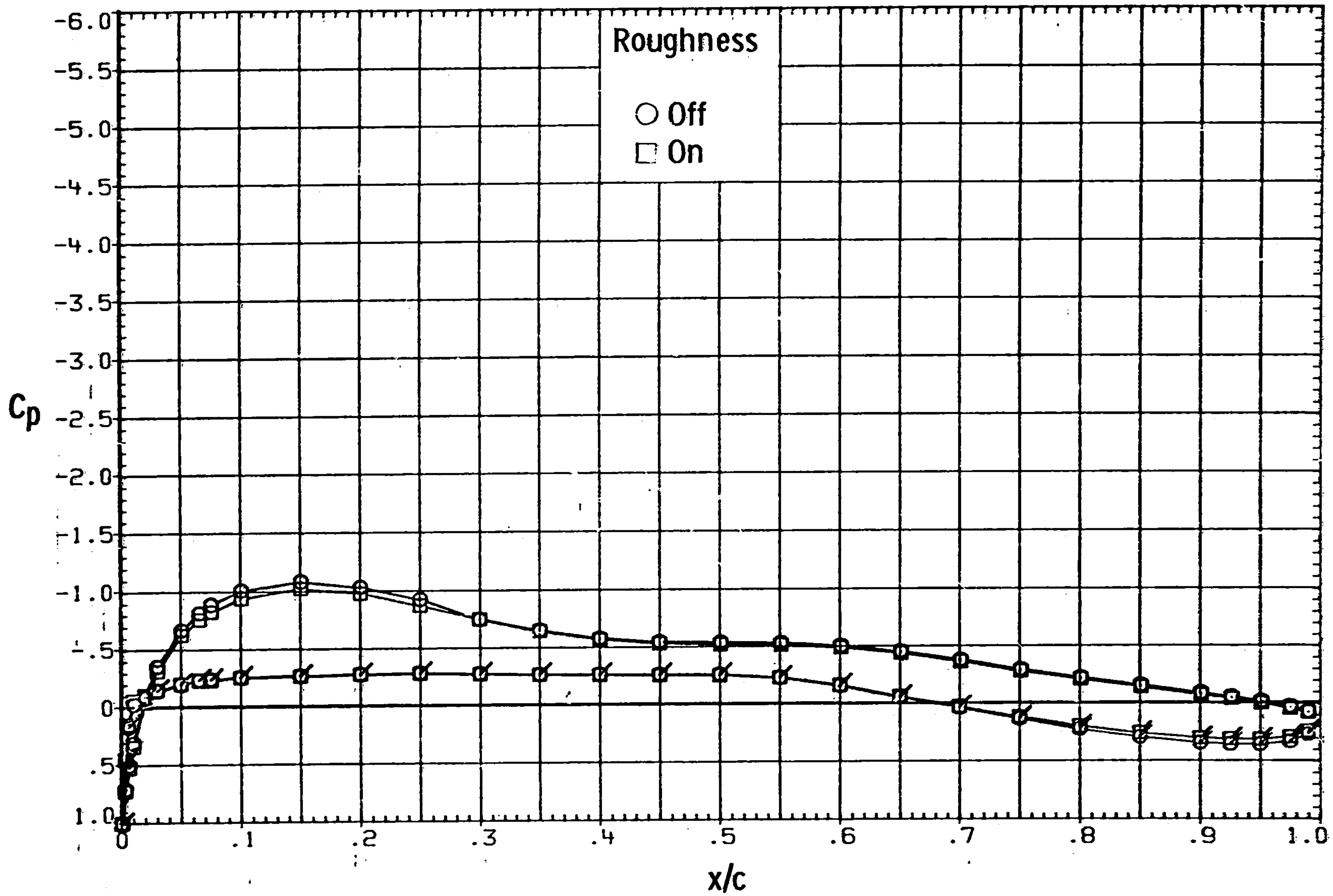

(b) $R = 4.0 \times 10^6$.

Figure 14.- Continued.

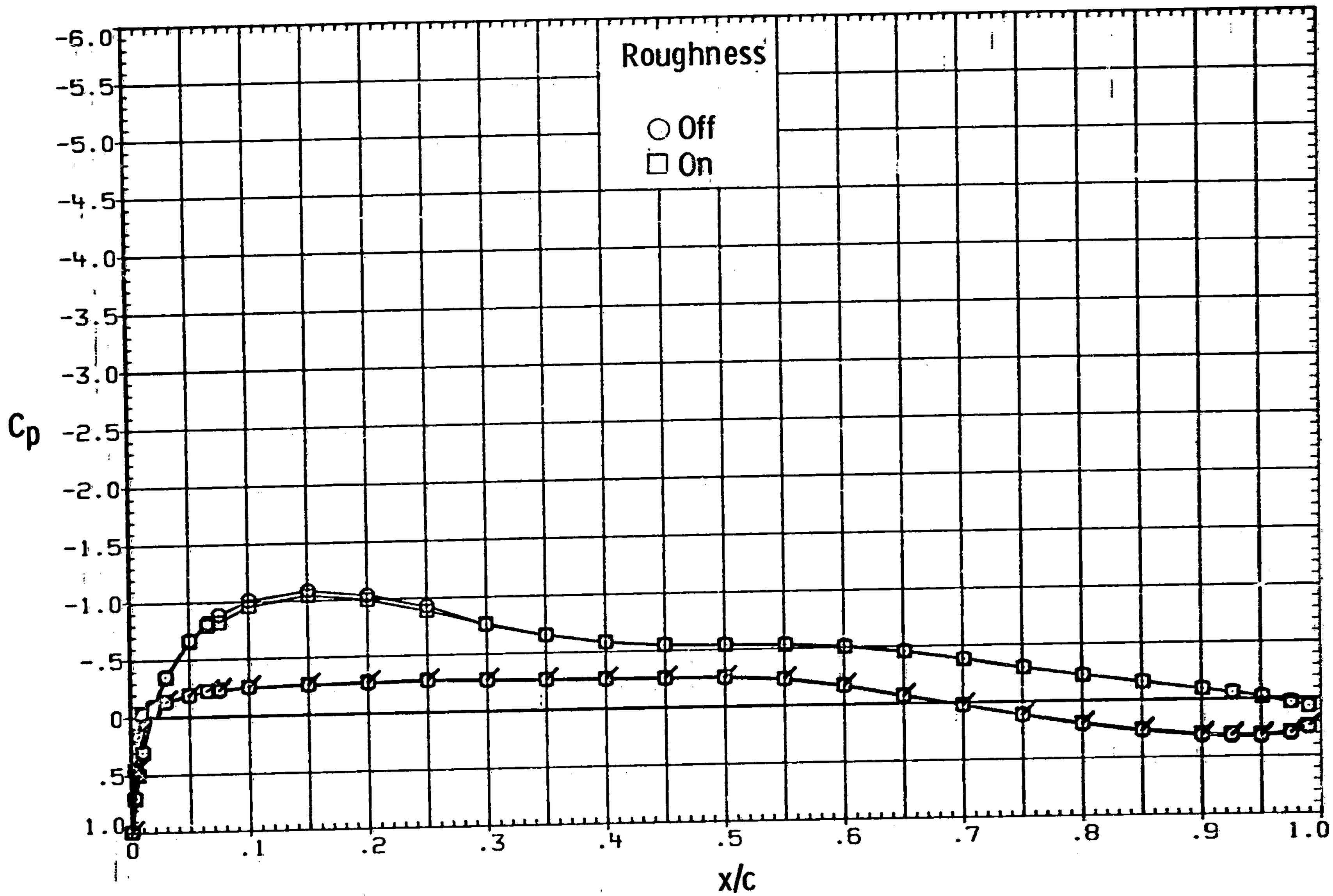

(c) $R = 6.0 \times 10^6$.

Figure 14.- Continued.

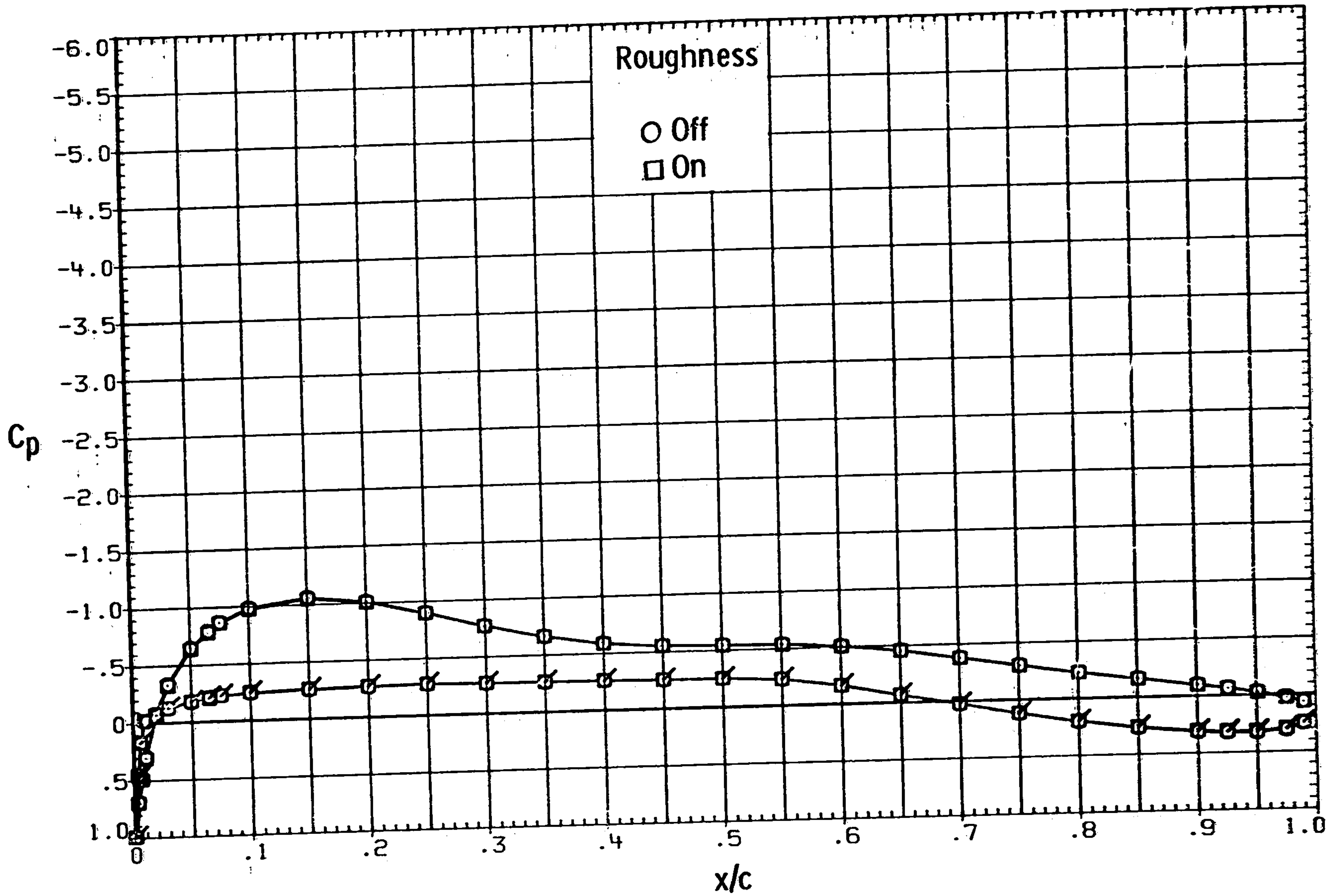

(d) $R = 9.0 \times 10^6$.

Figure 14.- Concluded.

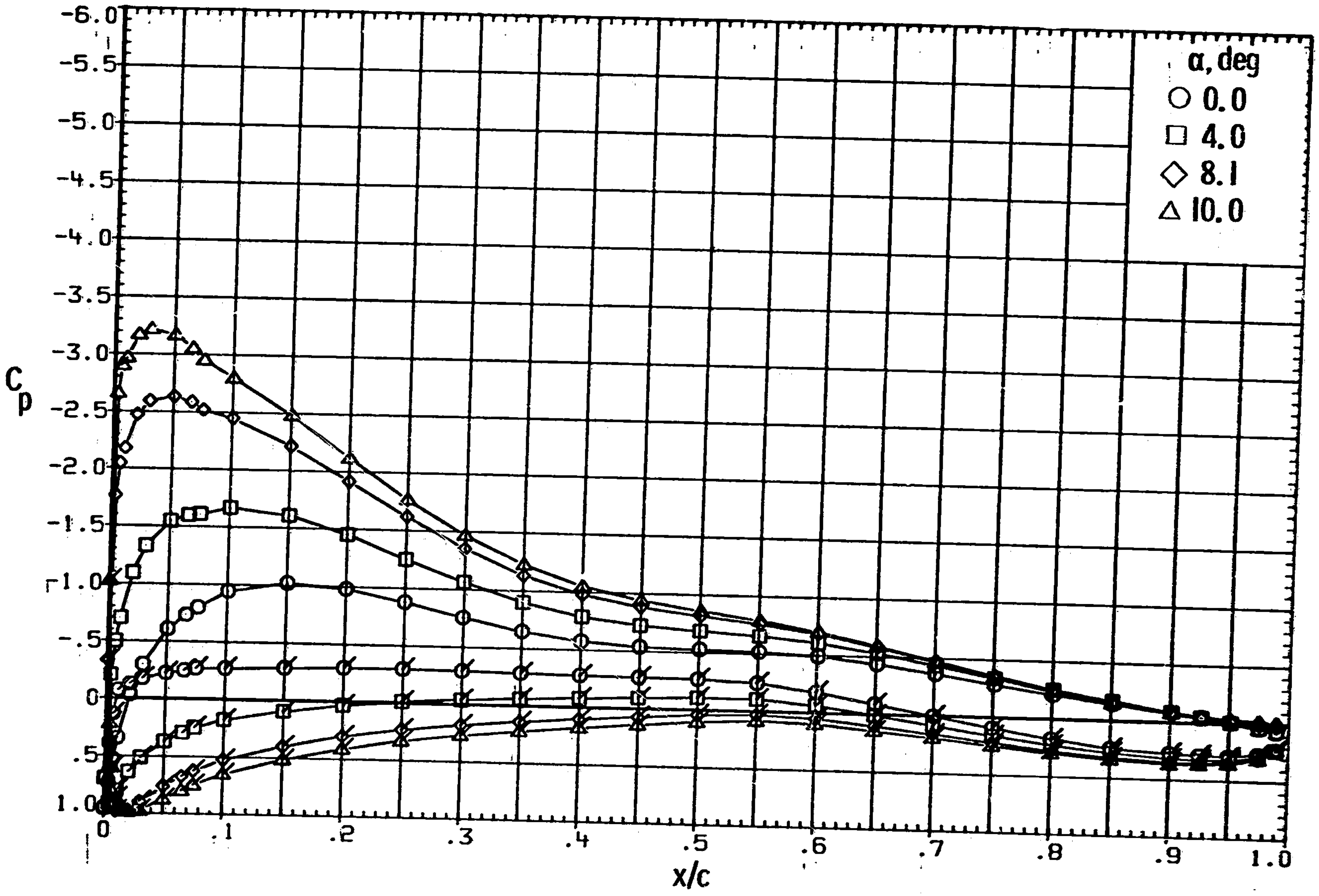

(a) $R = 2.0 \times 10^6$.

Figure 15.- Effect of angle of attack and Reynolds number on chordwise pressure distributions for LS(1)-0417 Mod airfoil. Roughness on; M = 0.15. Flagged symbols designate lower surface.

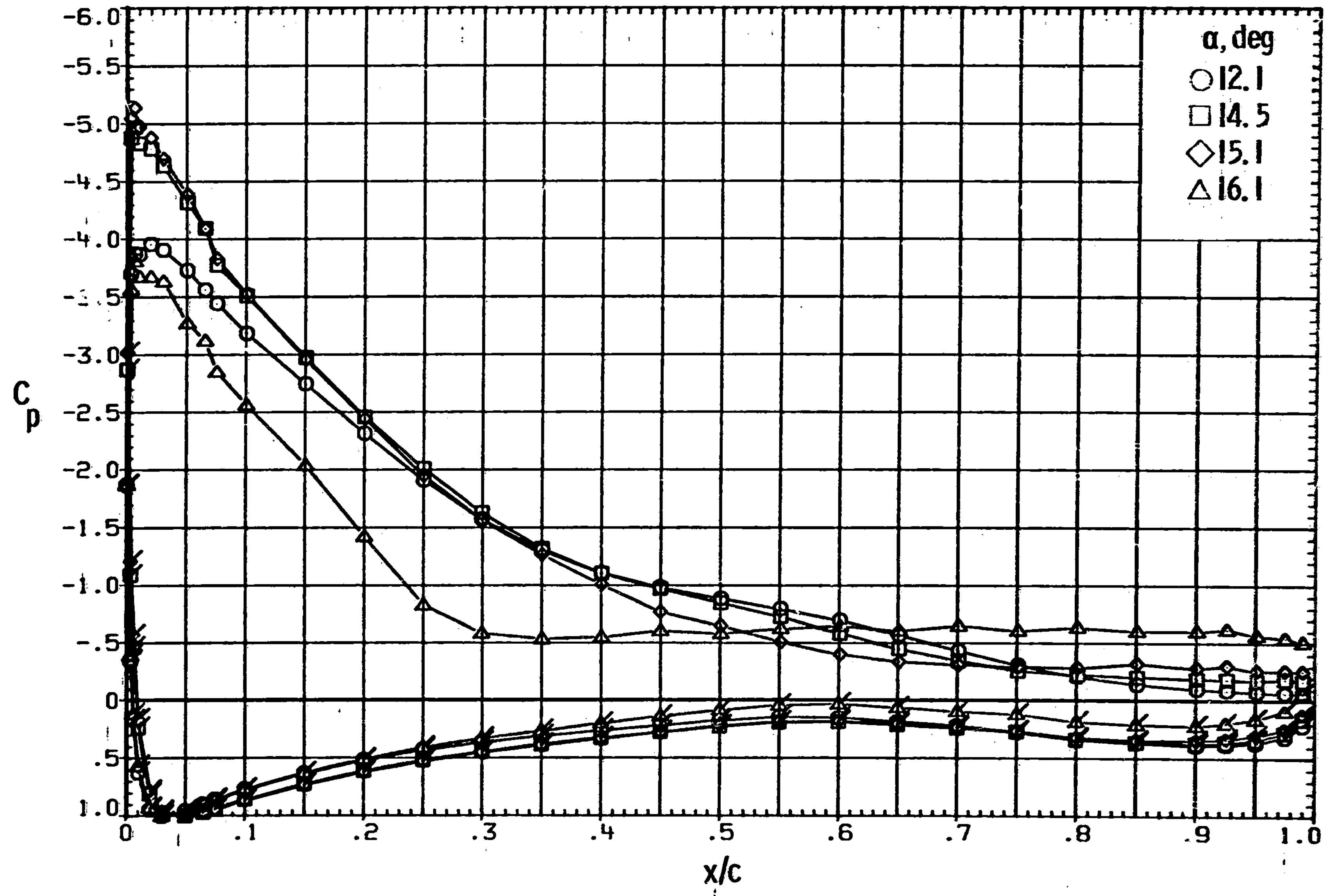

(a) $R = 2.0 \times 10^6$. Concluded.

Figure 15.- Continued.

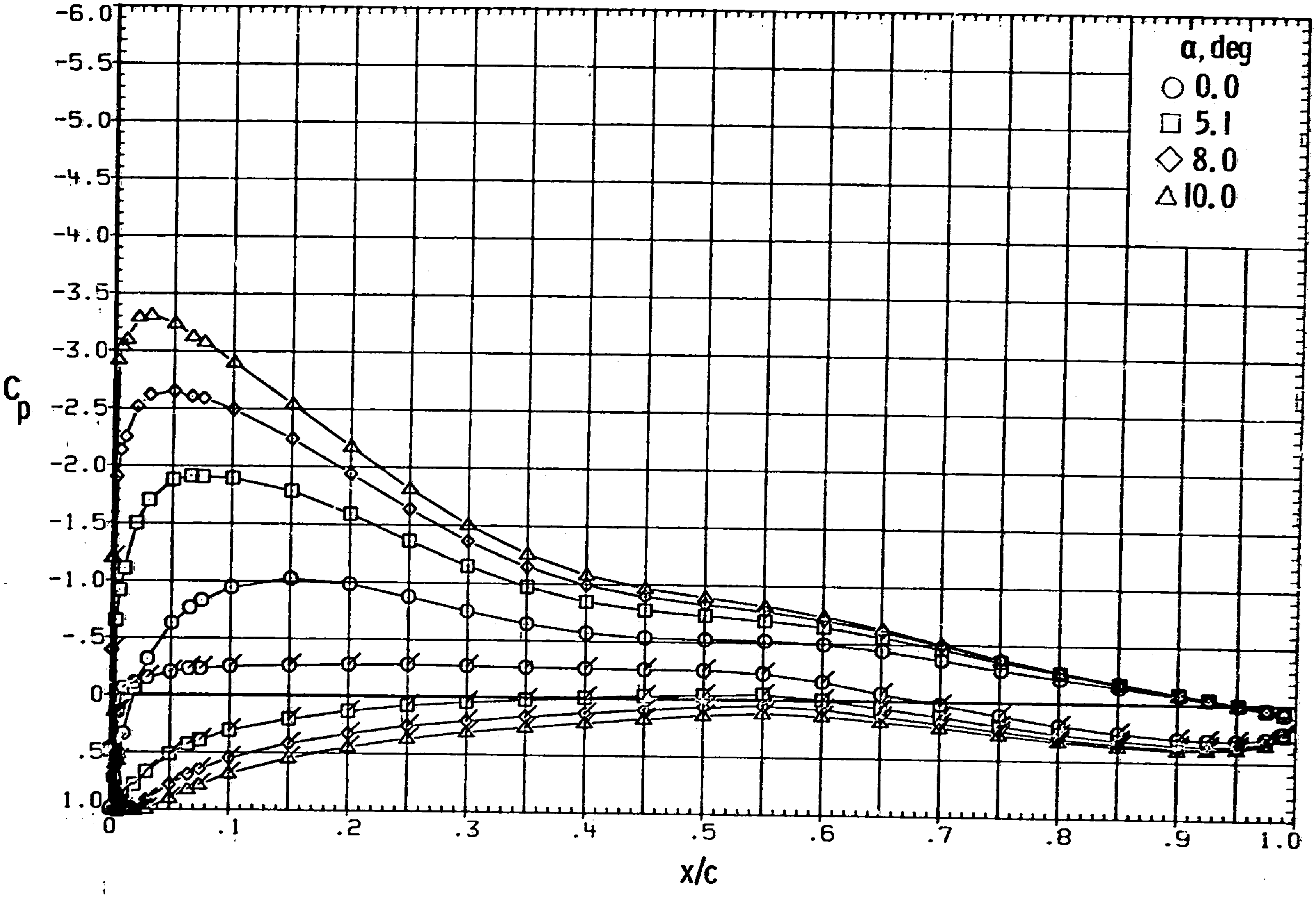

(b) $R = 4.0 \times 10^6$.

Figure 15.- Continued.

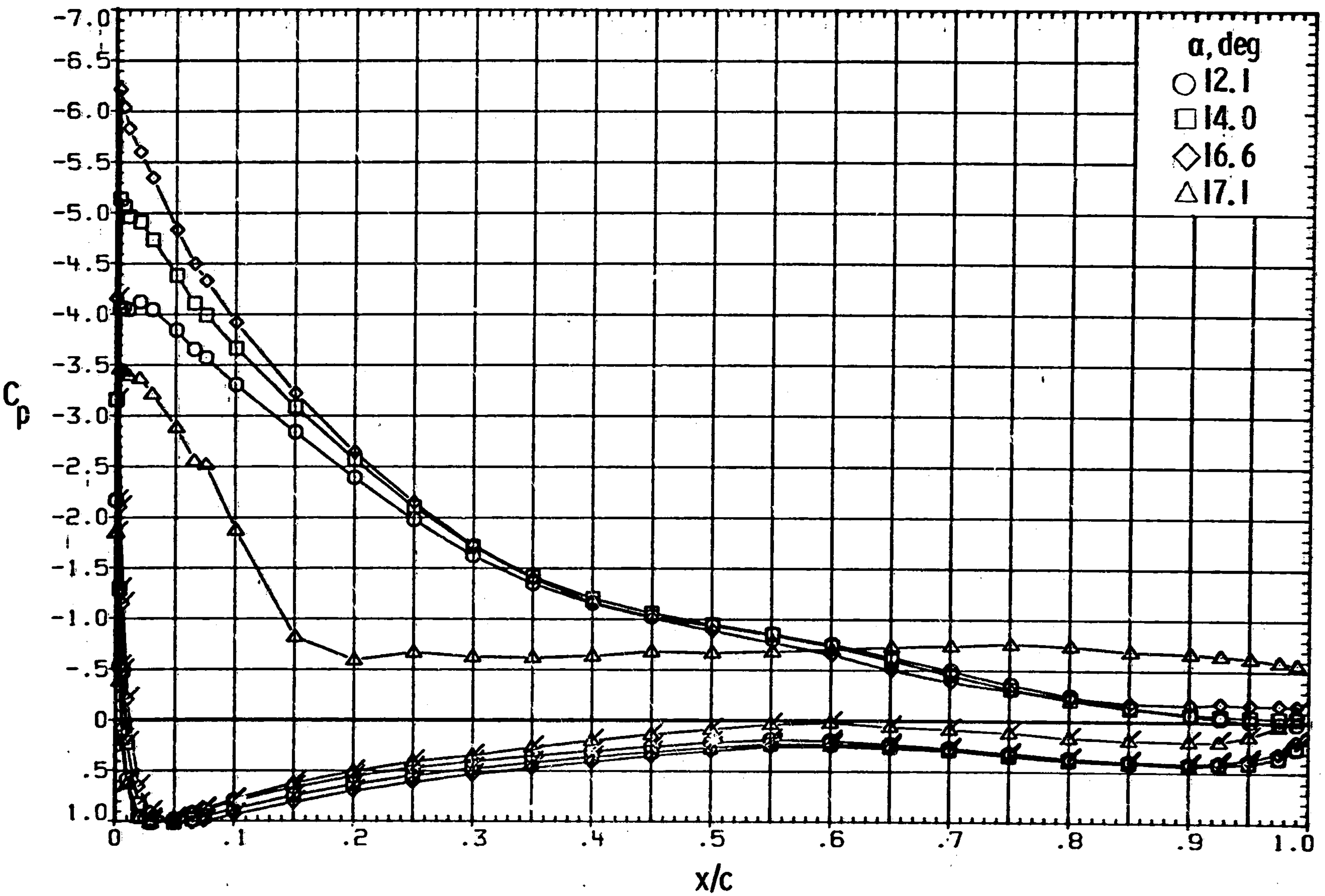

(b) $R = 4.0 \times 10^6$. Concluded.

Figure 15.- Continued.

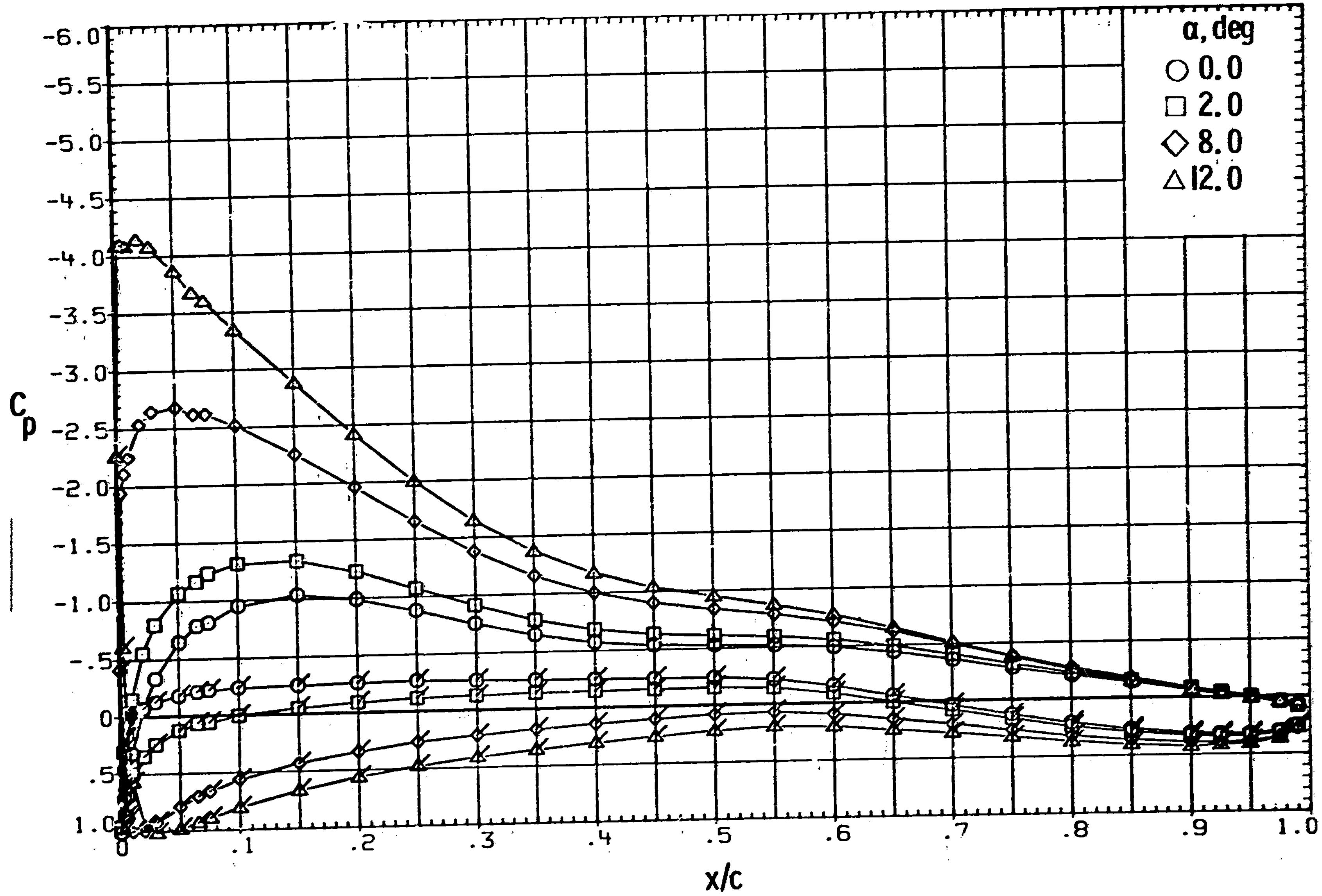

(c) $R = 6.0 \times 10^6$.

Figure 15.- Continued.

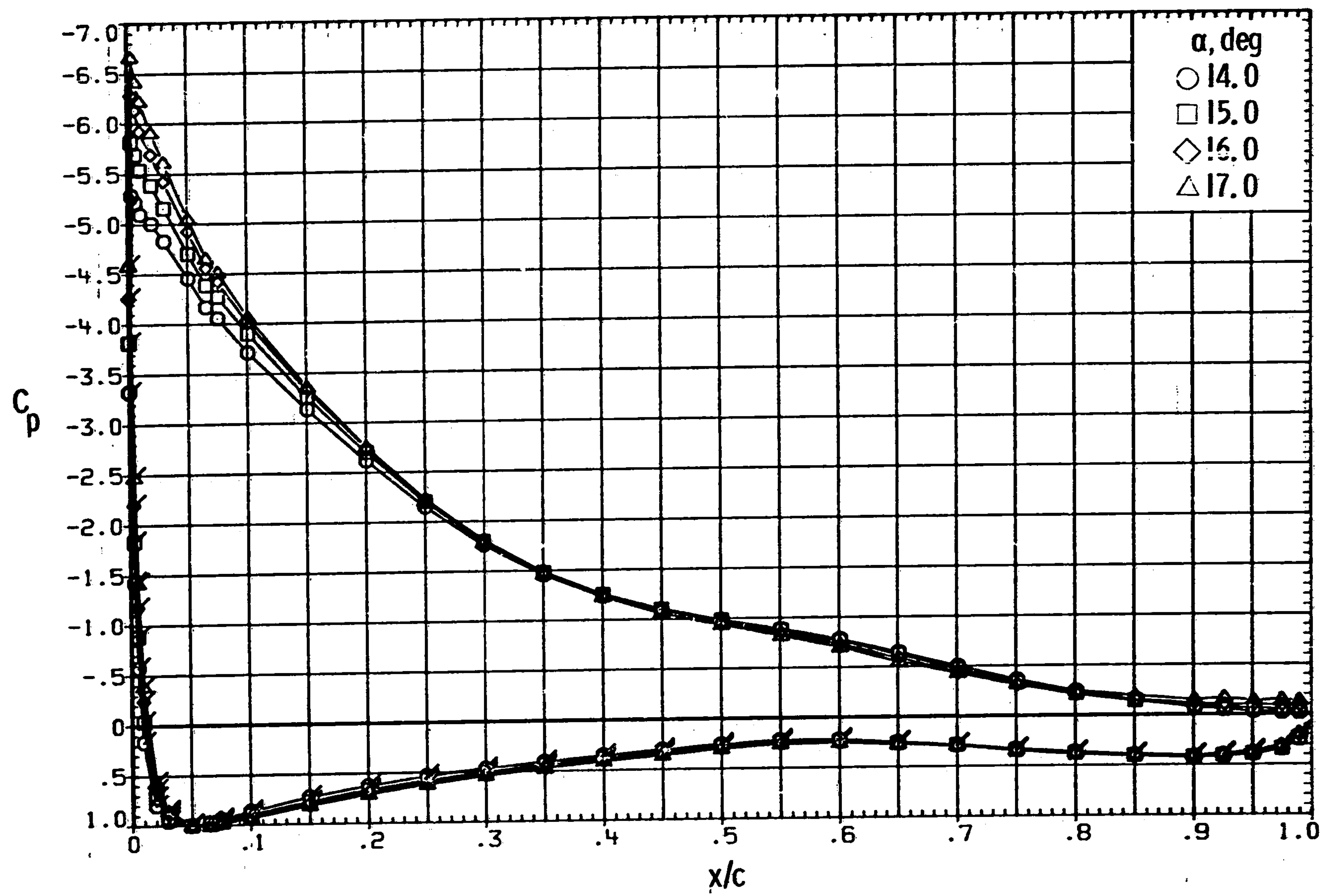

(c) $R = 6.0 \times 10^6$. Concluded.

Figure 15.- Continued.

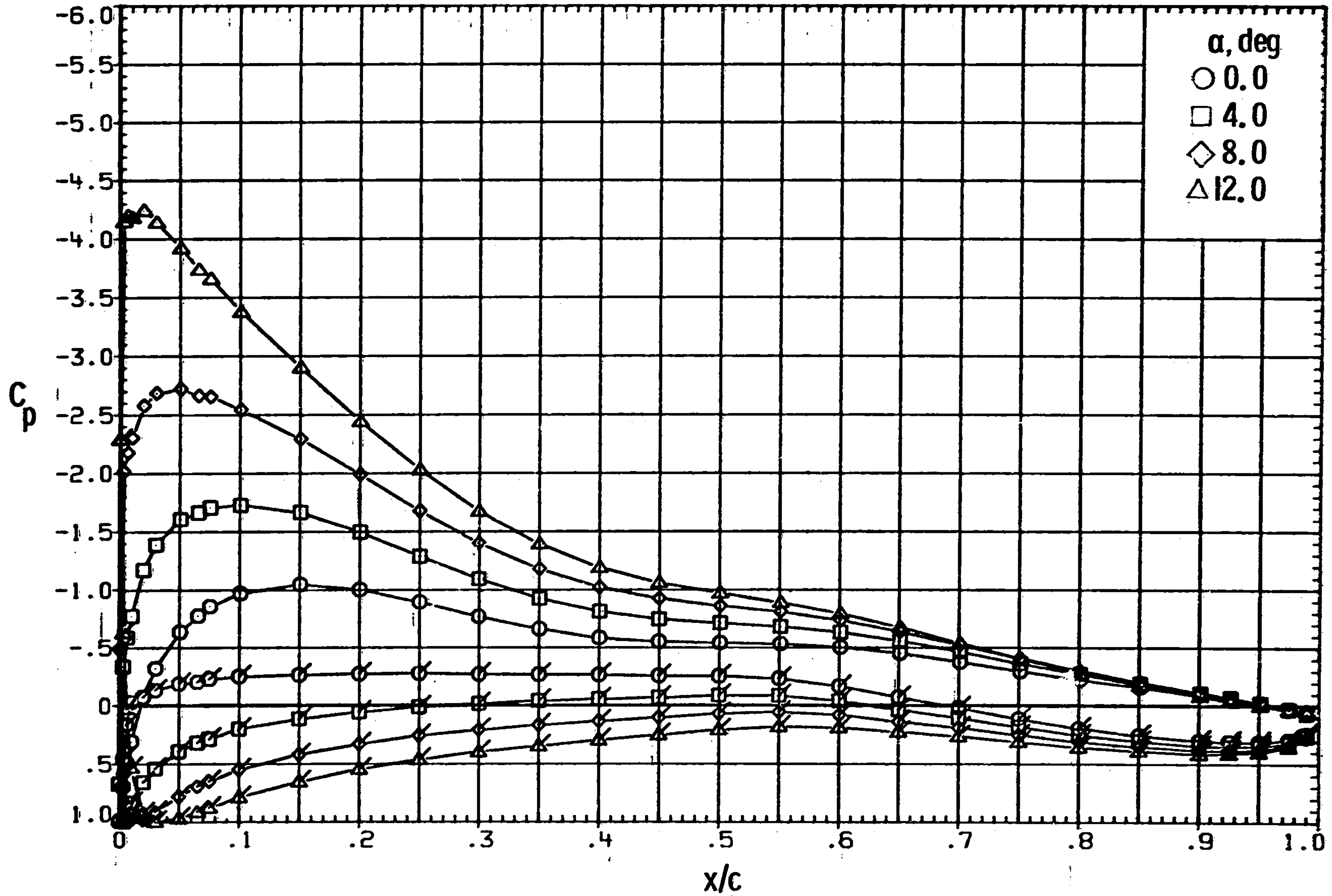

(d) $R = 9.0 \times 10^6$.

Figure 15.- Continued.

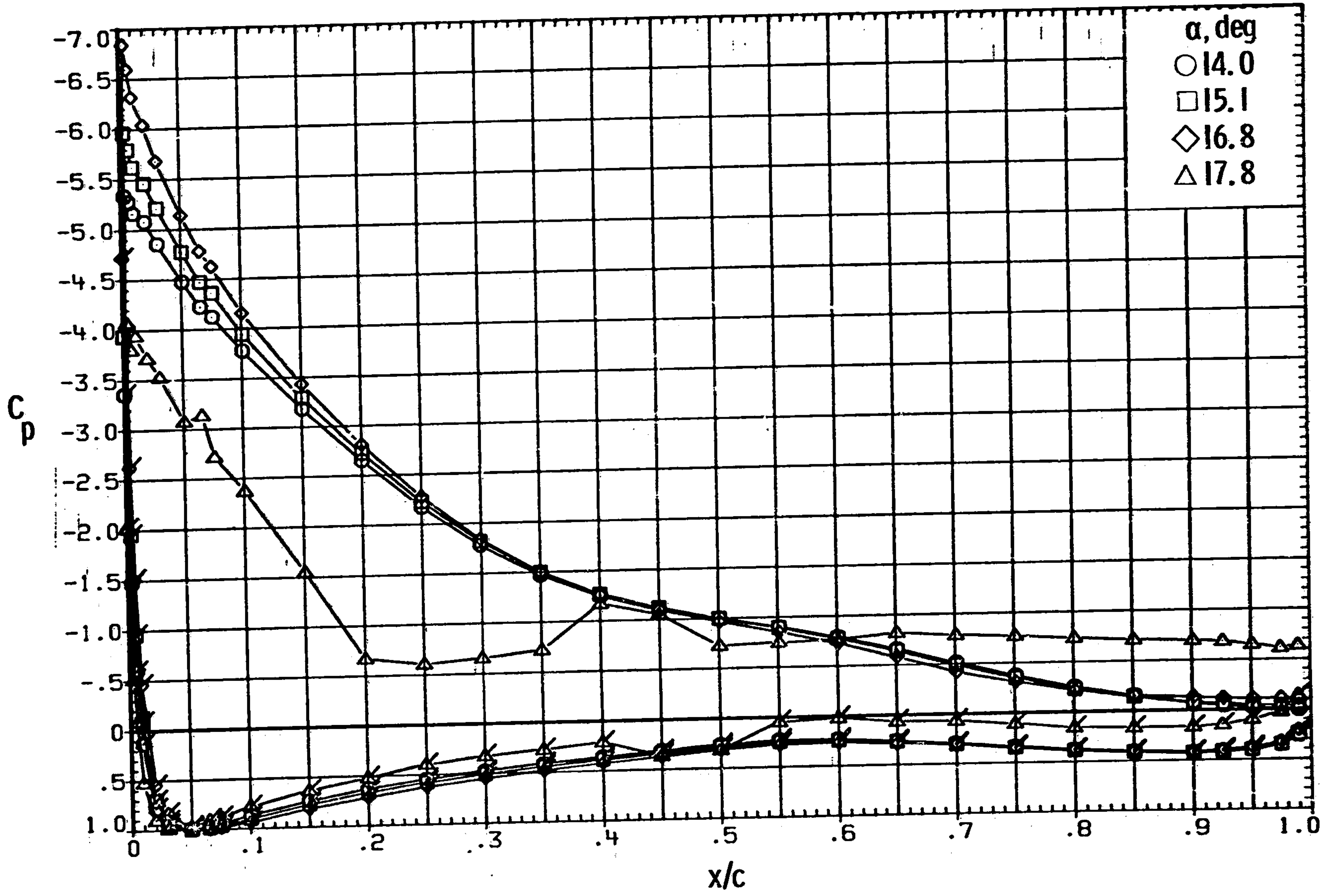

(d) $R = 9.0 \times 10^6$. Concluded.

Figure 15.- Concluded.

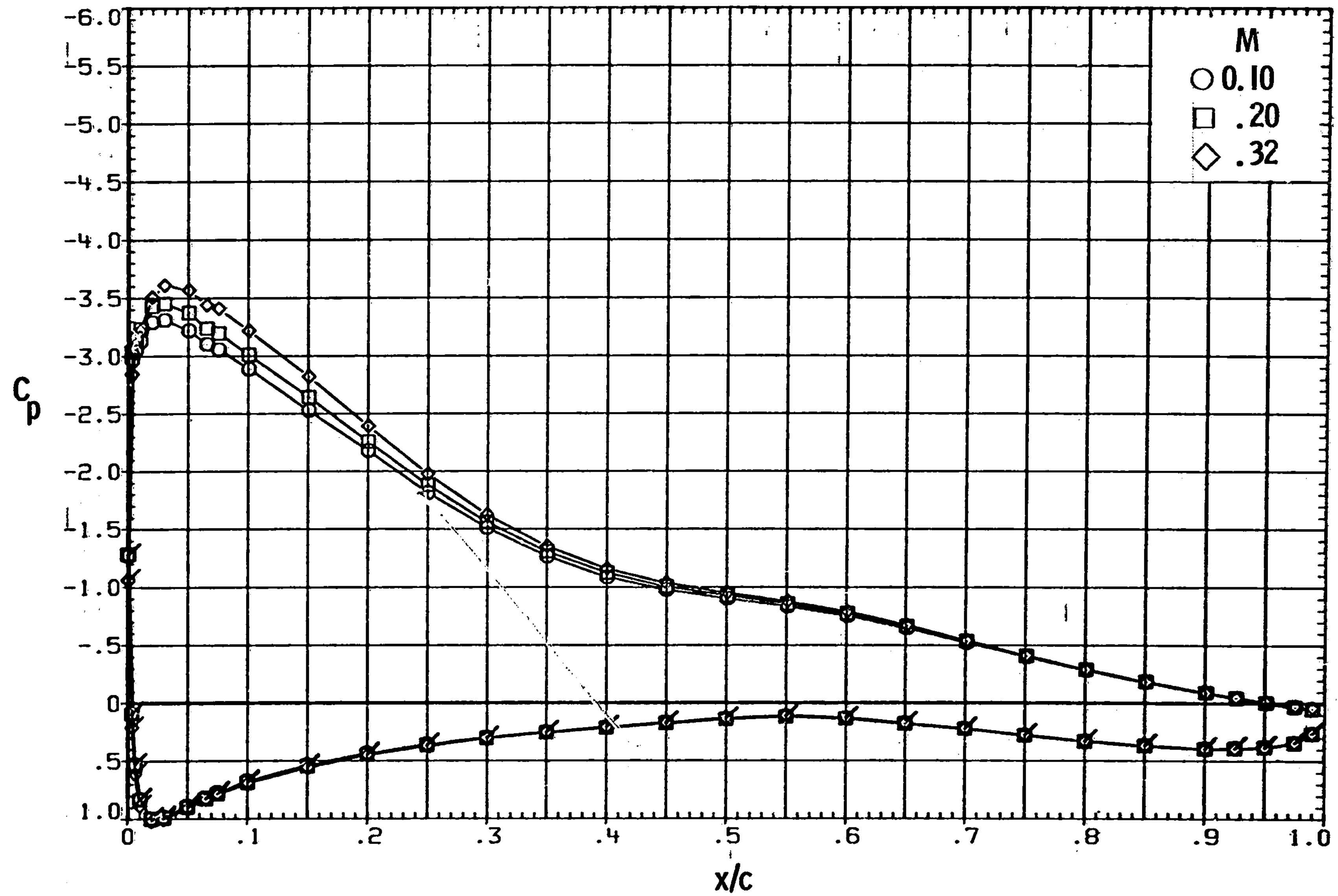

Figure 16.- Effect of Mach number on chordwise pressure distributions for LS(1)-0417 Mod airfoil. Roughness on; $R = 6.0 \times 10^6$; $\alpha = 10°$. Flagged symbols designate lower surface.

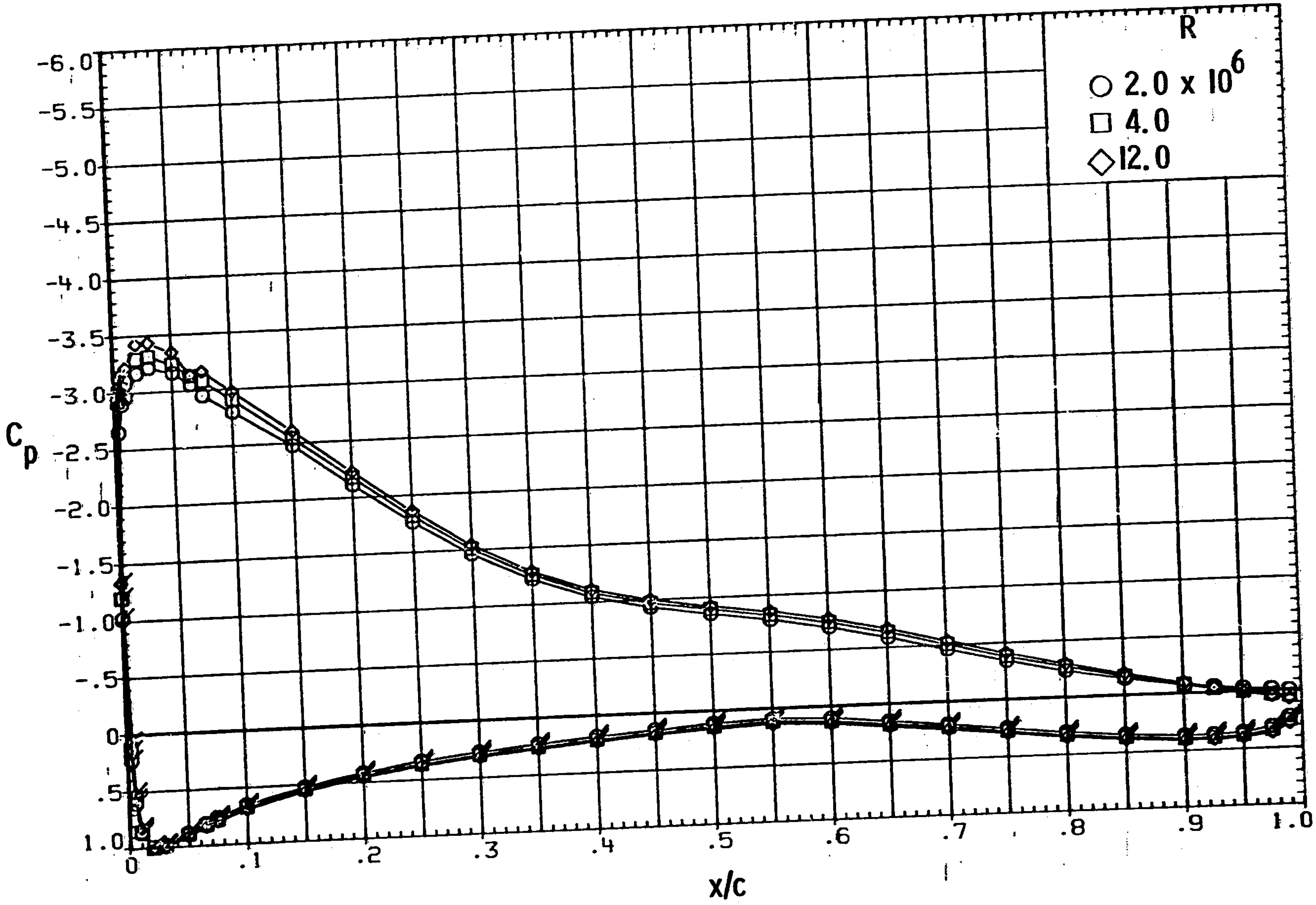

Figure 17.- Effect of Reynolds number on chordwise pressure distributions for LS(1)-0417 Mod airfoil. Roughness on; $M = 0.15$; $\alpha = 10°$. Flagged symbols designate lower surface.

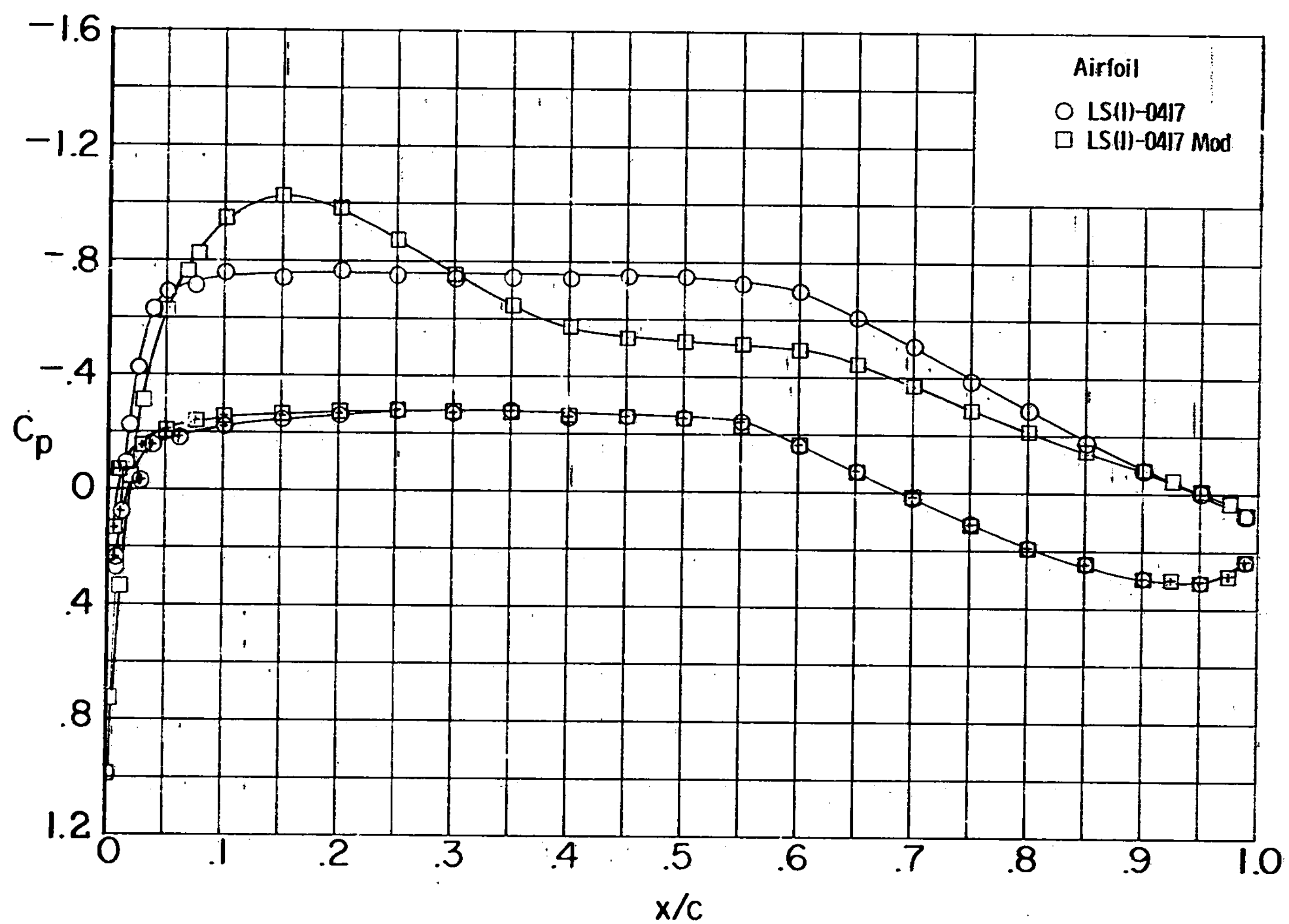

(a) $\alpha = 0°$.

Figure 18.- Comparison of chordwise pressure distributions for LS(1)-0417 and LS(1)-0417 Mod airfoils. Roughness on; $M = 0.15$; $R = 4.0 \times 10^6$. Symbols with + inside designate lower surface.

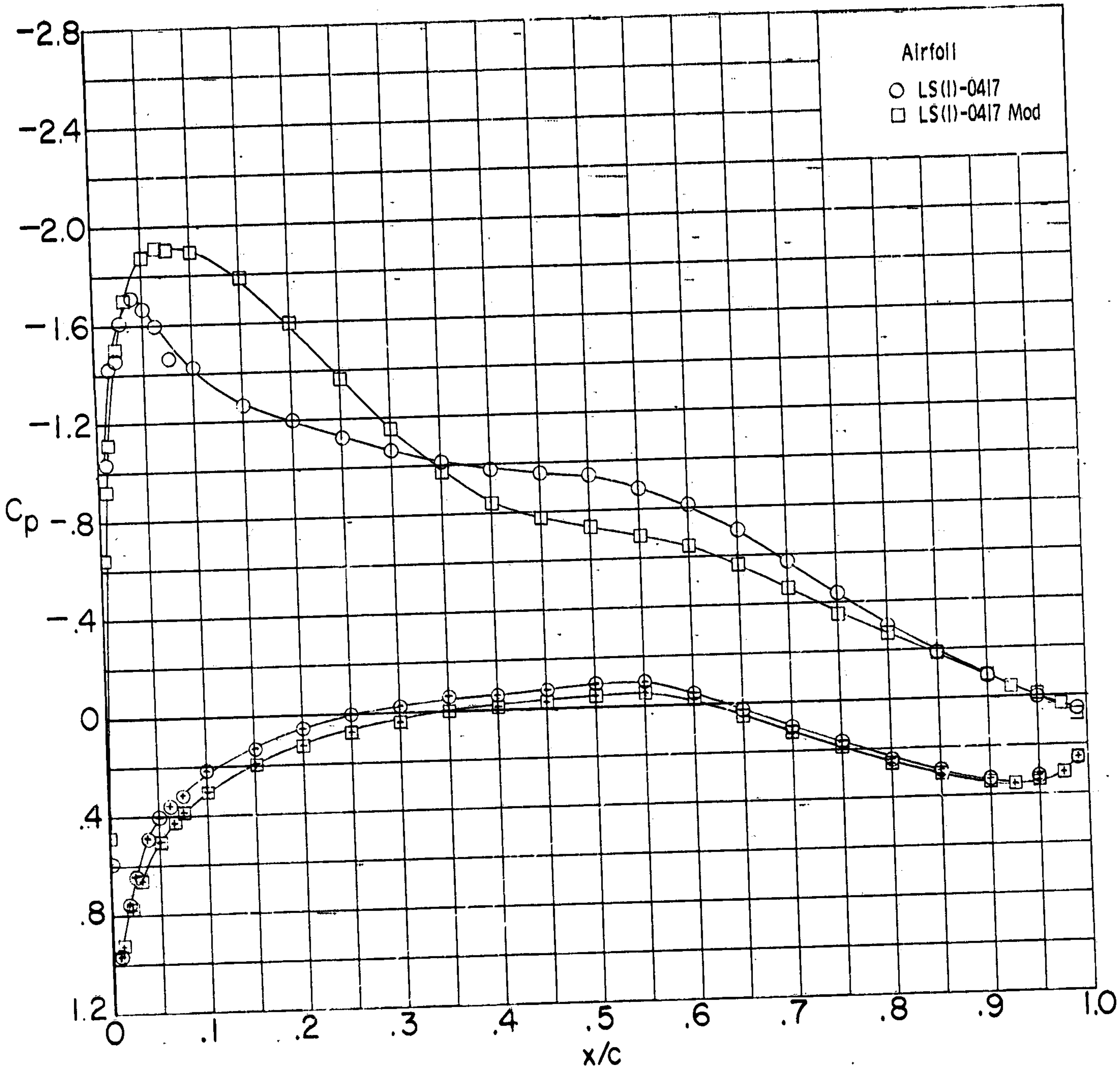

(b) $c_l \approx 1.0$.

Figure 18.- Continued.

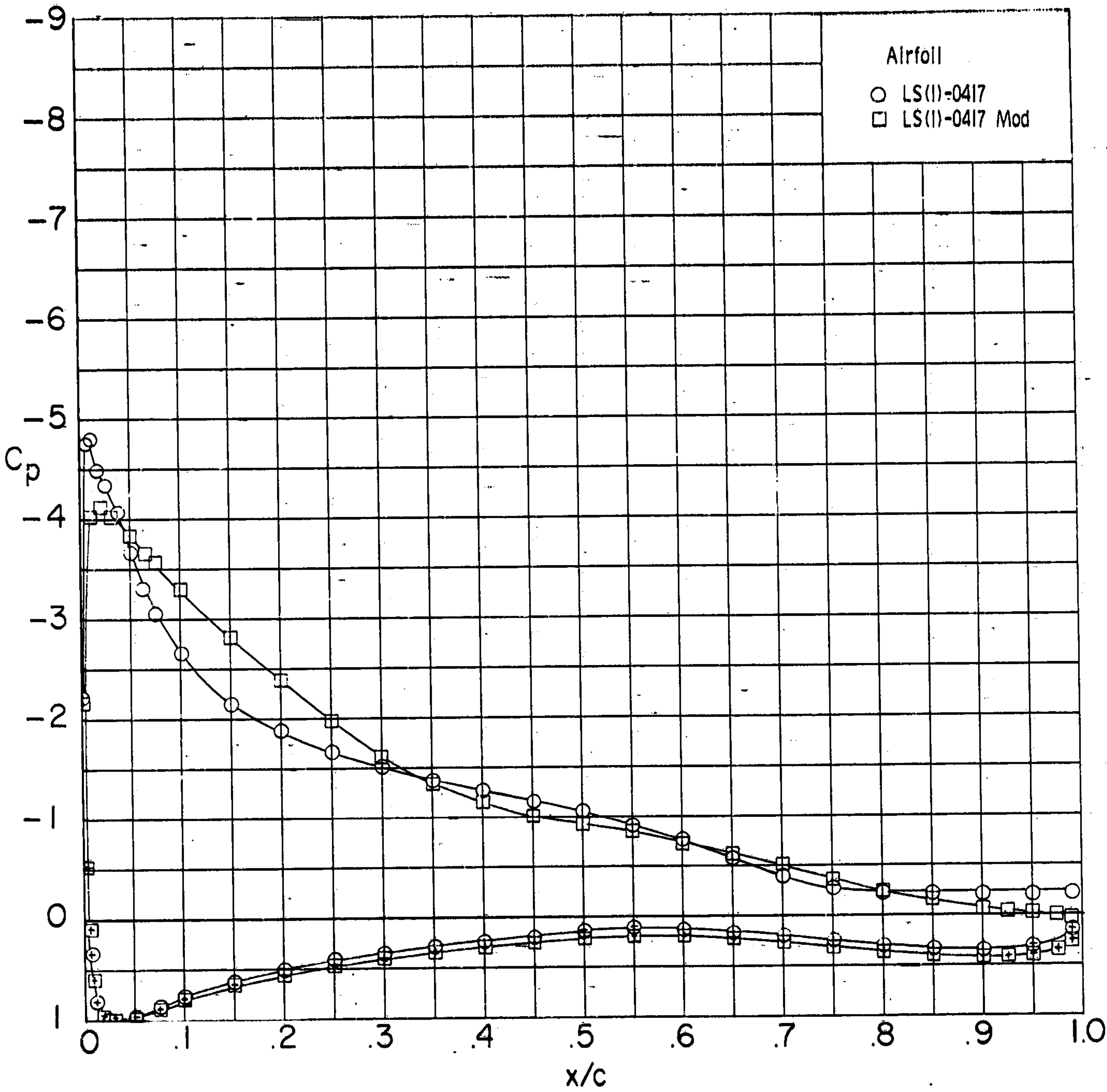

(c) $\alpha = 12°$.

Figure 18.- Concluded.

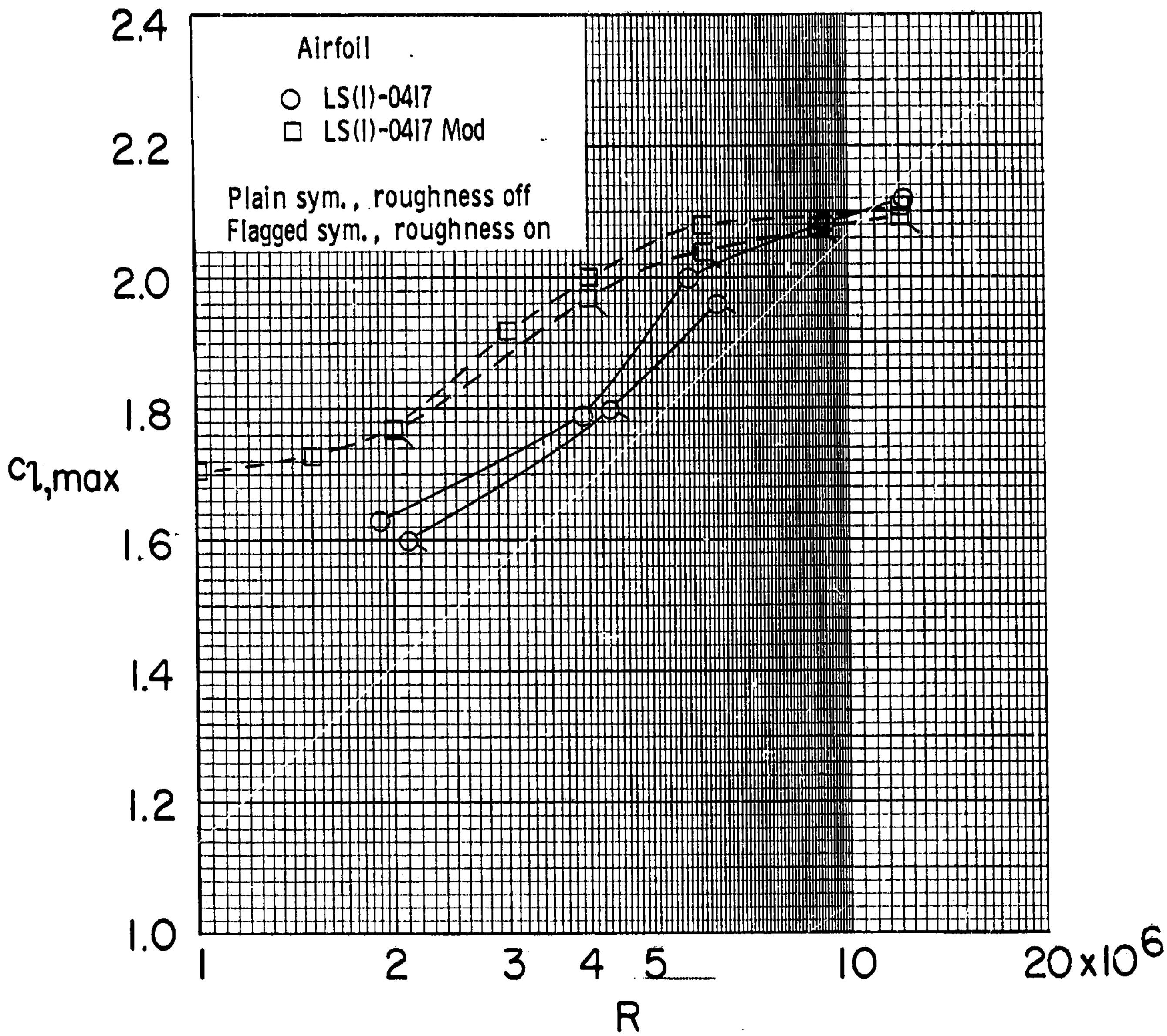

Figure 19.- Variation of maximum lift coefficient with Reynolds number for LS(1)-0417 and LS(1)-0417 Mod airfoils. M < 0.15.

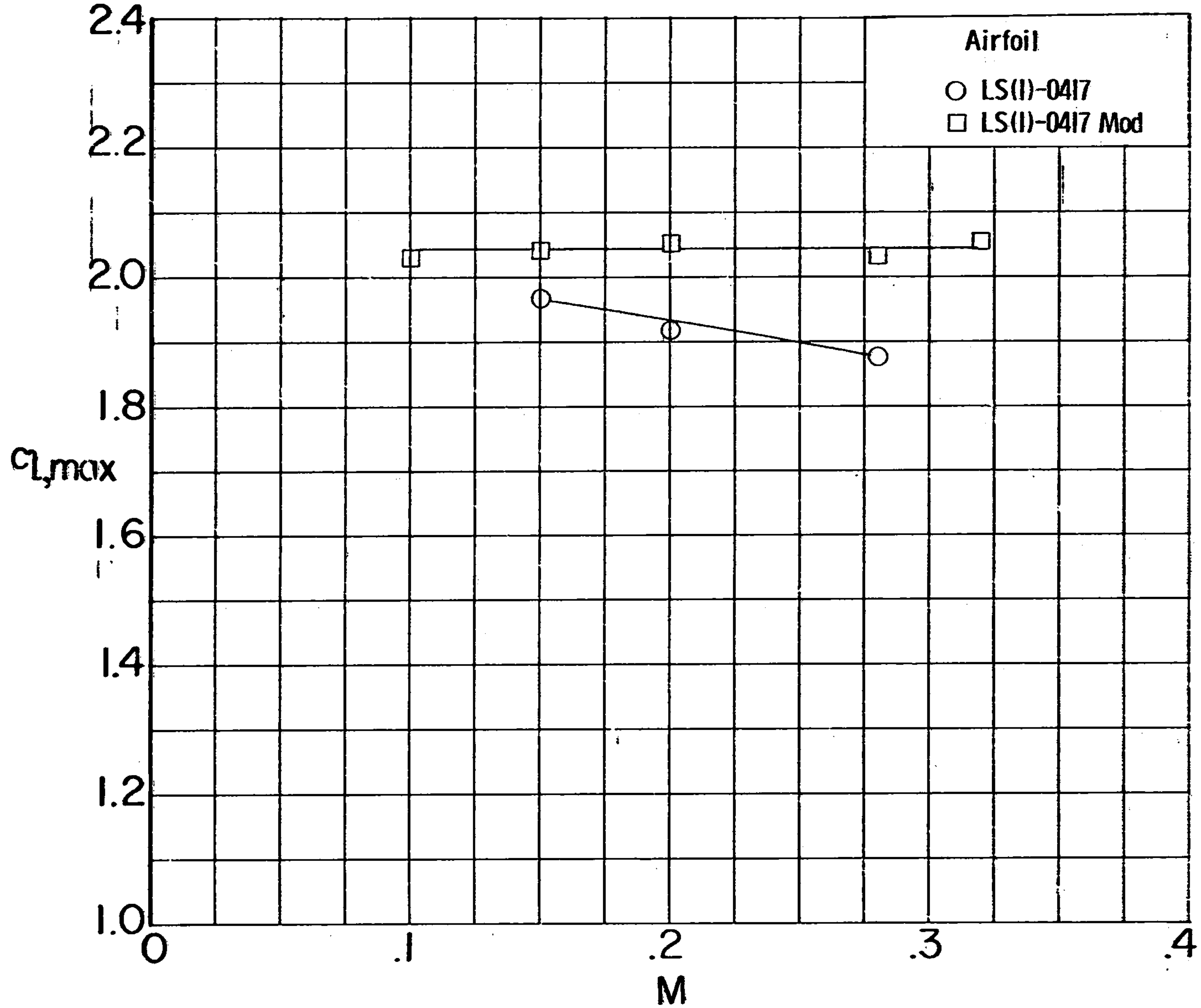

Figure 20.- Variation of maximum lift coefficient with Mach number for LS(1)-0417 and LS(1)-0417 Mod airfoils. Roughness on; $R = 6.0 \times 10^6$.

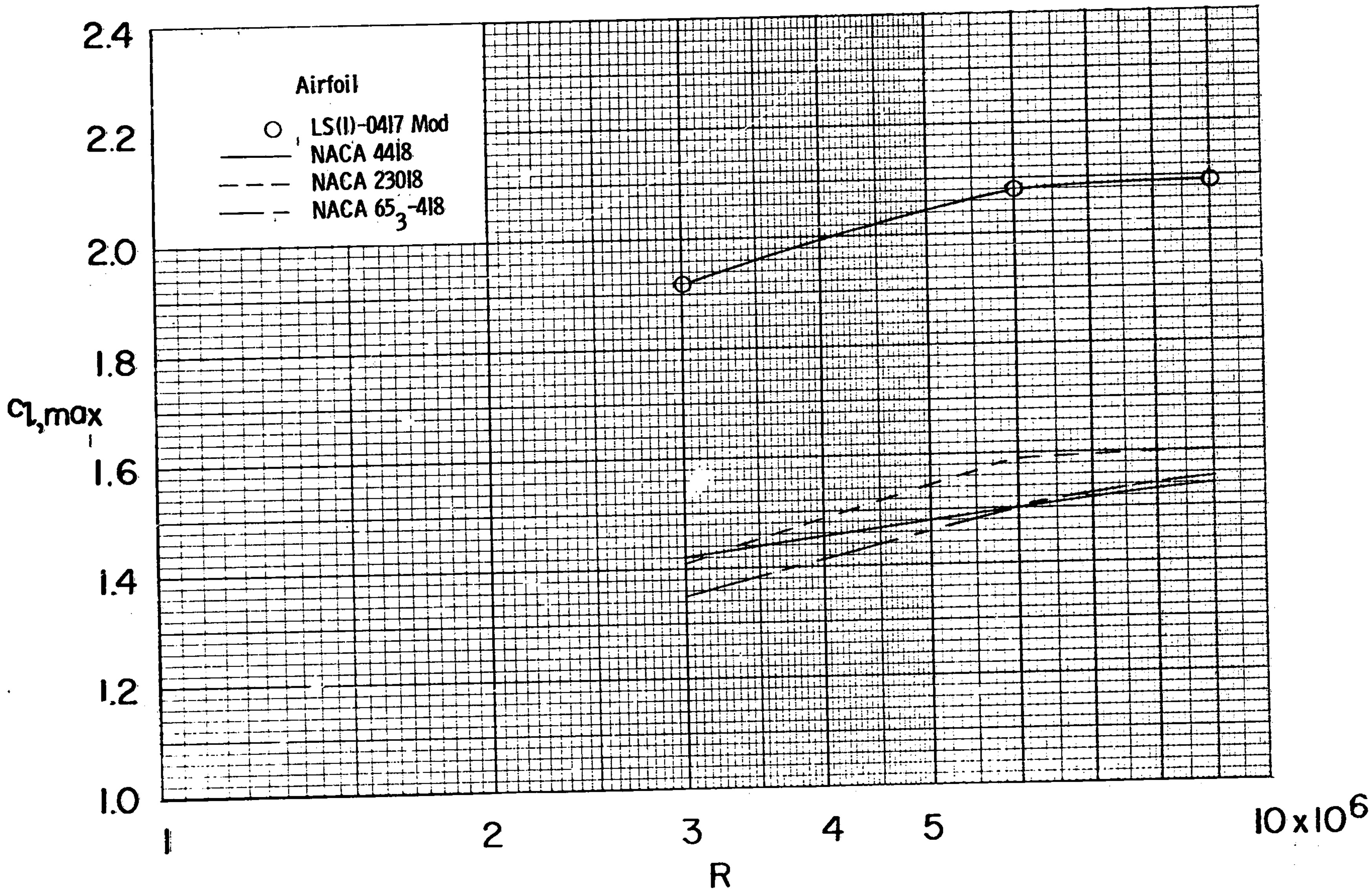

Figure 21.- Comparison of maximum lift coefficients of LS(1)-0417 Mod airfoil with those of NACA airfoils. Models smooth; M = 0.15.

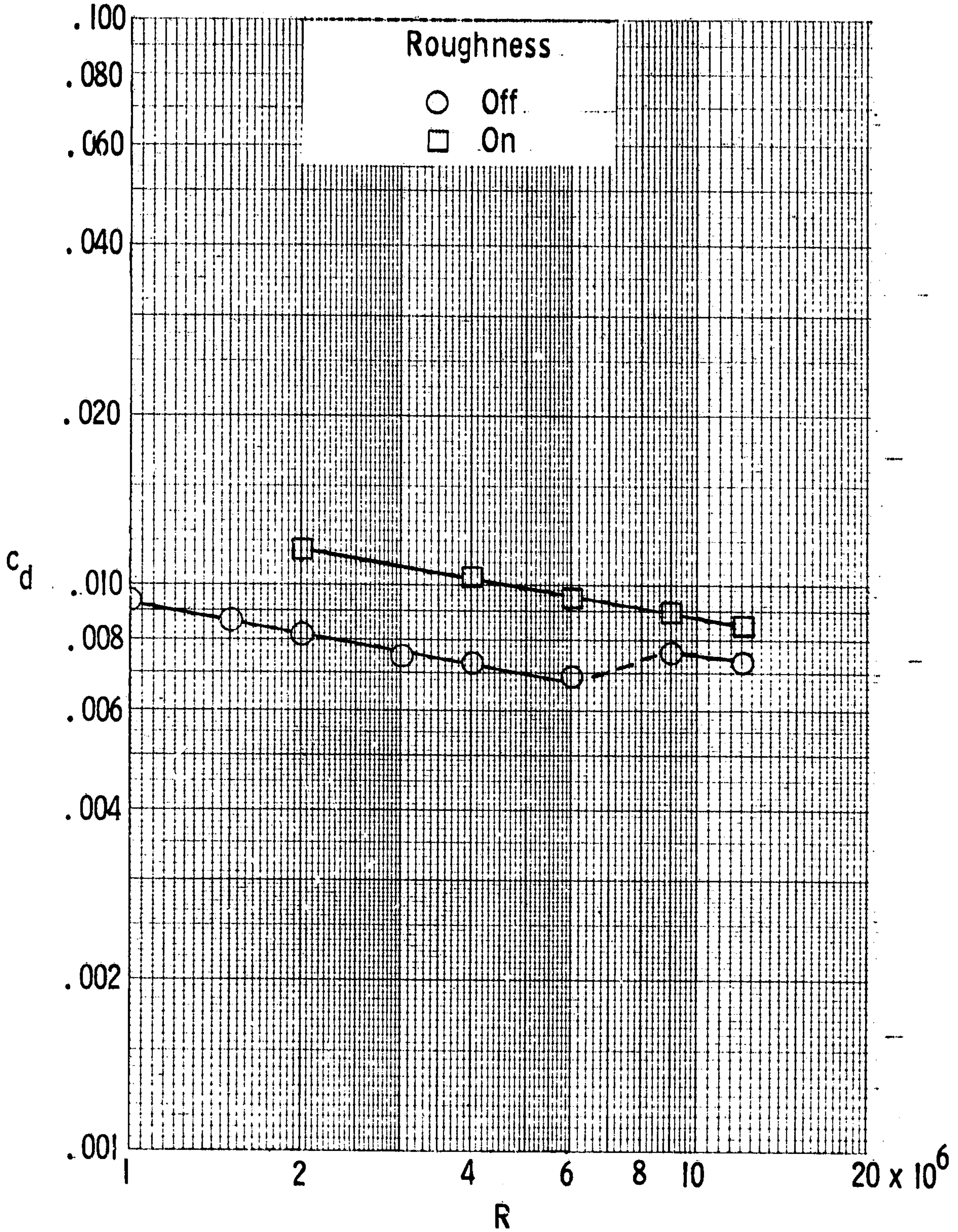

Figure 22.- Variation of drag coefficient with Reynolds number for LS(1)-0417 Mod airfoil. $M < 0.15$; $c_l = 0.40$.

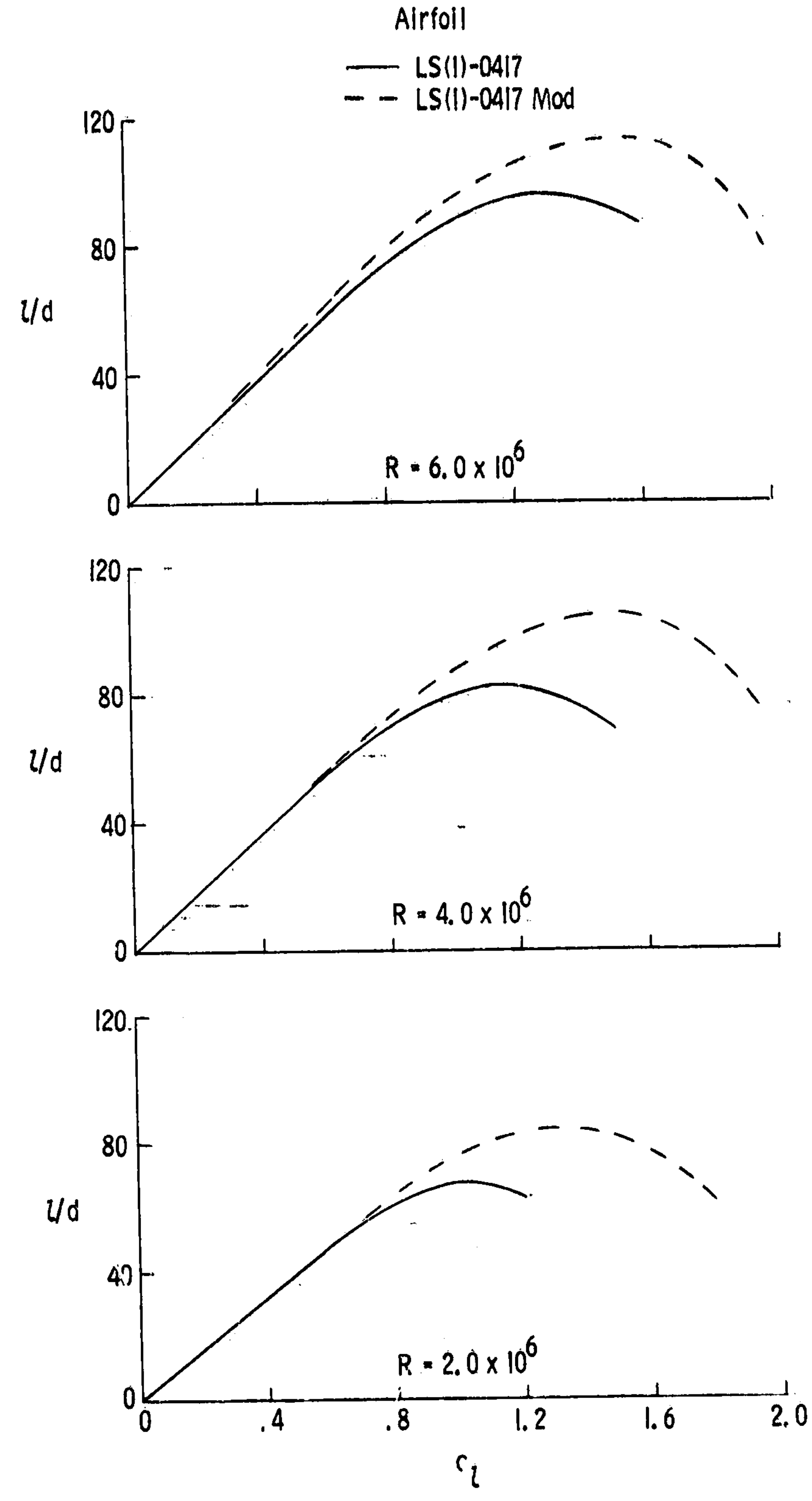

Figure 23.- Variation of lift-drag ratio with lift coefficient for LS(1)-0417 and LS(1)-0417 Mod airfoils. Roughness on; M = 0.15.